Author’s response on “Heterogeneous spatial and temporal pattern of surface elevation change and mass balance of the Patagonian icefields between 2000 and 2016”

***Authors*: Abdel Jaber, W., Rott, H., Floricioiu, D., Wuite, J., Miranda, N.**

The Cryosphere Discuss., https://doi.org/10.5194/tc-2018-258

Referee comments are shown in **black**, our response in **blue**, changes in **red**. Line numbers refer to the manuscript version (pdf) of 23 November 2018.

Anonymous Referee #1

General comments:

Comment (GC1): This manuscript applies advanced SAR processing techniques in order to derive spatially detailed maps of surface elevation change (SEC) of the Northern and Southern Patagonian icefields, NPI and SPI respectively. The text is well written, the figures are of good quality, the tables are clear and informative, the topic is of high interest and the results are very interesting, confirming previous studies showing as a whole a strong negative ice volume change with high spatial variability. The authors analyze in detail different sources of errors and gives precise estimations of uncertainties for every studied glacier, different data sets and analyzed periods.

Response: Firstly, we want to thank the anonymous Referee for the time and effort put in this detailed and thorough review. We carefully evaluated all comments and suggestions, which are extremely valuable in improving the paper. We are very glad about the positive feedback. We particularly value the Referee’s appreciation of the error estimation, in which we invested significant effort and which we believe is one of the strong points of this manuscript with respect to previous studies. Throughout this response, as well as in the paper, we refer to the surface elevation change (in m) as “SEC” and to the surface elevation change rate (in m a^{-1} or m d^{-1}) as “SECR”.

We recognize that the focus of this review is on the seasonal correction which we apply for filling gaps in the rate of surface elevation change, in particular for the four-year time span of epoch 2012 to 2016. This is an important side issue aimed at reducing the uncertainty in mean annual SECR. The main contribution of the paper is the generation of spatially detailed data sets on surface elevation and volume change of both NPI and SPI for two different epochs, including the assessment of communalities and differences in glacier behaviour between the two ice fields and the two epochs. We are not aware of any other publication showing homogenous high resolution data sets on surface elevation or volume change of both icefields for two different epochs.

Comment (GC2): The results are not totally novel, since the data sets employed in this manuscript were recently used in a paper published by Malz et al., (2018) with some variations in dates, error assessments and study area. Unfortunately, the results are not totally comparable between them since the glacier basins and dates are not the same. These differences preclude a precise estimation of discrepancies, but in general the results are statistically similar. The main contribution of Abdel Jaber et al, is their claimed much smaller uncertainties due to several correction that Malz et al didn't applied. After considering the analysis performed by Abdel Jaber et al, I think the error assessment is much more rigorous, effectively addressing many error sources of the data sets, but it is too ambitious when trying to extrapolate parameters from single stations/glaciers for correcting some issues related to the whole icefields. In those cases, is better to live with higher uncertainties and not adding more doubts as I think were added when using Perito Moreno as model for altitudinal gradients for example.

Thanks to the detailed error analysis, this manuscript provides a state-of-the art estimation of surface elevation change of both Patagonia Icefields. Unfortunately, the last data set of 2015 does not come from the end of ablation season, therefore, the authors applied a seasonal corrections to the derived surface elevation changes in order to provide estimates that correspond to full seasonal cycle. This seems to be a weak point of the study design. I guess this was caused by the availability of TanDEM-X imagery, however, employing a more recent datatake from the end of ablation season (later than 2015/16), would have considerably strengthen the importance of this contribution.

Response: While in fact some TanDEM-X raw data (Level-0) used in this study are the same as those used by Malz et al., (2018) we would like to highlight the main differences with respect to the latter publication. Malz et al., (2018) provides a SECR with full coverage of SPI for the epoch 2000-2015/2016 only, from which they derive the geodetic mass balance at an icefield level (with uncertainty) and at a basin level (without uncertainty). They furthermore provide two SECR maps covering the periods 2000-2012 and 2012-2015 which are based on SRTM and on the same pairs of TanDEM-X raw data that we use but they are restricted to the southern part of SPI (~2106 km², ~16% of SPI). Furthermore they do not exploit them to provide any mass balance estimation of the covered glaciers.

We argue that one of the strong points of this study is the use of a homogeneous set of methods and data to achieve SECR maps of both Patagonian icefields, featuring a very high coverage, for two similar observation periods. These maps are used to compute the geodetic mass balance (with uncertainty) of all glacier basins larger than 2 km² on NPI and larger than 9 km² on SPI. Hypsometric plots (with uncertainty) for both epochs are also reported for 15 main glaciers of NPI and 24 of SPI.

As correctly noted by the Referee a critical point of our study design is linked to the missing summer days in the "slave" elevation mosaic of the 2012-2015 SEC, caused by its acquisition time in December 2015, whereas February 2016 would have constituted the ideal setup. We hence understand that most of the constructive critique is linked to this issue. We firstly confirm the Referee's presumption: the choice of this dataset was indeed forced by the absence of more suitable coverages of the icefields at the beginning of this study.

As described in the manuscript, the seasonal elevation loss occurring on the icefields during the missing summer days is non-negligible. We show a map of measured seasonal changes on most of the SPI for a different summer, that of 2011/2012 (Fig. 8) which, however, was characterized by the same average air temperature as summer 2015/2016. We are not aware of any published seasonal SECR map of SPI.

Neglecting the impact of summer seasonal elevation variations on the SECR maps and on the corresponding geodetic mass balance would cause some bias, in particular for the second epoch. We hence devise different correction strategies for different sections of the icefields, according to the availability of SECR datasets and complementary data. We are aware of the limitations of such strategies and take into account these limitations in the error budget. Detailed information on the points correctly raised by the Referee is provided below. We are convinced that the seasonal corrections improve the accuracy of the mean annual SECR compared to the approach by filling temporal gaps with average SECR without taking into account the missing days in the melting season.

Comment (GC3): Assuming that the surface elevation changes in summers 2011/2012 and 2015/2016 are equal, based on similarity of monthly mean air temperature records in some neighbouring weather stations is very arguable.

Response: We agree that these weather stations, in some distance from the icefields, are not the best choice for checking summer temperature over the icefields. We checked the ERA Interim temperature data, showing agreement within 0.1°C for both summers. The 850 hPa mean summer temperatures (December, January, February) for point 47.25 S, 73.55 W over NPI are 5.9° C (2011/2012) and 6.0° C (2015/2016), for point 50.25 S, 73.55 W over southern SPI 3.6° C (2011/2012) and 3.5° C (2015/2016).

Changes: We dropped the station data and report the ERA Interim temperature data together with relevant information in Sect. 3.1.3.

Comment (GC4): The other weak aspects of the manuscript are the assumptions regarding altitudinal gradients only supported by Perito Moreno glacier data. This glacier cannot be considered representative for the entire icefield due to extreme longitudinal gradients of climate and mass balance associated with orographic barrier of the Patagonian Andes.

Response: Many thanks for stressing this topic. We recognise that the rationale and procedures for the seasonal corrections were not well explained in the first version of the manuscript. Section 3.1.3 contains now a completely revised version describing in detail the strategy, procedures and implications of the seasonal correction. In the Supplement to the manuscript (Section S4) we present an analysis on the applicability of the P. Moreno mass balance gradient for supporting the seasonal corrections on Jorge Montt, S. Rafael, S. Quintin and Benito glaciers (the only glaciers for which this type of correction is applied).

Changes: Sect. 3.1.3 (Seasonal correction) was completely re-written in order to assure a better explanation of the applied strategy and methods. An analysis on the applicability of the P. Moreno mass balance gradient for supporting the seasonal corrections on Jorge Montt, S. Rafael, S. Quintin and Benito glaciers is included in the Supplement to the manuscript (Section S4).

Comment (GC5): I would be keen to see maps of systematic error similar to Fig S7 that shows random error. This is especially important for some major outlet glaciers of SPI (Jorge Montt, Pio XI, O'Higgins, Viedma and Upsala) where seasonal correction was in the order of several meters (Fig. S4b).

Response: The systematic error maps do not feature a strong spatial variation, with exception of regions affected by high probability of signal penetration and regions not covered by the summer 2011/2012 SECR. The systematic error maps are per se not very informative and are hence not included in the Supplement, which file size cannot be further increased without affecting the resolution of the other figures. We instead preferred providing quantitative values of the different systematic error components in Table S7. The systematic error linked to the seasonal correction is considered as a bulk error derived from the systematic error of the summer 2011/2012 SECR (see Sect. 3.3.3 and also the response to specific comment below), which was increased on specific regions to take into account the extrapolation through hypsometric average values on regions not covered by the summer 2011/2012 SECR. The weighting by the number of corrected days was also applied. The systematic error dominates in the average SECR and VCR of individual glaciers reported in Table 3, 4 and S8 and can hence be easily compared among glaciers and epochs. We also noticed that the description of Figure S4 might have caused some confusion and changed it. Figure S4 represents the rasters (in meters) added during processing to the original SEC rasters (covering the entire observation period) to compensate for the missing/exceeding days.

Changes: Caption of Fig. S4 changed.

Comment (GC6): This work is largely based on the results and methods reported by Abdel Jaber (2016) PhD thesis. In order to avoid undesirable repetitions, I guess the thesis can be quoted only a couple of times, and then assuming that the results are the one obtained in this manuscript.
In synthesis, I think this manuscript is highly valuable and fits very well with the aim and scope of the journal.

Response: This work is based on methods applied in the Abdel Jaber (2016) PhD thesis which were further developed and adapted to this study. Abdel Jaber (2016) reported SECR maps of NPI (2000-2014) and SPI (2000-2011/2012) with mass balance only at an icefield level. The results presented in this study are completely novel (we note that a limited number of TanDEM-X raw data are in common but were newly processed). For this reason in the manuscript we treat Abdel Jaber (2016) as a separate scientific study. The good agreement between the results of this study and those obtained by Abdel Jaber (2016) by separate processing represents, in our opinion, an added value for both publications.
The only results reported in the manuscript and stemming from Abdel Jaber (2016) are the subaqueous ice volume changes and frontal distance variation of the main SPI glaciers in the epoch 2000-2011/2012 (Table S9) and the icefield-wide subaqueous volume change rate reported in Sect. 4.

Changes: A clarification on the novelty of the results presented in this manuscript and on the relation to the PhD thesis of Abdel Jaber (2016) was added in the Introduction and adequate reference to the thesis is made throughout the paper where relevant.

Specific comments:

Comment: P1 L20: ... and ..., respectively

Response: Wording changed to: "They stretch from 46.5° S to 47.5° S and from 48.3° S to 51.6° S, respectively, along the…"

Changes: as above.

Comment: P2 L9: any other reference? this is only review

Response: References added:

Åström, J. A., Vallot, D., Schäfer, M., Welty, E. Z., O'Neel, S., Bartholomaus, T.. C., Liu,, Y., Riikilä, T. I., Zwinger, T., Timonen, J., and Moore, J. C.: Termini of calving glaciers as self-organized critical systems, Nature Geoscience, 7, DOI: 10.1038/NGEO2290, 2014.

Benn, D. I., Warren, C. R. and Mottram, R. H.: Calving processes and the dynamics of calving glaciers, Earth-Science Reviews, 82, 143-179, 2007.

Warren, C. R. and Aniya, M.: The calving glaciers of southern South America, Global and Planetary Change, 22, 59-77, 1999.

Changes: as above.

Comment: P3 L8-9: You frequently refer to Abdel Jaber (2016), how different is its work from this submission? I presume is roughly speaking the same.

Response: Please see the response to the general comment GC6.

Comment: P3 L23-24: Later you refer to Abdel Jaber (2016) as a source for subaqueous ice loss estimates

Response: Please see the response to the general comment GC6.

Comment: P5 L15-20: Crippen et al. (2016) provided only a general description of NASADEM, and as far as I now, its performance has not been thoroughly compared with SRTMGL1. This I guess is one of main differences of this work compared to a very similar study by Malz et al. (2018) - how does it impact your final results? Were there really less voids compared to SRTMGL1?

Response: Voids, mostly caused by phase unwrapping errors, were filled using ASTER GDEM2 in the SRTMGL1 dataset (SRTM version 3). In the NASADEM (available in its void-filled and SRTM-only versions) voids were not very critical on great part of the icefield. We agree with the Referee that the performance of NASADEM has not been assessed yet. We hence performed our own assessment with the main focus being on sources of systematic errors, and particularly long-wavelength elevation biases. While not perfect (particularly around NPI) we concluded that NASADEM is certainly a step forward in this regard compared to SRTMGL1. We hence proceeded with this dataset for the production of the SECR maps and the computation of the mass balance. SECR maps based on SRTMGL1 were not produced; a quantitative comparison of volume change rates is hence not available.

Comment: P6 L25: How different were your glacier outlines from those used by Malz et al? The Randolph inventory is known to have problems in many places. Maybe you can discuss about this.

Response: Assuming reference to P5 L25. For the glacier outlines of NPI and SPI we use the Randolph Glacier Inventory in its latest version 6 with our own modifications. In RGI v6 significant changes compared to the previous version are found on NPI, where a complete new set of outlines was introduced based on those published by Rivera et al. (2007), while no changes are found on SPI. We are aware of the limitations of the RGI outlines, particularly in the definition of the internal divides between adjacent basins. We improved the external borders of the glacier outlines as described in Sect 2.3, whereas we did not modify the internal divides. The TanDEM-X DEMs have potential for such an improvement but this exceeded the scope of this study. We preferred to use the latest RGI for comparability of results, limiting changes to the termini.

The SPI outlines of Malz et al. (2018) are reportedly based on RGI version 5 with refinements based on optical images. Some non-negligible differences between our and their glacier outlines can be appreciated by comparing our Figure S9a with their Figure 2b. In particular differences are visible on Bernardo, Tempano, Occidental, Greve glaciers (the latter three appear as a single basin in their paper). Other differences are found on Chico/Viedma glaciers, Europa/Guilardi glaciers, and on smaller glaciers.

Comment: P7 L10: There is a problem when quoting equations along the whole manuscript. Only Eq. 2 is mentioned in the text and some equations are between lines without label numbers, don't helping in the fluent reading process. You refer here to Eq. (2) well before introducing it (and before Eq. (1))

Response: Agreed, many equations were written inline in order to reduce space and provide a flowing narrative. We will improve the manuscript on this issue.

Changes: The most relevant equations are now displayed on their own line and numbered, whether they are cited or not.

Comment: P8 L20. The temperature and balance altitudinal gradients in the SPI are highly different between east-west margins or northern - southern parts etc. Maybe you can check a recent paper by Bravo et al in JGR (DOI: 10.1029/2018JD028857) and comment on this.

Response: Many thanks for referring to this recently published paper providing very valuable data for advancing the modelling of surface/atmosphere exchange processes and surface mass balance across the icefield. We performed computations on mass balance gradients using different lapse rates on east and west coast glaciers and comparisons with Moreno balance gradients which happen to support our approach. See details in response to general comment GC3 and in Supplement Section S4.

Changes: We clarified this point in the re-written Sect. 3.1.3 and in the Supplement (S4), including the suggested reference to Bravo et al. (2019).

Comment: P8 23-36: Can you please clarify this part? For example Perito Moreno and Jorge Montt have very different climatic setting (Lenaerts et al., 2014), I wonder if Perito Moreno is a best choice for a reference in this case.

Response: See the detailed descriptions and checks in Section 3.1.3 and Supplement (S4) and the response to comment P8 L20.

Changes: Information on mass balance gradients for different glaciers and checks on representativeness of Moreno data are reported in Supplement S4.

Comment: P8 L30-32: Again, issue of transferability of parameters of Perito Moreno to entire SPI. Why was it not necessary for NPI, because of the day of data take, I guess?

Response: The 2000-2012 SECR of NPI was not corrected because the SRTM and the TanDEM-X data takes were acquired approximately in the same days of February. The seasonal changes on the scene with index 1, not involving summer days, were deemed to be negligible and much less than the systematic errors on a 12-year time frame. Furthermore, the seasonal ratio in ablation rate (summer vs. full year), based on P. Moreno measurements, is not used for supporting the seasonal correction of the full icefields, but only for four glaciers. See also the detailed descriptions in Section 3.1.3 and Supplement (S4) and the response to comments above.

Comment: P8 L36-37; Fig S4: There are sharp boundaries between zones corresponding to different time spans, do they propagate to the final product introducing discontinuities?

Response: The discontinuities are caused by the different Δt in days to be corrected between adjacent master-slave pairs. These do not propagate in a noticeable way to the final SECR product. In fact light discontinuities might already be present in the uncorrected SECR, the correction would, at least in theory, reduce such discontinuities by compensating different amplitude of seasonal changes according to the actual Δt in days.

Comment: P9 L19: Uncertainty bound on glacier-wide density seems to be too low. Cogley (2009) refer to Sapiano et al. (1998) 6% estimate as reasonable. In similar work, Malz et al. (2018) provide three scenarios of different densities, it is their main source of uncertainty for the final results.

Response: The main scope of this study is to provide reliable volume change rate estimates at a basin scale and the core of the error estimation focuses on the volume change rate estimates. (Tables 2, 3, S8). These can then be converted to mass change rates using a constant density assumption with a corresponding error of choice. Furthermore we also provide a reference mass change rate at an icefield level (Table 1). For this purpose we used in the first version of the paper the common scenario of glacier-wide density of 900 kg m^{-3} facilitating the comparison of results with other studies. We agree that the assigned error of ±17 kg m^{-3} is a small one for firn areas. The high mass loss rates on the Patagonian icefields refer to ice areas. Therefore it makes sense employing separate density estimates for the volumes in ice areas and firn areas. We use ±17 kg m^{-3} in the ice areas and ±54 kg m^{-3} in the firn areas, assuming a mean elevation of 1150 m on NPI and 1050 m on SPI for separating ice and firn areas. The resulting uncertainty in density for icefield-wide mass changes is obtained by rounding up to ±36 kg m^{-3} (4 %).

Changes: This point is taken into account by employing an error on the density of 36 kg m^{-3} (4 %) for icefield-wide mass changes reported in Table 1. This value (together with explanation) is not cited anymore in Sect. 3.1.4 but appears only in Sect 3.3.4 to avoid repetition.

Comment: P10 L7-10: Please back it up with some reference

Response: References added:

Garreaud, R., Lopez, P., Minvielle, M., and Rojas, M.: Large Scale Control on the Patagonia Climate, J. Climate, 26, 215–230, 2012.

Schaefer, M., Machguth, H., Falvey, M., and Casassa, G.: Modeling past and future surface mass balance of the Northern Patagonian Icefield, J. Geophys. Res.-Earth, 118, 571–588, doi:10.1002/jgrf.20038, 2013.

Changes: as above.

Comment: P10 L24: Finally, what exactly was the criterion for masking regions prone to penetration? Was it only manually outlined based on expert knowledge?

Response: In each DEM mosaic, regions prone to signal penetration were not masked-out, instead they were manually outlined according to backscatter intensity and assigned a certain penetration bias, which was then used to compute the corresponding systematic error component of the SECR (Sect. 3.3.3). The penetration bias was assigned based on the average σ^0 within the region. Measurements of signal penetration in TanDEM-X data over NPI at varying σ^0 are reported in Abdel Jaber (2016). These, together with knowledge on relations between X-band σ° and signal penetration length (see e.g. Mätzler, 1987) were used to assign the elevation bias taking into account the relation between penetration length location of the scattering phase center within the snow pack. During summer the top snow layers on the main ice plateau are either wet (low σ°) or include melt/freeze metamorphic layers with rather small penetration for X-band signals also in frozen state (Reber et al., 1987).

Mätzler, C.: Applications of the interaction of microwaves with the natural snow cover, Remote Sensing Review, 2, 259-387, 1987

Reber, C., Mätzler, C., and Schanda, E.: Microwave signatures of snow crusts, modelling and measurements, Int. J. Remote Sensing, 8 (11), 1649 – 1665, 1987.

Changes: Section 3.2 was improved including the aspects and references reported in this response.

Comment: P11 L8-9: See comment above.

Response: The average σ^0 of the SRTM acquisitions were analyzed to reach this conclusion. This is another novel aspect of this publication; we are not aware of an empirical assessment of the backscatter of C-band SRTM to assess possible signal penetration in glaciological remote sensing studies. Relations between snow wetness, penetration depth and backscatter intensity can be looked up in radar textbooks (e.g. Ulaby and Long, 2014). Furthermore, the good agreement between our volume change rates 2000 to 2012 over NPI and the results of Dussaillant et al. (2018) based on optical data confirm the validity of our approach regarding signal penetration. See also their conclusion: " our study confirms the lack of penetration of the C-band SRTM radar signal into the NPI snow and firn except for a region above 2,900 m a.s.l.".

Ulaby, F.T and Long, D.G.: Microwave Radar and Radiometric Remote Sensing, The Univ. of Michigan Press, Ann Arbor, 2014.

Comment: P11 L11: Bippus (2007) assumed this lapse-rate for summer season on Perito Moreno, however as far as I know this value was not based on measurements. Additionally, she accounted for an off-glacier location of AWS, resulting in additional temperature offset. Maybe you can compare your numbers with Bravo et al 2019

Response: Thank you for this input. However, we want to stress that the conclusion about signal penetration is primarily based on the backscatter assessment. Regarding penetration see also the comment on P11, L8-9.

Changes: Based on our response the reference to Bippus (2007) was removed and the explanation made clearer. The suggested reference is included in the manuscript.

Comment: P12 L26: Is 0.1 m based on literature?

Response: The bulk systematic error of 0.1 m for the remaining pixels above 1000 m a.s.l. accounts for undetected regions (a very small percentage of the total area) and possible small offsets for areas with refrozen upper layer of snow and firn, affecting only very small areas; see response above. The typical X-band one-way penetration depth of a frozen crust of 10 cm thickness is about 0.1 m, increasing with decreasing crust thickness (Reber et al, 1987).

Changes: We added here a reference to Sect. 3.2 which refers to the response above, and the corresponding reference to Reber et al. (1987).

Comment: P13 L1-5: I think that the error linked to the seasonal correction may be underestimated as it does not seem to cover all uncertainties related to the transferability of hypsometric averages shown in Fig. 8 (see previous comments).

Response: For details see the response to the general comment on seasonal correction (Sect. 3.1.3) and Sect. 3.3.3 on error analysis. The systematic error linked to the seasonal correction is derived from the systematic error for the summer 2011/2012 SECR used for the correction on most of the glaciers. This systematic error was increased to account for the different year to correct, although summer air temperatures were nearly the same (see response above). It was also increased on regions where the summer 2011/2012 SECR has no coverage (NPI, north-west SPI and many gaps throughout SPI) in order to account for the transferability of hypsometric averages. Such increases might even lead to an overestimation of this error source; this is accepted as it tends towards a more conservative error budget.

Changes: Revisions and clarifications on seasonal correction have been implemented in Sect. 3.1.3 and on related error analysis in Sect. 3.3. See response to related comments above.

Comment: P15 L26: It that is true than your seasonal correction should use lower density in accumulation area.

Response: P15 L26 does neither refer to seasonal correction nor to density in the accumulation area. It is a statement pointing out that measured (or modelled) surface ablation cannot be directly converted into SEC, as it is necessary to account for emergence or submergence. Regarding the question on the density used: there is no need for using snow or ice density in SEC retrieval by means of DEM differencing. The correction refers to seasonal differences (summer vs. rest of the year) in surface elevation and fills the missing days in observed SEC.

Changes: Revisions and clarifications on seasonal correction have been implemented in Sect. 3.1.3. The procedure of separate accounting for seasonal corrections of SEC due to surface melt and submergence is detailed in Supplement, Section S4. The latter procedure is applied to those four glaciers with significant dynamic downwasting that are not (completely) covered by the summer 2011/12 SEC maps.

Comment: P15 L30: Perito Moreno glacier

Response: Corrected.

Changes: as above.

Comment: P16 L28: Results were recently published in Frontiers - Langhamer et al. (2018)

Response: Thank you; we included the reference to this publication in the revised paper.

Changes: as above.

Comment: P16 L37: Again, I doubt that Perito Moreno is representative for entire SPI and SPI, Steufer (2007)

Response: This comment refers probably to P16 L30 (there is no L37): "Assuming a degree-day factor of 0.7 cmd^{-1} on ice areas (Stuefer et al., 2007), the melt loss for an increase of surface temperature by 0.7 °C during November to March corresponds to an additional loss ...... ". This average degree-day factor, based on ablation measurements on Perito Moreno Glacier over several years, is similar to the average degree-day factor of 0.65 cmd^{-1} reported by Rivera (2004) for Chico Glacier. Consequently this factor can be well used for an estimate on the impact of melt due to different summer temperatures in the discussion.

Comment: P17 L26: This issue is a critical factor in the whole analysis of the elevation changes in the high plateau of the icefields. We know that the accumulation is extremely high, an in between few days you can have huge accumulation events. I think this high temporal variation of snow fall must be taken into account. See Schwikowski et al 2013 for snow accumulation on the SPI.

Response: At first, we want to point out that we are well aware on the spatial and temporal variability of accumulation on SPI. The work reported in this paper (as in other papers on SPI or NPI mass balance) does not deal with single events, but addresses the retrieval of spatially detailed maps on changes in surface elevation and volume over SPI and NPI, providing mean values over epochs of 12 years and 4 years. The contribution of single events during this period is implicitly included in this analysis. Regarding spatial variability, this is fully taken into account by the high spatial resolution of the TanDEM-X elevation data and the high percentage of spatial coverage (Tables 2 and 3). Regarding the summer periods 2011/2012 vs. 2015/2016, there is no indication on exceptional events as according to ERA Interim there is perfect agreement for air temperature and the difference in precipitation between these two summers is 15 % (within the uncertainty of precipitation estimates for this region of complex topography).

Comment: P18 9? What analysis? It is missing in methods and results sections. Maybe you wanted to quote Abdel jabber 2012?

Response: Assuming this comment refers to P18 L3, L4. Thanks for pointing out the lack of information on the source of the velocity data used in the Section 5 (Discussion) for supporting the discussion on differences in volume change between the two icefields and two epochs. The analysis refers to novel ice flow velocity results from a study which we performed complementary to the work on DEM differencing. It is based on TerraSAR-X repeat-pass SAR data, as explained now in the revised text. Within the ESA project SAMBA (mentioned in the Acknowledgements of the paper) we generated digital maps of ice velocities of SPI and NPI derived from TerraSAR-X and Sentinel-1 data, including time series. In Section 5.1 we report some numbers out of these results for supporting the discussion. We added one figure with velocities for four main glaciers in different years.

Changes: We explain the origin of the velocity results at the beginning of Sect. 5.1 and include a new figure which shows results for four main glaciers of SPI.

Comment: P18 L25: See comment above P33 Fig.4: Why is there a sharp transition in the terminal part of the glacier on panel a? Frontal retreat I guess?

Response: Yes, exactly. The sharp transition is in fact a physical signal in the elevation difference between the glacier front in 2012 (abrupt step in elevation) and what in year 2000 was the glacier surface (smooth increase in elevation). **References mentioned in this review:**

Bravo, C. et al (2019) Air Temperature Characteristics, Distribution and Impact on Modeled Ablation for the South Patagonia Icefield. JGR, DOI: 10.1029/2018JD028857

Langhamer, L., Sauter, T., & Mayr, G. J. (2018). Lagrangian Detection of Moisture Sources for the Southern Patagonia Icefield (1979-2017). Frontiers in Earth Science, https://doi.org/10.3389/feart.2018.00219

Lenaerts, J. T., Van Den Broeke, M. R., van Wessem, J. M., van de Berg, W. J., van Meijgaard, E., van Ulft, L. H., & Schaefer, M. (2014). Extreme precipitation and climate gradients in Patagonia revealed by high-resolution regional atmospheric climate modeling. Journal of Climate, 27(12), 4607-4621.

Sapiano, J.J., W.D. Harrison and K.A. Echelmeyer. 1998. Elevation, volume and terminus changes of nine glaciers in North America. Journal of Glaciology, 44(146), 119- 135.

Schwikowski, M., M. Schläppi, P. Santibañez, A. Rivera and Casassa G. (2013): "Net accumulation rates derived from ice core stable isotope records of Pío XI glacier, Southern Patagonia Icefield". The Cryosphere 7, 1635-1644. doi.org/10.5194/tc-7- 1635-2013

Anonymous Referee #2

General comments:

Comment (GC1): The study presented by Wael Abdel Jaber and co-authors is an overview of surface elevation change rate (SECR) and geodetic mass balance (MB) values for the Southern Patagonia Icefield (SPI) and Northern Patagonia Icefield (NPI) for the two epochs 2000-2012 and 2012-2016. The results are calculated on the entire icefield as well as on glacier basis, mean SECR and volume change rates (VCR) are listed in a table including observed area and error budget. For most important glaciers the hypsometric distribution of those variables is depicted in graphs. The study provides a detailed description of the error analysis and several steps to correct for biases and penetration and ablation uncertainties. The language is correct and understandable. The subject is of high interest to the community, the method and study areas are not completely novel. In the last years, there have been publications covering the study area with the same topic (Foresta, Dussaillant, Malz, Abdel Jaber himself), but partly using different approaches. This new study cites and discusses those adequately. I recommend to add the recent work of Braun et al. (2019) which also includes SPI and NPI, but only covers the first observation period (2000-2011/15). The authors point out two aspect as main progress to previous studies: 1) The comprehensive and simultaneous observation of both icefields at two epochs. 2) The variety of corrections and assumptions made to guarantee a precise observation of SECR and following products. The line of argumentation is clear as far as (1) is concerned and thus I support publication in TC. Nevertheless, concerning (2), revisions should be performed to significantly improve the traceability of results and assure the validity of some of the applied steps described in the method section before publication.

Response: We thank the anonymous referee for the detailed review and the appreciation of our work. Although similar studies were published already we want to point out the main novelties of our manuscript. We provide the first geodetic mass balance for NPI and SPI also for a recent epoch (2012-2016) by TanDEM-X DEM differencing and discuss causes for differences between the two icefields and the two epochs. Besides the entire icefields we give average SECR and VCR (incl. error) for individual glacier basins (up to 9km^2 on SPI and 2km^2 on NPI) and hypsometric plots of main glaciers (incl. error bars). We used the same method as for the preceding epoch (2000-2012) and this allows the comparison of individual glacier and icefield behavior in the two epochs. Also we present an up to now unique analysis of the backscatter coefficients of all SAR acquisitions (SRTM and TanDEM-X) to assess the error due to signal penetration, a known issue when using InSAR based DEMs. Abdel Jaber et al. (2016) is a doctoral thesis. It has not been published in any scientific journal, neither in its entirety nor any part of it, but it is available online to everybody. The thesis, reporting many details on the methods used for SECR and VCR, provides also the basis for the technical approach applied in this paper. This review asks for many details on techniques for TanDEM-X DEM differencing and retrieval of SECR which are relevant for a technical paper on DEM differencing. As this is not the main scope of our paper, we tried to focus in the methodology sections on essential points, nevertheless resulting in an already quite comprehensive description. We provide in this response information on specific technical issues raised by the referee and explain how these we taken into account in the revisions.

Thanks also for pointing to the recently published paper by Braun et al. (2019). We make reference to this paper. Regarding DEM differencing SRTM-TanDEM-X, for SPI, the numbers seem to be based on Malz et al. (2018). The reported number for NPI 2000 - 2011/2015 lacks full traceability regarding the TanDEM-X data used and processing methods so that in depth comparison with our results is not possible.

Changes: We took these issues into account for paper revision (see response to specific comments). We added the reference to Braun et al. (2019) in Sect. 5.2.

Comment (GC2): Methods: The utilization of several thresholds or distinct values is not always transparently explained. At some decisive points, it remains vague if the method or decision follows own reasoning, own previous work or an external reference (cf. specific comments)

Response: We thank the referee for pointing out this aspect. We provide relevant information in the response to specific comments and in the revised paper.

Comment (GC3): The correction for the observation date in epoch 2, for not being at the end of ablation period, is an unprecedented venture. However, it forms also a weak point of the study. In the reviewer's opinion, the error induced to the SECR (Epoch 2 – Epoch1) by this step is not adequately represented by the mapped datasets nor is it transparently addressed as error contribution in the text. Moreover, an interpolation of missing areas based on only two weather stations and adjusted to sparse hypsometrical patterns has to be regarded rather experimental compared to the robust methodology used for the rest of the study. It is hard to judge the validity of the seasonal correction. A Δh map outside the icefields and the unfiltered dataset Δh could help justifying, at least for the observed parts(cf. specific comments)

Response: We are aware that the correction applied for the missing days in the ablation season to complete the 4 years period of epoch 2 has some limitations. On the other hand performing such a correction for the short period is fundamental for obtaining reliable annual SECR for comparisons with other results. This reduces a possible bias compared to the case without seasonal correction. Regarding the station data: we replaced these by ERA Interim data over the icefields.

We recognise that the rationale and procedures for the seasonal corrections were not well explained in the first version of the manuscript. Section 3.1.3 contains now a completely revised version describing in detail the strategy, procedures and implications of the seasonal correction. In the Supplement to the manuscript (Section S4) we present an analysis on the applicability of the P. Moreno mass balance gradient for supporting the seasonal corrections on Jorge Montt, S. Rafael, S. Quintin and Benito glaciers (the only glaciers for which this type of correction is applied). Regarding the impact of the seasonal correction on the error budget, this is specified in Table S4 at the icefield level and taken into account in the total error budget for the icefields and the individual glaciers. The spatial patterns on the magnitude of the seasonal correction are shown in Fig. S4. Outside the icefields no seasonal correction is applied. Therefore additional delta h maps are not deemed to be necessary, in particular as they would further inflate already a long paper and Supplement. Concerning the unfiltered Summer 2011/2012 SECR please see the answer to corresponding specific comment.

Changes: Sect. 3.1.3 on seasonal correction was completely re-written. Further information is supplied in the Supplement, Section S4.

Comment (GC4): The error indicated for SECR is spectacularly low in this paper. Although there is a section explaining the calculation it is not totally clear, why a DEM comparison could come up with such low elevation error budget. It appears, the systematic error budget, as the main contributor, is calculated partly in favor of a small total error. Some steps along this path should be under discussion or described in more detail for traceability (cf. specific comments).

Response: The errors of SECR and of VCR (Table 1) are comparable to most of the recent results obtained by other authors based on elevation change approach (see Table S10). Therefore we do not understand the reason for the reviewer's statements "spectacularly low" error and "the systematic error is calculated in favor of a small total error". Furthermore, the agreement between our volume change rate 2000 to 2012 over NPI and the results of Dussaillant et al. (2018) is well within the combined error bound. This supports the validity of our error estimate, as the results of Dussaillant at al. are based on completely different data sets and methods. As suggested, we provide further clarification on the error estimate in the revised manuscript and Supplement.

Comment (GC5): Structure: The work is based on the PhD thesis of Abdel Jaber (2016). However, since it is sometimes difficult to follow what is actually new in contrast to what was already in place, that presents the reader with challenges. A clear line between parts that were newly implemented and those that were adopted needs to be drawn by the authors. I recommend that the authors revise the methods and result section with regard to this aspect to make the paper a full stand-alone document. This also concerns the length of some descriptions that could be kept more concise for this paper, with reference to the thesis (or other original source).

Response: In our view the first version of the paper is already a full stand-alone document, as all essential information on scientific background, methods, results, discussion, etc. is presented in a logical and traceable way, including references to the sources. As mentioned before, the PhD thesis of Abdel Jaber (2016), nor parts of it, have been submitted to or published in any journal. In this respect everything reported out of the thesis would be novel for a journal paper (with adequate reference to the thesis). However, the results on surface elevation and volume change presented in this study are completely novel also compared to the thesis which covered SECR maps of NPI (2000-2014) and SPI (2000-2011/2012) with mass balance only at an icefield level. Only a limited number of TanDEM-X raw data are in common, but these were newly processed. For this reason we refer in the manuscript to Abdel Jaber (2016) as a separate scientific study. The good agreement between the results of this study and those obtained by Abdel Jaber (2016) by separate processing represents, in our opinion, an added value for both publications. The methodology builds on the development work for the thesis with some further evolution. This paper includes an overview on key components of the method, with reference to the thesis where the reader can look up details. However, we realize that the related explanations are not clear enough in the first version of the paper and took this into account in the revisions.

Changes: A clarification on the novelty of the results presented in this manuscript and on the relation to the PhD thesis of Abdel Jaber (2016) was added in the Introduction and adequate reference to the thesis is made throughout the paper where relevant.

Specific comments:

Comment: P 6 l27 ...(in order of impact, the latter being negligible in our Raw DEMs)." This and further statements could be corroborated by a similar Figure as Fig S 2 for SRTMTDM, displaying same Δh for outside the icefields for SRTM-TDM(Ep1) and TDM(Ep1)- TDM(Ep2).

Response: Off-glacier SECR close to some termini are included for this purpose in the detailed maps from different locations of the icefield shown in Figures 2 - 7. Adding these four figures would inflate the already extensive size of the paper. Furthermore the file size of the Supplement cannot be increased further without affecting the resolution of the other figures.

Comment: P 7 ll3 -13 The weighted averaging of the offset values leaves the question if a spatial pattern was analysed and fitted by an offset function. A simple averaging could lead to regional maladjustment, if the sign / magnitude of the offset is a function of geographic position (tilted dataset, described in this manuscript p6 l20). For the precision of the applied method a mapped Δh (cf. comment to P6 ll26) could be convincing.

Response: See previous response.

Comment: P7 ll13 How is the absence of horizontal shifts checked? The detection is slope dependent (cf. Nuth and Kääb (2011)), thus cannot be efficiently performed on an area without slope as the CRs (avr. Slope below 4◦)

Response: The horizontal shifts (in our case possibly acting in the ground range direction) were not checked analytically directly on our datasets, but relying on visual analysis of all available off-glacier terrain. Analytical checks using the method of Nuth and Kääb (2011) was done for the TDM-SRTM SEC datasets during the preparation of the thesis (Abdel Jaber et al., 2016) corroborating the validity of this calibration procedure. Because the same method was applied for this paper as for the thesis, the conclusions regarding this procedure can be adopted for this work.

Comment: p7 ll23 Please provide reference

Response: Rivera (2004) Fig. 6.3 shows in January higher density in the upper metres of snowpits in the accumulation area of Chico glacier, compared to density in September and October. We added the reference:

Rivera, A.: Mass balance investigations at Glaciar Chico, Southern Patagonia Icefield, Chile, Ph.D. thesis, Univ. of Bristol, UK, 2004.

Changes: as above.

Comment: P 7 ll30 What kind of filtering was applied? It would be interesting to see the original dataset and a Δh map outside the icefields.

Response: Since the Summer 2011/2012 daily SECR is used only for the seasonal correction, we applied the following procedure for eliminating outliers: (i) conservative masking on glaciated terrain of regions with high backscattering and peaks in the daily SECR values followed by (ii) 2-step filtering with sliding window: (a) median filters with kernel size 9 and (b) smoothing with kernel size 9. The raster posting is 0.4 arcsec. This way the localized seasonal changes or outliers were eliminated and thus the SECR map can be used for the purpose of compensating the temporal gap in 2015/2016. Such a figure representing the unfiltered Summer 2011/2012 SECR would not provide any additional significant scientific or methodological contribution as it is a minor technical detail of rather limited impact.

Comment: P8 ll10 What does similar mean here? +-0◦C? Please add a number for consistency.

Response: The 2 stations data we used are confirmed by ERA Interim temperature data (see also response AC#1 page 3) which provide even higher agreement between the summer epochs. According to ERA Interim the average temperatures of summer 2011/2012 and summer 2015/2016 agree within 0.1°C. This means that the SECR maps of summer 2011/2012 (scaled to the length of the missing period) can well be used as substitute for the missing days in summer 2015/2016. We will add this info in this paragraph.

Changes: The reference to the two stations was dropped and reference is made to the ERA Interim data in the re-written Sect. 3.1.3.

Comment: P7 ll32 -p8 37 A comprehensive series of comments concerning the temperature variability and spatially variable ablation patterns resulting in a rather speculative adjustment in the seasonal correction section is given by referee #1. I agree on those.

Response: Please see –our response to your general comment GC3 that refers to the same issue.

Changes: Sect. 3.1.3 on seasonal correction was completely re-written to better explain the rationale and strategy of the seasonal correction. Supplement, Section S4, provides analysis on the applicability of the P. Moreno mass balance gradient for supporting the seasonal corrections on Jorge Montt, S. Rafael, S. Quintin and Benito glaciers (the only glaciers for which this type of correction is applied), confirming the validity of this approach. As mentioned before, there is no other glacier on SPI or NPI (except P. Moreno Glacier) for which multi-year seasonal and annual ablation measurements are available and a seasonal ratio for ablation (summer vs. full year) based on observation is available.

Comment: P8 ll28-32 Please explain the justification of 20% reduction in correlation to a temperature value. Based on what assumption does it translate into a percentage?

Response: For epoch 1, although the daily SECR is from the same year (ablation season 2011/2012) and was obtained from December to March, the days which have to be compensated are in late summer and therefore we reduced the estimate for ablation by 20 % compared to the summer average. As we mentioned in the manuscript, this scaling factor is based on a time series of daily air temperature measurements from 1995 to 2003 near the front of Perito Moreno Glacier and ablation measurements on the terminus (Stuefer et al., 2007). Furthermore, we want to point out that this correction factor, applied on the hypsometric curve in Fig S3, affects only a very small area of the icefield.

Changes: The justification was added in the re-written Sect. 3.1.3.

Comment: P9 ll8 Can you please add more information to increase reproducibility when data gets available: what threshold on SEC values? What morphological operators?

Response: We did not include these details because we do not think that this is an interesting point and would inflate an already very long paper. For each of the 4 SECR maps we produced a raster starting from the flag mask (FLM) layer that resulted from the processing with ITP which provides roughly the regions affected by layover and shadow. Thresholds $\Delta h/\Delta t < -10$ m/a and $> +6$ m/a were applied. A morphological operator of closing followed by a 5 x 5 median filter was applied on the mask raster in order to "clean" the mask, avoiding noise due to thresholding.

Changes: This is a minor methodological step; we avoid entering in such details in the manuscript given its length and scope. The procedure can be found in the response above.

Comment: P9 ll16-19 Where are the 17 kg m-3 uncertainty taken from? Citation of Cogley et al. (2009) is misleading here, because reader would expect a reference for the density uncertainty. I found it to be mentioned in Abdel Jaber (2016), but it seems to be taken from Gardner et al. (2012) – this is not referenced here. Anyway, why using this value when recent large area studies like Brun et al. (2017), Dussaillant et al. (2018), Malz et al. (2018) use 60 kg m-3? Choosing that latter value would lead to comparable error budget.

Response: Yes, the uncertainty ±17 kg m^{-3} comes from (Gardner et al, 2012). Regarding this issue, we want to mention again the statement in response to Referee 1, that he main scope of this study is to provide volume change rate estimates at basin scale (Tables 2, 3, S8). These can then be converted to mass change rates using a constant density assumption (which provides full traceability). Furthermore we provide a reference mass change rate at an icefield level; these are the only four numbers in the paper reporting mass change estimates (Table 1). We decided to use the common scenario of glacier-wide density of 900 kg m^{-3} facilitating the comparison of results with other studies. We agree that the assigned error of 17 kg m^{-3} is a small one (1.8%) for firn areas. However, large mass losses on the Patagonian icefields refer to ice areas. Therefore it makes sense employing separate density estimates for the volumes in ice areas and firn areas. We use ±17 kg m^{-3} in the ice areas and ±54 kg m^{-3} in the firn areas, assuming a mean elevation of 1050 m on NPI and 1150 m on NPI for separating ice and firn areas. The resulting uncertainty in density for icefield-wide mass changes is ±36 kg m^{-3} (4 %).

Changes: This point is taken into account by employing an error on the density of 36 kg m^{-3} (4 %) for icefield-wide mass changes. This value (together with explanation) is not cited anymore in Sect. 3.1.4 but appears only in Sect 3.3.4 to avoid repetition.

Comment: P9 ll 31 Please provide reference

Response: The following reference will be added:

DLR-CAF. 2013 (October).TerraSAR-X Ground Segment Basic Product Specification Document. 1.9 edn. German Aerospace Center (DLR) - Cluster Applied Remote Sensing (CAF). TX-GS-DD-3302.

Changes: as above.

Comment: p10 ll21-24 and P11 ll8 Why manual outlines? What is the decision to delimit these areas based on? If that information can be found in Abdel Jaber (2016) it should be indicated (or the original study it referes to).

Response: The outlining was performed manually based on the backscatter coefficient (σ^0) and taking also into account the corresponding elevation to ensure that areas of high backscattering are on the smooth firn plateau and not in the ice areas. A fixed thresholding of the σ^0 layers would have added noise because this would include regions of rough glacier ice. The penetration height offsets assigned to each region are based on the relation between difference in σ° for dry and wet snow and Δh (Figure 8.12 of Abdel Jaber (2016), Sect. 8.4).

Comment: P11 ll3-7 Is any of the values mentioned in these paragraphs used for determining the outlines? What is the interpretation of the sigma0 ranges based on? Abdel Jaber (2016) / other? Please reference it.

Response: The σ°-values and related interpretation are based on multi-year experimental and theoretical work on X-band and C-band radar signal interaction with snow and ice by two of the co-authors, including several field campaigns on Alpine glaciers related to ERS-1/ERS-2, ASAR of Envisat, Shuttle Radar SIR-C/ X-SAR SRL-1 and -2, and TerraSAR-X. See e.g. Nagler and Rott (2000); Floricioiu and Rott (2001). Relations between snow wetness, snow morphology, penetration depth and backscatter intensity can also be looked up in radar textbooks (e.g. Ulaby and Long, 2014). Concerning the SRTM data (Sect.3.2.2), to which this comment refers, such an analysis was already performed in (Abdel Jaber, 2016) and the processing was not repeated for his study. Only the analysis of TDM backscatter (Sect. 3.2.1) is new because the data used in this study have not been used in Abdel Jaber (2016).

Floricioiu D. and Rott, H.: Seasonal and short-term variability of multifrequency, polarimetric radar backscatter of alpine terrain from SIR-C/X-SAR and AIRSAR data. IEEE Trans. Geosc. Rem. Sens., Vol.39(12), 2634 –2648, 2001.

Nagler T. and Rott, H.: Retrieval of wet snow by means of multitemporal SAR data. IEEE Trans. Geosc. Rem. Sens., Vol 38(2), 754-76, 2000.

Ulaby, F.T and Long, D.G.: Microwave Radar and Radiometric Remote Sensing, The Univ. of Michigan Press, Ann Arbor, 2014.

Changes: This issue has been clarified in Sect. 3.2 and references have been added.

Comment: P11ll 17 First sentence would be well supported by a formula. Is the HEM for the TDM elevations calculated by the phase difference to the interferometric phase of 12 m TDM products? Is it always TDM 12m as a reference (also in 3.3.3 (1))? It is mentioned once briefly in 2.1, but I think I should be emphasised there, that it is especially used as reference for elevation error assessment.

Response: The HEM does not depend on the reference DEM (the global TDM DEM) but it is processed by ITP for each TDM RAW DEM. The HEM is only the interferometric error and reflects point per point the actual error. This is the alternative of computing it over ice free terrain, as other authors did. This error is used to compute the random error of each sample. When averaging on an elevation bin this error becomes negligible compared to the systematic components.

In 2.1 (p 4 lines 13-14) we state only that the global TDM DEM is used as reference for the processing, the details of how this is used are given in 3.1.1. It is also used for the DEM coregistration (see sect. 3.1.2 p 6 lines 24-25). We never mention that we used the global TDM DEM in error calculation.

Changes: We improved the explanation and added the requested formula even if it is a basic uncertainty propagation rule, but we will avoid repeating the quadrature sum formula in the rest of the Section.

Comment: P11 ll25: How was it included? Add some mathematical explanation of the error propagation through seasonal correction. Is it sqrt($\sigma t1^2 + \sigma t2^2 + \sigma seas^2$) for each pixel?

Response: The random error (addressed in this comment), using pixelwise correction, is applied for the portions of SPI which are covered by the summer 2011/2012 SECR. It is included in the formula for the total random error as shown in the comment above. We do not see the need for adding also this formula as it refers to basic uncertainty propagation, already described by the (standard) formula provided in response to the comment P11 L17.

Changes:. We changed the text to better clarify this operation.

Comment: P12 ll14 Enhance precise and illustrative explanation to this whole section 3.3.3. The reader is interested how exactly the systematic error is calculated, for it is key to the low elevation error budget presented. Please provide formulas to enhance comprehensibility. That could spare some explanatory text passages, that are less illustrative.

Response: As already explained in the response to general comment GC4, the elevation error budget is not particularly low, being in line with several other studies. We agree with the request to improve the comprehensibility of Section 3.3.3 and revised this section, trying to address a broad community interested in mapping of glacier volume change.

Changes: Sect. 3.3.3 was revised in order to improve its clarity.

Comment: p 12 ll14 Is the IQR of the areas that were adjusted (CR, calibration) addressed as the measure of error (validation) on each DEM? I do not agree with this method from a scientific perspective. On top, choosing the IQR reduces or eliminate slope dependent effects (avr. Slope below 4°, IQR slope?). But on glacier these are present for sure, so they are a source of systematic error to be addressed in the budget. It would be more reliable if validation is performed on the entire DEM (glaciers excluded), but assessed with regard to absolute elevation and slope.

Response: Assuming the comment concerns p 12 ll17-20.

The IQR is chosen to characterize the spread of the elevation difference between the TDM Raw DEM and the global TDM DEM within each scene over calibration regions covered by that scene. Large difference means larger uncertainty of the DEM calibration. The IQR was chosen instead of standard deviation because the distribution is not Gaussian. A tilt of a specific Raw DEM was excluded through the comparison to the reference global TDM DEM. If still present it would lead to an increase of the spread, since the calibration regions (visible in Figure S1) are relatively well distributed geographically.

Slope dependent elevation offsets are caused by horizontal shifts between the two DEMs, which according to our checks are negligible compared to vertical ones. The glaciers are rather flat, except on the small regions of the mountain ranges sticking out of the plateau. Therefore, the combination of small shifts and small slopes would make these effects negligible. We focus on vertical offsets. Evaluating on the entire off-glacier surface would have been another possibility. But this would have been biased by the higher slopes of the off glacier mountains of Patagonia and would lead to a larger error than what we found on the glaciers which have low and moderate slopes. Since this error is linked to the calibration procedure we compute it on the calibration regions themselves.

Comment: P12 ll21 Why 1 – 6 m? Reference, calculation or explanation for decision should be provided. Where does that assumption 1000 m.a.s.l come from? Please provide reference.

Response: The penetration height offsets of 1 to 6 m were assigned based on explanations given in Sections 3.2.1 and 3.2.2 and in (Abdel Jaber, 2016) based on the observed backscatter coefficient. See response above. We assign the mentioned systematic error only to altitudes above 1000 m (as a conservative threshold) to compensate for undetected regions on the plateau.

Below 1000 m a.s.l. are ice areas where the C-and X-band radar signal does not penetrate. For the SRTM data set (C-band) penetration is no issue because the snow and ice surfaces were wet during the SRTM mission. Regarding the TanDEM-X data, only a quite small percentage of the total data set exhibited partly frozen or dry snow. The penetration height offsets for completely dry snow and firn are based on the relation between $\sigma°$ for dry and wet snow and Δh in Figure 8.12 of (Abdel Jaber, 2016) showing for dry snow a mean offset of 4 m and a maximum offset of 6 m. This is in agreement with the number on X-band one-way signal penetration for dry snow reported by Mätzler (1987) if converted into two-way penetration and also with the TanDEM-X penetration bias in the percolation zone of the Greenland ice sheet (Rizzoli et al., 2017). The penetration depth of refrozen snow crust is smaller (see response to Referee 1, P12, L26). The good agreement between our volume change rates 2000 to 2012 over NPI and the results of Dussaillant et al. (2018) based on optical data confirms the validity of our approach regarding signal penetration.

Mätzler, C.; Applications of the interaction of microwaves with the natural snow cover, Remote Sensing Review, 2, 259-387, 1987

Rizzoli, P., Martone, M., Rott, H., and Moreira, A..: Characterization of snow facies on the Greenland Ice Sheet observed by TanDEM-X interferometric SAR data. Remote Sens., 9(4), 315; doi:10.3390/rs9040315, 2017.

Changes: Relevant explanation was added to Sect. 3.2 and 3.3.

Comment: P13 ll1 According to this paragraph: for interpolated seasonal correction, the last epsilon term should dominate the quadrature sum and thus the total SECR error ,if I understand correctly. What does ‘increase by a factor of three’ mean in this context? Times 3 (*3) ? I compared SECR uncertainty value for extrapolated glaciers (e.g. Jorge Montt, Bernardo, Tempano) in Tab. 3 with values for not extrapolated glaciers. First ones are not near triple of latter. And they should even be higher than triple, following this paragraph: scaling by year (divided by 0.27. for 99 days for example) is performed as well as a *1.5 increase for the timespan difference. Please explain where I've gone wrong and/or revise the explanations in this paragraph.

Response: Thanks for pointing this out. It seems there is some misunderstanding regarding the seasonal correction and its impact for the retrieval of SECR. The term seasonal correction refers to the difference between mean annual SECR over epochs spanning 12 years (2000 to 2012) and 4 years (2012 to 2016) without accounting for seasonal differences in SEC of the missing days vs. the mean annual SECR taking seasonal differences into account. For the extrapolated glaciers 53 to 103 summer days are missing in order to cover the full 4 year period (1461 days). This means that the missing days to be substituted correspond to 3.6 % to 7.0 % of the 4 year period for which the mean SECR is computed (and not 27 % which would refer to a single year). The impact of missing days to be substituted for the 12 year period is still much smaller. This is now made clear in the revised section 3.1.3 and in Supplement S4.

Changes: Sect. 3.1.3 was revised providing a better explanation of the seasonal correction. We updated the results (tables and plots) to correctly take into account the spatial variability of the systematic error.

Comment: P13 ll9 A formula containing the total SECR error would be helpful for traceability. Is it δSECR = sqrt(εb^2 + SE^2). Just to make sure I got the method correctly and the comment above (ll1) is justified.

Response: We do not see the need for adding this formula as it refers to basic error propagation, already described by the formula added in response to comment P11 L17.

Comment: P13 ll15 I would assume a factor of 3 to be very low for the icefields concerning a factor 5 was applied e.g. by Brun et al. 2017 in High Mountain Asia, whereas the variability of SECR patterns in the icefields (especially SPI) is rather high.

Response: This comment seems to be based on some misunderstanding, as already explained in the response to P13, L1. The revised Section 3.1.3 and Supplement S4 provide full traceability on this issue. The analysis on the validity of the mass balance gradients (in S4) used for estimating the seasonal difference in the ablation component of the four unsurveyed glaciers in S4, for example, indicates that the increase of error by a factor of 3 for unsurveyed regions is an overestimate. Nevertheless, we keep this (rather conservative) factor as it anyway does not have a large impact on the VCR rates because the extrapolation refers to a limited subset of the total data sets in respect to area and time span.

Comment: P13 ll19 A formula for the complete error propagation throughout mass balance computation would be appropriate.

Changes: We improved the text in Section 3.3, added and highlighted formulae so that it should provide adequate understandability and traceability of the error estimation procedure.

Comment: P15 ll19 The processes described should be perfectly correct. However, I doubt the values found through the seasonal correction analysis are able to significantly support this interpretation. As mentioned, I assume this daily SECR as a study design feature hard to accept. Also, a precise description of the method that smoothed the SECR field in Fig 8 would be of interest– or even better a display of the original data (SECR field). If it is clearly shown, that the process introduces more precision to the data, than it introduces measurement/ interpolation uncertainty (also regarding comments to 3.3.3) I am willing to accept it. So far, I find it difficult to support it.

Response: This comment refers to the seasonal correction which is not the topic addressed on page 15, line 19 to 26 (In Section 4, "Results"). Here we discuss processes of relevance for the observed SECR pattern during the summer period, pointing out the main factors responsible for surface lowering. The reference to a daily ablation rate provides a hint on the magnitude to be expected for the contribution of surface melt during summer, based on measurements. There is no claim for measuring ablation by DEM differencing because these data provide the sum of SEC due to ablation and emergence/submergence (as explained in the paper). In our view the information provided in this section is clear and without any fault. On suggestion of Referee 1 we added a reference on firn densification. During summer firn densification is a general feature in firn areas of temperate glaciers.

Changes: Reference on firn densification on SPI in summer added (Rivera; 2004)

Comment: P15 ll28 For the subaqueous loss Abdel Jaber (2016) is referenced. But for the basal cross-sections an original source should be cited.

Response: The references for the bathymetric data on the four mentioned glaciers (Upsala, Jorge Montt, Tyndall and Ameghino) will be added. The calving cross sections of these glaciers are deduced from bathymetric data in front of the glaciers and the freeboard. References to the bathymetric data:

Ameghino Glacier:

Stuefer, M: Investigations on mass balance and dynamics of Moreno Glacier based on fieldmeasurements and satellite imagery, PhD Thesis, Univ. Innsbruck, Austria, 1999.

The thesis reports also on two field campaigns on Ameghino Glacier, including pre-frontal bathymetricmeasurements.

Jorge Montt Glacier:

Rivera, A., Koppes, M., Bravo, C. and Aravena, J.C.: Little Ice Age advance and retreat of Glaciar Jorge Montt, Chilean Patagonia. Clim. Past, 8, 403–414, 2012.

Tyndall Glacier:

Raymond, C., Neumann, T., Rignot, E., Echelmeyer, K., Rivera A., and Casassa, G.: Retreat of Tyndall Glacier, Patagonia, over the last half century, J. Glaciol., 51(173), 239-247, 2005.

Upsala Glacier:

Naruse, Renji and Skvarca, Pedro, "Dynamic features of thinning and retreating Glaciar Upsala, a lacustrine calving glacier in southern Patagonia", Arctic, Antarctic, and Alpine Research (2000), 485--491.

Skvarca, P and De Angelis, H and Naruse, R and Warren, CR and Aniya, M, "Calving rates in fresh water: new data from southern Patagonia", Annals of Glaciology (2002), 379--384.

Changes: The original sources of bathymetric data have been cited in the Supplement.

Comment: P18 ll 9 It is unclear here if that paragraph refers to previous work (Abdel Jaber 2016) or a different publication. Any citation would help. Also I would suggest a reference to the Figures displaying those datasets (provided in the supplement if it is own work)

Response: A similar remark was made by Referee #1. The analysis refers to ice flow velocity results which we performed complementary to this study. It is based on TerraSAR-X as explained now in the revised text. Within the ESA project SAMBA (mentioned in the Acknowledgements of the paper) we generated digital maps of ice velocities of SPI and SPI derived from TerraSAR-X and Sentinel-1 data, including time series. In Section 5.1 we report some numbers out of these results, for supporting the discussion on differences between epoch 1 and 2. We added one figure with velocities for four main glaciers in different years. Including a comprehensive report on all these results is not the objective of this paper and would overrun the maximum length of TC papers.

Changes: Information has been added in Section 5 to clearly indicate the origin of all cited ice flow velocity results. Furthermore, a new figure displaying novel unpublished plots of TerraSAR-X ice flow velocities along the central flowlines of four main SPI glaciers was included.

Technical Corrections:

Comment: p4 l1 'Method and error estimation'

Response: Not clear what is wrong here.

Comment: P7 l1 Check formula. This way it says δhoff is equal δhoff times the factor.

Response: Assuming p7 ll 11: "." is not a multiplication but a punctuation mark. We will avoid starting the sentence with δhoff.

Changes: Formula was isolated and sentence not starting with a Greek letter.

Comment: Also the distinction, when formulas are a) formatted as objects to be numbered b) written as part of continuous text c) omitted, but have a text description instead is not clearly structured. This should be reconsidered thoroughly.

Changes: Improvements were implemented as suggested. Formulae which are relevant to the method and error estimation are now displayed as object and numbered. Generic or less important formulae are left inline. Text description of operation is used to avoid repeating with variations a numbered formula which is already provided (ex. Quadrature sum for error propagation).

Comment: P14 l 'Figs' Fig. /Figure consistency Check throughout the text, also Table /Tab.

Response: We checked the Fig/Figs vs Figure. “Tab.” does not occur.

Changes: We checked this issue according to the rules of the Journal, one instance of Figure was corrected.

Heterogeneous spatial and temporal pattern of surface elevation change and mass balance of the Patagonian icefields between 2000 and 2016

Wael Abdel Jaber[1], Helmut Rott[2,3], Dana Floricioiu[1], Jan Wuite[2], and Nuno Miranda[4]

[1]Remote Sensing Technology Institute (IMF), German Aerospace Center (DLR), Oberpfaffenhofen, Germany
[2]ENVEO IT GmbH, Innsbruck, Austria
[3]Institute of Atmospheric and Cryospheric Sciences, University of Innsbruck, Innsbruck, Austria
[4]European Space Agency (ESA) - ESRIN, Frascati, Italy

Correspondence to: Wael Abdel Jaber (wael.abdeljaber@dlr.de)

Abstract. The Northern and Southern Patagonian icefields (NPI and SPI) have been subject to accelerated retreat during the last decades with considerable variability in magnitude and timing among individual glaciers. We derive spatially detailed maps of surface elevation change (SEC) of NPI and SPI from bistatic SAR interferometry data of SRTM and TanDEM-X for two epochs, 2000–2012 and 2012–2016 and provide data on changes in surface elevation and ice volume for the individual glaciers and ~~for~~ the icefields at large. We apply advanced TanDEM-X processing techniques allowing to cover 90 % and 95 % of the area of NPI and 97 % and 98 % ~~of the area~~ of SPI for the two epochs, respectively. Particular attention is paid to precisely coregistering the DEMs, ~~assessing and~~ accounting for possible effects of radar signal penetration through backscatter analysis, and correcting for seasonality biases in case of deviations in repeat DEM coverage from full annual time spans. The results show a different temporal trend between the two icefields and reveal a heterogeneous spatial pattern of SEC and mass balance caused by different sensitivities in respect to direct climatic forcing and ice flow dynamics of individual glaciers. The estimated volume change rates for NPI are -4.26 ± 0.20 km^3 a^{-1} for epoch 1 and ~~-5.60 ± 0.71~~-5.60 ± 0.74 km^3 a^{-1} for epoch 2, while for SPI these are ~~-14.87 ± 0.51~~-14.87 ± 0.52 km^3 a^{-1} for epoch 1 and ~~-11.86 ± 1.90~~-11.86 ± 1.99 km^3 a^{-1} for epoch 2. This ~~am~~correspo~~u~~nds for both icefields to ~~0.047 ± 0.005 mm a^{-1}~~an eustatic sea level rise of 0.048 ± 0.002 mm a^{-1} for ~~b~~epo~~t~~ch ~~icefiel~~1 and~~s~~ ~~during~~0.043 ± 0.005 mm a^{-1} ~~the~~for epoch 2~~000–2016~~. On SPI the spatial pattern of surface elevation change is more complex than on NPI and the temporal trend is less uniform. On terminus sections of the main calving glaciers of SPI temporal variations of flow velocities are a main factor for differences in SEC between the two epochs. Striking differences are observed even on adjoining glaciers, such as Upsala Glacier with decreasing mass losses associated with slowdown of flow velocity ~~between the two epochs~~, contrasting with acceleration and increase of mass losses on Viedma Glacier.

1 Introduction

The Northern and Southern Patagonian icefields (NPI and SPI) are the largest contiguous temperate ice bodies in mid-latitudes of the southern hemisphere. They stretch from 46.5° S to 47.5° S~~, respectively~~and 48.3° S to 51.6° S, respectively, along the main ridge of the southern Andes and cover areas of about 4000 km^2 and 13000 km^2 (Davies and Glasser, 2012). The perturbation of the strong and consistent westerly flow caused by the Andes leads to one of the strongest precipitation gradients on earth (Garreaud et al., 2013). Because the icefields are located on the only significant land mass between 45° S and Antarctica, they offer unique possibilities for studying the impact of changes in southern-hemisphere westerly flow on glacier evolution and for inferring Holocene climate history from glacial evidence (Rasmussen et al., 2007; Lopez et al., 2010; Glasser et al., 2011; Davies and Glasser, 2012; Garreaud et al., 2013).

Precise, spatially detailed data on changes of glacier area and volume and on the mass balance are essential for establishing reliable relations between climate signals and glacier records in order to reconstruct the past climate and to develop accurate predictive tools of glacier response to climate change (Fernández and Mark, 2016; Marzeion et al., 2017). The dynamic adjustment of a glacier to changing external forcing does not happen instantaneously. In particular for calving glaciers the dynamic behaviour and mass balance may be largely decoupled from direct climate forcing ~~(Benn et al., 2007)~~(Benn et al., 2007; Åström et al., 2014). The main outlet glaciers of the Patagonian icefields are tidewater or freshwater calving glaciers, showing heterogeneous patterns of changes in frontal position and hypsometry (Warren and Aniya, 1999). This stresses the need for spatially detailed geodetic repeat observations covering different epochs in order to resolve the complex pattern of glacial responses. High resolution topographic satellite data from SAR interferometry, as employed for the work reported in this paper, provide an excellent basis for handling these issues.

There has been a general retreat of SPI and NPI glaciers since the Little Ice Age (Davies and Glasser, 2012), however with considerable variability in magnitude and timing~~ of retreat~~ for individual glaciers. Only few glaciers advanced intermittently during recent decades. The most striking case is the Pio XI Glacier showing a large cumulative frontal advance since 1945, including recently a general advancing period of its southern and northern branches starting in 2000 and 2005, respectively (Wilson et al., 2016).

Geodetic mass balance estimates of NPI and SPI have been derived from various sources. The first remote sensing based estimates of NPI and SPI volume change and mass balance were reported by Rignot et al. (2003), comparing Shuttle Radar Topography Mission (SRTM) elevation data of February 2000 with topographic maps of 1968/1975 to estima~~s~~te ~~w~~the vol~~l~~ume ~~as~~ chan~~d~~ge of~~ 1995 on a~~ ~~limi~~the~~d~~ large~~a~~st ~~of~~63 ~~SPI~~glaciers. Elevation changes measured at low elevations were fitted to a polynomial as a function of elevation in order to extrapolate the results to higher elevations where the topographic maps ~~w~~have large ga~~ff~~ps. A similar analysis was pe~~et~~rformed ~~by~~for 20 glacier~~g~~s of SPI, where 1995 cartography is~~.~~ available, and scaled to infer the volume loss of the entire icefield.

The SRTM DEM was used in several studies as baseline for deriving volume change of the icefields during periods spanning the subsequent 10 to 15 years. Willis et al. (2012a, b) analyzed the ice volume change of NPI between 2000 and 2011 and of SPI between 2000 and 2012 by comparing the SRTM DEM with time series composed of 55 DEMs f~~o~~r~~f~~ NPI and 156 DEMs f~~o~~r~~f~~ SPI which were derived from data of the Advanced Spaceborne Thermal Emission and Reflection Radiometer (ASTER) operating on the Terra satellite. The authors used all suitable ASTER scenes and applied a weighted linear-regression to the time-series of elevations on a pixel-by-pixel basis in order to obtain the elevation change for the full time spans. Willis et al. (2012b) assumed a 2 m radar signal penetration bias for SRTM without taking into account the melting state of the surface. ~~Acco~~Introducing~~ly~~ the~~y~~ same penetration bia~~l~~s~~o~~, Willis et al. (2012b) revised also their previous volume loss estimate of NPI.

This underlines the importance of correct treatment of radar signal penetration in case of interferometric DEMs. Dussaillant et al. (2018) determined the NPI volume change for 2000 to 2012 with two methods, on one hand by differencing the SRTM DEM and a SPOT-5 DEM from March 2012, on the other hand by fitting pixel-based linear elevation trends over 118 DEMs calculated from ASTER stereo images acquired between 2000 and 2012. Icefield-wide rates of volume change by both methods agree very well.

Foresta et al. (2018) exploited swath processed CryoSat-2 interferometric data to produce maps of surface elevation change over the Patagonian icefields and estimated the mass balance for six years between April 2011 and March 2017. The maps cover 46 % of the total area of NPI, and 50 % of SPI with large gaps on ~~s~~the~~v~~ ter~~al ~~m~~a~~ini of most glaci~~er t~~er~~mini~~s. Relations between CryoSat-2 elevation change and surface elevation in the SRTM DEM were used to fill the gaps in the surface elevation change (SEC) maps.

The TanDEM-X (TerraSAR-X add-on for Digital Elevation Measurements) mission (shortly TDM) (Krieger et al., 2007), composed of the two formation-flying radar satellites TerraSAR-X and TanDEM-X, is operational since December 2010. The mission opened up excellent new capabilities for high resolution topographic mapping of the global land surfaces including glaciers and ice sheets. Abdel Jaber (2016) generated DEMs based on comprehensive TanDEM-X data sets, over NPI mostly acquired in austral summer 2014 and over SPI between March 2011 and March 2012. DEM differencing versus the SRTM DEM yielded volume loss rates over NPI for the period 2000 to 2014 and over SPI for the period 2000 to 2011/2012. Abdel Jaber (2016) also presented~~ also~~ detailed information on the methods used for DEM generation and calibration, on error assessment and on the analysis of radar backscatter signatures of SRTM and TDM drawing conclusions on radar signal penetration. For Jorge Montt Glacier, featuring the highest thinning rate on the icefield, the geodetic mass balance for 2011 to 2014 was also derived from TDM DEMs. Malz et al. (2018) performed DEM differencing of TDM DEMs of December 2015 versus the SRTM DEM over SPI. For the southern part of the SPI they further differentiated the SRTM elevation versus TDM DEMs from January–March 2012, autumn 2014 and winter 2016 and computed the TDM-based~~ surface elevation change (~~SEC~~)~~ for the epoch January–March 2012 to December 2015. Seasonal variations of surface elevation and of radar signal penetration were not taken into account for retrieving SEC rates.

The studies cited above use different data sets and methodological approaches and cover, at least to some extent, different epochs. This impairs the comparison of results, the evaluation of temporal trends and the analysis of commonalities and differences between the two icefields. In order to tackle these issues, we derive volume change of NPI and SPI exclusively from bistatic SAR interferometry (InSAR) data (SRTM and TDM) for two multi-annual periods, spanning from 2000 to 2012 and from 2012 to 2016. Furthermore, for the main retreating glaciers of SPI an estimate of subaqueous ice loss is provided for the period 2000–2011/2012. The generation of surface topography products and the analysis of elevation change build upon methods developed by Abdel Jaber (2016) with various upgrades regarding TDM data selection and processing methods. The results presented here are completely novel, unless clearly stated. Particular attention is paid to the acquisition dates of the different DEMs, applying corrections for deviations of repeat DEM coverage from full annual time spans in order to avoid seasonality biases when deriving annual SEC rates. Significant effort is dedicated to the assessment of the wetness of the snow and firn surface through a careful analysis of the backscatter of SRTM and TDM data, and to modelling and quantifying different sources of uncertainty.

The paper presents the first spatially detailed analysis of surface elevation change and the derived total net mass balance over the Patagonian icefields for two different epochs based on the same observation technique, including a catalogue of volume change for the epoch 2000 to 2012 and 2012 to 2016 for all glaciers > 2 km^2 of NPI and > 9 km^2 of SPI. The results indicate a different temporal trend between the two icefields and reveal the complex spatial pattern of SEC and mass balance as result of intricate interdependencies between direct climatic forcing and effects of ice flow dynamics.

2 Data

For the generation of surface elevation change rate (SECR) maps we rely exclusively on pairs of multitemporal bistatic InSAR DEMs. This technique provides wide-coverage surface elevation, overcoming issues affecting optical DEMs, such as lack of contrast on smooth snow or the presence of clouds, as well as the limited spatial coverage and resolution of altimeters. In this study we exploit data from TanDEM-X and SRTM, the sole earth observation systems equipped with single-pass radar interferometers.

2.1 TanDEM-X

The primary objective of the TanDEM-X mission is the generation of a global, consistent DEM with high resolution and accuracy (Krieger et al., 2007). The main payload of the twin satellites is a SAR instrument operating at X-band (9.65 GHz), capable of a swath width of 30 km in the operational Stripmap single-pol (HH) mode. The global DEM product (DLR-EOC, 2018), whose performances are analyzed in Rizzoli et al. (2017) and Wessel et al. (2018), is the result of the combination of four years of bistatic data acquisitions with different baselines and geometries. This product is hence not suitable for the derivation of surface elevation changes, nevertheless we exploited the 0.4 arcsec (~ 12 m) release as a reference DEM of the region for various processing aspects (Sect. 3), after proper editing of unreliable samples.

In this study we processed single, selected TDM bistatic raw datatakes into so-called Raw DEMs (Rossi et al., 2012; DLR-CAF, 2010) using ITP, the operational TanDEM-X processor (Breit et al., 2012; Fritz et al., 2011), in order to generate two elevation maps completely covering the icefields in the years 2012 and 2015. The TDM data selection for each coverage was based on various criteria like the reduction of temporal span and of the number of datatakes, warm seasons to minimize SAR signal penetration, small height of ambiguity (HoA) to reduce interferometric noise and similar imaging geometry. Ideally data acquisitions should be at the end of the ablation season when the surface is at its lowest, but most importantly the two coverages should be acquired at the same time of year in order to minimize seasonal changes, which can be significant on the Patagonian icefields. Since data availability restricted fulfilling the last criterium, the residual temporal gap had to be compensated.

The TDM acquisitions used to generate the two elevation maps are summarized in Tables S1 and S2 in the Supplement for NPI and SPI, respectively. The footprints of the individual Raw DEMs are shown in Fig. S1. The first elevation map is composed of descending acquisitions from austral summer 2012. An exception are the western termini of NPI where, due to data unavailability we had to rely on an acquisition from May 2011. The second coverage is achieved with descending acquisitions from December 2015 (beginning of austral summer). On part of SPI we additionally processed three acquisitions from December 2011 acquired with the same geometry of the 2012 datatakes in order to measure seasonal elevation changes during summer. Three TDM datatakes from December 2015 (scenes 6 and 7 on NPI and 13 on SPI) feature a steep look angle ($< 27°$) leading to increased layover.

For each Raw DEM the ITP provides additional geocoded rasters (Rossi et al., 2010; DLR-CAF, 2010) which were used in different phases of this study: height error map (HEM), uncalibrated SAR amplitude, backscattering coefficient, interferometric coherence and flag mask indicating critical areas.

2.2 SRTM

The SRTM (Farr et al., 2007; Rabus et al., 2003) was launched 11 February 2000 and produced in 9 days of acquisition a near-global DEM (60° N–56° S) with 1 arcsec (~ 30 m) posting. The main payload was a bistatic C-band (5.36 GHz) SAR capable of a 225 km swath achieved applying the ScanSAR technique to four sub-swaths featuring different polarization (HH, VV, VV, HH) and look angles between 30° to 56°. The large number of interwoven acquisitions at higher latitudes contributed to both absolute and relative accuracy as well as to reducing voids: the 9 ascending and 9 descending datatakes covering the Patagonian icefields (Seal and Rogez, 2000) are listed in Table S3. The performance of SRTM was assessed among others by Rodriguez et al. (2005); Brown et al. (2005); Carabajal and Harding (2006); Wendleder et al. (2016). The main issue is the presence of long-wavelength height errors with magnitude up to ~ 20 m globally and spatial variation scales of hundreds to thousands of kilometres, mainly caused by residual roll errors due to the attitude adjustment manoeuvres of the Shuttle and by the applied absolute calibration of the sub-swaths.

The NASADEM (Crippen et al., 2016) is a new version of SRTM DEM, consisting of a complete reprocessing of the raw data, with improved phase unwrapping (significantly reducing voids) and an ICESat-based calibration, tackling issues such as limited absolute vertical accuracy and long-wavelength height errors. In this study we used a provisional version of NASADEM (NASA JPL, 2018) as the elevation map of year 2000 for both icefields. The choice was done after comparing on a vast region surrounding the Patagonian icefields the NASADEM and the SRTM ver. 3 (SRTMGL1) (NASA JPL, 2013) to the TDM global DEM rescaled to 1 arcsec. The SRTMGL1 data set, besides suffering from a vertical offset of ~ 1 m against the reference (statistics are given in Table S4), displays a stronger presence of long-wavelength elevation and geo-location biases (Δh images are shown in Fig. S2) and a higher RMS when compared to the NASADEM. On the icefields the differences between the two SRTM data sets are larger on NPI and in the very south of SPI.

We furthermore retrieved the SRTM radar brightness images (SRTMIMGR) (NASA JPL, 2014) for the sub-swaths covering the icefields (Table S3) with the purpose of assessing the melting state of the glacier surface. We also used the SRTM Water Body Data (SWBD) (Farr et al., 2007) for statistical and visualization purposes.

2.3 Glacier outlines

We relied on the Randolph Glacier Inventory (RGI) version 6 (RGI Consortium, 2017; Pfeffer et al., 2014), which contains improved basin divides of NPI by Rivera et al. (2007). We manually updated the RGI outlines at the glacier termini (including internal rocks) using the SAR amplitude, the DEM and optical images in order to reflect the exact extent of the glaciers at the time of acquisition of each elevation map (2000, 2012, 2015).

3 Method and error estimation

3.1 Methods for SEC and mass balance

3.1.1 Raw DEM processing

The use of ITP to process the single Raw DEMs allows a great degree of flexibility with respect to processing parameters and algorithms. The beginning and end times of each scene were adapted (up to $\sim$ 30 s total length) in order to minimize the number of scenes and to include the widest possible ice-free terrain suitable for DEM coregistration (Sect. 3.1.2). The ruggedness of the topography of the study region with its steep mountains and intricate water bodies poses a significant difficulty for the ITP operational algorithms of phase unwrapping (Lachaise, 2015) and absolute height determination (Rossi et al., 2012). We hence relied on an alternative algorithm of ITP (Lachaise and Fritz, 2016) which tackles both issues by exploiting an external reference DEM (Sect. 2.1).

The absolute phase simulated from the reference DEM is subtracted from the interferometric phase of the data. The fringe frequency of the differential phase is significantly lower and its unwrapping is unproblematic as long as elevation differences versus the reference DEM are not too large (maximum half of the HoA). The absolute phase of the data is then reconstructed by summing to the unwrapped differential phase the phase simulated from the reference DEM, this way removing any influence of the latter on the relative elevation in output. The output Raw DEM is finally obtained by geocoding in ITP the absolute phase of the data, implicitly determining an absolute phase offset (APO) value, on which the absolute height and the across-track position of the Raw DEM depends. ITP allows to manually update the APO value and perform a new geocoding, for instance to fine-tune the coregistration with a reference DEM, as described in Sect. 3.1.2.

3.1.2 DEM coregistration

The master and slave DEMs may be affected by vertical biases with respect to each other, these can be constant (offset), linear (tilt) or even varying with low frequency. They can furthermore be affected by horizontal shifts causing an additional slope- and aspect-dependent elevation bias in the SEC which couples with the vertical bias resulting in a systematic error with high potential impact on the volume change rate estimated over large areas. To obtain two consistent TDM elevation maps, coregistered to each other and to the SRTM DEM we coregistered the single Raw DEMs and the SRTM DEMs of NPI and SPI to the reference DEM (Sect. 2.1).

An error in the APO of a TDM Raw DEM leads to a vertical height offset, an across-track horizontal shift and a tilt around the master flight trajectory (in order of impact, the latter being negligible in our Raw DEMs). These three effects are solved by fine-tuning the APO through an accurate estimation of the height offset versus the reference DEM and by repeating the geocoding with ITP. This method assures high precision by exploiting the geometrical parameters of the SAR acquisition and allows avoiding critical aspects of the generic coregistration problem, accurately tackled by Nuth and Kääb (2011), such as estimation of horizontal shifts, interpolation, etc.

To estimate the height offset we manually selected a large number of calibration regions (CRs) over stable terrain around the icefields relying on the SAR amplitude, the TDM slope and optical imagery. Tall vegetation was avoided because of physical changes and varying scattering phase centre at different incidence angles and radar frequencies. The CRs were chosen to be as flat as possible in order to isolate the actual vertical height offset. Layover and shadow regions were avoided as well as water pixels, affected by low coherence. The footprints of the CRs are visualized in Fig. S1 and their features are summarized in Table S5.

From the elevation difference Δh between the reference DEM and the single Raw DEMs (or the SRTM DEMs of NPI and SPI) we computed on each CR with index r the mean μ_r, the standard deviation σ_r and the standard error of the mean: $\cancel{\mathrm{SE}_r = \frac{\sigma_r}{\sqrt{N_r}},}$

$$\mathrm{SE}_r = \frac{\sigma_r}{\sqrt{N_r}}, \tag{1}$$

where N_r indicates the number of spatially uncorrelated samples on CR r and was estimated through a semivariogram analysis as described in Sect. 3.3.2~~ and in particular computed with Eq. (5)~~. A height offset estimate for each DEM was obtained through the weighted average $\cancel{\delta h_{\mathrm{off}} = \frac{\sum_r \frac{\mu_r}{\mathrm{SE}_r{}^2}}{\sum_r \frac{1}{\mathrm{SE}_r{}^2}}.}$

$$\delta h_{\mathrm{off}} = \frac{\sum_r \frac{\mu_r}{\mathrm{SE}_r{}^2}}{\sum_r \frac{1}{\mathrm{SE}_r{}^2}}. \tag{2}$$

Values of δh_{off} ranged in ma~~bsolu~~gnit~~e val~~ude between 0 m and 1.8 m for the TDM Raw DEMs and was used to fine-tune the APO. For the NASADEM it was equal to 0.3 m and 0.1 m in absolute value on NPI and SPI, respectively, and was subtracted after checking the ~~absence of significant~~ horizontal ~~sh~~coregi~~f~~strat~~s~~ion with respect to the TDM reference DEM at 0.4 arcsec in the proximity of the icefields.

Furthermore range and azimuth tilts caused by baseline errors (Hueso González et al., 2010) were verified and found to be negligible for all Raw DEMs. Height consistency between overlapping Raw DEMs was also checked in order to ensure a seamless elevation map.

The coregistration procedure partly compensates the crustal uplift rates due to the glacial isostatic adjustment affecting the region, characterized by rates up to 40 mm a^{-1} on the plateau of SPI and decreasing with distance as reported by Dietrich et al. (2010).

3.1.3 Seasonal correction <This section was completely re-written>

To derivSe ansonual variateions of SECR shourface eld bev tatioken chaingeto accoundt massfor balancede,riving seasonnual variationes of speciurfic mass balance shoueld be vataken ionto accouhantge if the time span of the repeat DEMs does not exactly match yearly intervals. TCommonly the meannu daily mean SECR of the giveneo timplete speriodan is commonly extrapolatused tfor the mfissling temporal gap.s However, infor summer inebtreased melcting andthe compaentribution of excesnow/firns edauyse. Thissignific approach introducevs a biats ions from the annual mean SECR. Iin ordcaser tof mseasonitor suchal devariations. The magnitude tof comthe bias dependsate on them poercental gape of miss-ing (our excess) datys and sets whe coamplitutded onf SPIthe seasonal higcycle. Th-re seasonalu correction, asumm elaborated SECRhere, refers mapto bythe differencinge bethrween mean additionnual SECRaw DEMs of December 2011 versus the correseponding chsame-beam Raw DEM of Januar4 y/Mearehs (2012 to 2016), alreadspectively p12 yearts of(2000 theo 2012), DEM mostakieng (Tseasonable S2). Thdiffe Drencembes in SECR for 2011missing days intao account versus SPImean annualm SECR withosut accompleuntelying for soutch odif 49ferences.4°

The S,temporal mismand tch versus centrxactl/y 4 yearst and 12 yearns pvarties fofr the two epochs and forth different section.s of Tthe timce span fis 99 eldays. fFor 2012 to 2016 the impactw of wseasteonal corrections bis moreams, importand 33t daysue ftor the eashortern timost be spamn. TFor NPI the numbere of missulting dailys SECR,corresponds to 3.6 % to 4.8 % aof ther cons4-yervar tivme maskipang, of aor thefae tswo maind filteracks acquing (mred ian Februandry 2012. A smooall secthiong), of NPI (coverisng sthe lowner termin Fig of S. 8Rafael, S.

I Quin thisn stuandy thBe 2012–2016 SECR nisto glaffectied byrs) was signifieanst temporald gap dcqurired ong summer28 May 2015/2016, whi(NPI schene Non. 1; Table shortS1, tFimeg. spS1an). Fof 4 years makthes main corrsections nof SPI thee pessary. Thce numbtager of missing days (5ranges from 3.6 % to 75.0 on NPI%, 53 excepto 103 fonr SPI)a vsmall sub-aries acco wherde ingt is 7 %. tFor SPI the e2000 to 2012 mbinsmatch ion percentage of TDM datatakhes (Tabfull period S1 randges S2from and Fig0.1 S1)% to 1.0 In% of the 12-yeard period. Nevertheless, we applied seasonal comprrections also to this data set. fFor the mistwo tracks covering summther dmays wein rselctiedons onf NPI the filtegap corresponds daito only SECR0.1% of summther 2011/2012. This wyears, usgivedn pixthe lwimited surface whcovered availably the onthird SPItrack, ino pacorrectieulon was arpplied to theis 33-daytaset.

Here bwe explam coinei details on the seasonal corregction whefore 53 the epoch 592012–2016 dbecayuse musof their blarger coimpensact. Depend.ing Forn the mavaisslabing parlity of Padditional XITDM GIDEM dataeier, the hyfollowing psromcetdurices mwean (aggreg atpplied for different 100 m elsevaction bins) of low-lossthe glaicefierlds:

– Three (Padditional XI,TDM Peracquisitions Morf Deno,cember Grey,2011 (Tyndabll, HPSe 13,S2) Eurcopa, Pvenguin,r Guilardi)the was-ousthed (green, curve in Fig. S3).tral Oand north-western rsesctions of SPI (except59.4 % Jorgef MonttSPI, GlacFierg. 8.). tThe hypsome data werice museand tof computhe 99-dailys summer SECR wasover susmmedr (2011/2012 bluey curveDEM differen Fcing vs. S3).TDM Ondata NPIof (exMarcepth 2012 (99 days) coverine 1)g the hypsometraien gpareet of SPI and evs. TDM data of 31 January 2012 (33 days) cove rin Fig. S3 was sub-sedction sine the south-erast. The eSECR malvingps ofl suxmmes are a2011/2012, smcalled etompon the length of totalhe maiss balaineg period, wherea used fon SPIr substroituting dynathe miessing downwayst ing lsummer 2015/2016, a valids tappro achig as ther nmegan tive SECR on glaeimper atongures.

In of the two seummenarios addgressed above we used ithein 2011/20.12 sum°C. Air temperatures SECRof tohe sEubsropean Centre for Medititm-Range Weather miForecasts Interingm dRe-Analysis of(ERA-Interim) (Dee et al., 2011; Berrisford et al., 2011) summhow at ther 20185/2016. At thPa level synfoptier stathe grid poin Balmacedat (457.925° S;, 713.6855° W) near (NPI) thea moeanthly summean air temperatures of summer5.9 °C in 2011/2012 comparend to6.0 summer°C in 2015/2016, wefore hpoigher in December and Januaryt (+250.25° °CS, +1.5 73.55°C), IW (sowuther in FSPI) thebr values arye (−1.53.6 °C) in 2011/2012 and similar3.5 °C in Ma2015/2016.

- Foreh. ASPI simiglaciers not coverend wasby mthea summered at2011/2012 PuntaSEC Arenmasp (53.00° S;except 70.85°Pio W),XI leanding usJorge Montot glacierssum) we ruseld datively sSECR imilarn mdependean ice abof elevation deraived from the 99-day SECR maps in bothf summers 2011/2012 (blue curve in Fig. S3).

On For the ablasection area of JPiorge MonttXI Glacier (that is not covered by the Dsummeer SEC map we use the hypsombetric 2011SECR curve of low-loss glaciers (green curves) itn Fisg. importaS3). Ont toNPI, except onsider the termini croveasred dby scenamice dNo. 1, wnwe alstingo comparused to the avhypsometraic gre of then icurve of Fieldg. ToS3 thsis endce wthe sepmajoraitely of glaecouiers are noted calving for the surfcaee lowerving fluxes are a smalatedl tcompo neinther surof totaeel mass balance or ice flow dynamies(Schaefer et al., 2013).

- For the lathree NPI termini wcove assumred aby scene Nonst. 1 antd vefortical velJoeity throughe Mount the yGlaciear, forwhich is nothe fcovermerd by the summeasonalr eycle2011/2012 SECR wmaps takend subject to significanto dynaemic douwnwast.ing Wwe addsed paratoe the dynamieSEC component in the seablastion areas related eto surface melt from SEC duee tio dynamic fdor wnwablastiong. TFor this eopurreetipon wase estimateds by usiong the elevation adependenualce of the lspecifinc surface marss balance (SMB) during summer adiend the ofull −1.37year m a⁻¹are pner 100eded. mTo ofur eknowlevationdge, up to now the eqonly muiltib-year tiume lserines (of ablased tion field measurements on Perito Moreanoy Gglacier (Stuefer et al., 2007))of sSPI and NPI, incaleuding withe thseparation of summer-to-and annual peratiods, ohas been performed ablation Moreno Glatcier (Stuefer et al., 2007).

W The applied ca simbilarity approaehf tohe seMorene 1 of NPImass balancover elevationg mgradienlyt thas been tchercked by mieanis of S. Rafamodel, S. Qoutpuintin aond SMB for NPI wenist coast glaciers (Fig.(Schaefer et al., 2013) S1).and Beingmass balancquire data onf 28Chico MGlaycier 2011(Rivera, 2004), accounting for the wexest/eedast by 189difference aind 200temperature dlaypse rathe 4 yeacross the imcefield span(Bravo et al., 2019). Furto ther ovderltapping sls avre seengives 4 and 5 (3 aind 14 Dthee Supplember 2015)nt, respSectively. S4. The eratio between daily SMB-relatribed SEC dutriong dsummer vs. tohe rest bof the dyneamr ien imbaladependence andof melt wevas obtaion is used byfor esetimalting the uincorreetased 2011–2015 SECR contribution thdue aeto surfal excess pmelt during summer od.n Tthe dJorgevia Montt termionus and fromr the mreduceand annuamelt acontriblaution during May teo was Deceemputbedr for withe thre balanee gNPI teradmient ofi. MFor theno Gldynaemier (Stuefer et al., 2007),c downwhastiehng aecoumponents forwe reduesed ablationhe duaveringage SECR of the f-summll period.

For months.

~~A~~e epoch 2000–2012 a seasonal correction w~~as al~~s~~o~~ applied on SPI to the TDM elevations of 2012 ~~wi~~t~~h~~o co~~resp~~rect for the gap to the SRTM acquisition mid-date (17 February). The effect of the correction ~~over the 12 year time span i~~s small, being of main relevance for TDM scenes 6/7, ~~(~~acquired on 15 March 2012~~)~~, covering ~ 6000 km^2 with a temporal gap of 38 days. The two 99-days beams of the 2011/2012 summer SECR ~~(which shares the 2012 acquisitions to be corrected),~~ were used pixelwise where available. The~~ir~~ hypsometric mean (blue curve in Fig. S3) was used elsewhere, with a reduction by 20 % to account for the late summer season (mid-February to mid-March). This scaling factor for late summer is based on a time series of daily air temperature measurements from 1995 to 2003 near the front of Perito Moreno Glacier~~. A~~and ~~simi~~abla~~r correc~~tion ~~w~~das ~~no~~t ~~necess~~ary ~~on NPI~~(Stuefer et al., 2007).

Finally the correction rasters were obtained by scaling pixelwise the daily correction rate by the temporal gaps in day~~s and are~~ ~~shown in~~ (Fig. S4).

3.1.4 Derivation of SECR maps and estimation of mass balance

Two DEM mosaics were obtained for each icefield from the main TDM coverages by means of stacking, where the most reliable scene (evaluated through the height error, the look angle and the backscattering) was prioritized fo~~n~~r overlapping regions. The WGS84 (EPSG:4326) projection with posting 0.4 arcsec was enforced through cubic convolution on a common geographic frame. Corresponding mosaics of the additional geocoded rasters computed by ITP were also obtained, as well as the SRTM DEM and its error layer. For each icefield two SECR rasters including seasonal correction were obtained differencing the DEM mosaics for the epochs 2000–2012 (12 years) and 2012–2016 (4 years), with the end of summer as reference start/end time of each epoch. To avoid biases of the mass balance we masked-out artefacts due to phase unwrapping, layover, shadow, etc. ~~by means of the flag mask, thresholds on the SEC, morphological operators and visual inspection.~~ The elevation of the water surface subject to frontal retreat, usually decorrelated, was manually edited in order to correctly capture the freeboard SEC.

By multiplying the average SECR with the corresponding glacier area over elevation intervals of 50 m the altitude-depend~~a~~ent volume change rate (VCR) was computed. The reference elevation used for the hypsometry is the 2012 TDM DEM (small voids are filled with the global DEM), which is common to the two investigation epochs. The mass balance was computed on the entire icefields as well as on single glaciers defined by the updated RGI glaciers outlines. The maximum extent of each glacier, either at the beginning or at the end of the observation period, was used to spatially capture all changes.

We used a glacier-wide density of ~~900 ± 17~~900 kg m^{-3} for the conversion of the VCR to mass change rate. This value is commonly used for geodetic mass balance measurements and provides traceability for comparisons with other studies (Cogley, 2009). The main mass losses on the Patagonian icefields refer to ice areas, and for the accumulation areas assumptions on changes of the vertical profiles of snow/ice density would be speculative.

3.2 Impact of radar penetration

A critical issue affecting InSAR-based elevation data is the penetration of the radar signal in dry snow and firn. In this case the scattering phase centre is situated below the surface, causing an elevation bias in the DEM (Dall, 2007), ranging from decimetres to metres at C- and X-band. This represents an important source of local systematic error on the SEC and consequently on the resulting total net mass balance. The penetration depth depends on the microstructure and the dielectric properties of the snowpack, which are in turn strongly dependent on the liquid water content (LWC). Several models (Tiuri et al., 1984; Mätzler, 1987) show how at C- and X-band the penetration depth drops rapidly below 0.2 m already with a LWC of approximately 0.5 $\%^{\mathrm{vol}}$. We used the backscattering coefficient σ^0 as a proxy to assess the wetness status of the snow and firn ~~(Stiles and Ulaby, 1980; Ulaby and Stiles, 1981; Mätzler, 1987)~~(Ulaby et al., 2014; Mätzler, 1987). The C- and X-band radar return from the bare rough ice of the glacier termini is dominated by surface scattering so that penetration is not an issue here.

3.2.1 Assessment of TanDEM-X backscatter

The TanDEM-X sensor features an absolute and relative radiometric accuracy of 0.6 dB and 0.3 dB, respectively (DLR-CAF, 2013), allowing precise measurements of backscatter. For each Raw DEM we processed with the ITP the geocoded backscatter image including the annotated noise contribution. This typically varies between −29 dB and −17 dB along the range direction and can thus have a significant impact on σ^0 of weak scatterers such as smooth wet snow. The σ^0 mosaics corresponding to the 2012, 2015 and 2011 DEMs are shown in Fig. S5. No masking of artefacts was applied.

TDM austral summer datatakes were chosen in order to increase the likelihood of imaging wet snow and firn. The mid-range look angle (θ_l) ranges between 35° and 45°, except for scenes 6 and 7 of NPI and scene 13 of SPI which have steeper look angles (Tables S1 and S2). The satellite overpasses were at approximately 6:00 local time (UTC−4h), which is generally the coldest time of the day, although the plateaus of NPI and SPI usually feature limited daily variations of air temperature due to the dense clouds and strong precipitation occurring most of the year (Garreaud et al., 2013; Schaefer et al., 2013).

On the plateau of NPI (covered by scenes 2, 5, 6 in Table S1) $\sigma^0 < -18$ dB dominates in our dataset up to approximately 2300 m of altitude in 2012 and 2015 confirming high LWC on most of the surface. Above this altitude $\sigma^0 > -10$ dB can be found on limited areas (particularly in December 2015), implying the presence of dry snow. Some regions with $-15 < \sigma^0 < -11$ dB are found ~~o~~in scene 2 ($\theta_l = 38.4°$) at altitudes below 2000 m. Given the season and time of day, these can possibly be explained by the formation a refrozen crust layer on top of wet snow or firn, implying an offset of the scattering phase centre ~~within~~up t~~he~~o a few decimetres (Reber et al., 1987; Mätzler, 1987).

The backscattering of SPI is more heterogeneous compared to NPI. The 2015 coverage features ~~$\sigma^0 < -19$~~$\sigma^0 \leq -19$ dB revealing wet snow on large parts of the plateau (particularly on the western margin). The σ^0 of the 2012 coverage is in average higher (especially on scene 4/5 acquired at the end of March)~~,~~. ~~s~~Over t~~ill, w~~he main parts~~sume~~ of the plateau ~~mo~~σ^0 is still lo~~f~~wer th~~e~~an ~~surf~~−16 dB, an indic~~e~~ation ~~was~~for wet ~~(~~sno~~r~~w, p~~art~~ossi~~a~~bl~~l~~y ~~r~~cove~~f~~red lo~~zen)~~cally by a~~nd~~ the~~re~~in frozen cr~~e~~ust th~~e~~at ~~DEM~~would i~~s~~ n~~o~~t~~ affe~~roduct~~e~~d ~~b~~only a s~~ignifie~~ma~~nt~~ll elevation bias. The December 2011 coverage displays values of $\sigma^0 < -18$ dB imputable to wet snow on most of the plateau. Some isolated regions with higher σ^0 in the southern sector have been conservatively masked out in the 2011/2012 summer SECR prior to using this dataset for seasonal correction (Sect. 3.1.3).

Based on the analysis of the backscatter and of the SEC maps we manually outlined regions on the plateau which we considered prone to signal penetration ~~o~~in each DEM mosaic (Fig. S5). The outlining was performed manually in order to identify areas on rough ice surfaces and on radar fore-slopes, where high σ^0 is not an indicator for signal penetration. We assigned a potential penetration height offset to each of these polygons according to its average σ^0 and look angle~~,~~. This offset~~o~~ ~~b~~is taken into acc~~l~~ou~~ded~~nt in the error budget. The offsets are based on empirical observations of the relationship between σ^0 and height offset performed on multiseasonal TDM Raw DEMs of NPI, showing a mean penetration bias of 4 m for an increase of σ^0 by 10 dB from wet to dry snow (Abdel Jaber, 2016).

3.2.2 Assessment of SRTM backscatter

The SRTM absolute and relative radiometric accuracy nominal values are 3 dB and 1 dB, respectively (Farr et al., 2007). The SRTMIMGR product provides the radar brightness β^0 at 1 arcsec corrected for flat earth for all the sub-swaths acquired during the mission. Lacking the orbital parameters of each acquisition, we coarsely removed the flat earth correction using the mid-look angle of each sub-swath, introducing this way an error up to ±0.6 dB and computed the backscattering coefficient using the provided local incidence angle (θ_{loc}) mask as $\sigma^0 = \beta^0 \cdot \sin\theta_{\mathrm{loc}}$ ~~(Abdel Jaber, 2016)~~.

Figure S6 shows the arithmetic mean ($\bar{\sigma}^0$) and the standard deviation computed pixelwise from the sub-swath σ^0 images covering the icefields (4 to 7 stacked pixels are usually found). The measure of spread supports the interpretation of $\bar{\sigma}^0$. While σ^0 is similar for the HH and VV polarizations of the sub-swaths, variations of several dB are induced by the wide range of look angles (30° to 56°) at parity of snow conditions ~~(Ulaby and Stiles, 1981)~~(Ulaby et al., 2014). ~~Fu~~The ERA Interim data show mean 850 hPa air temperatures between 3.3 and 3.8°C in February 2000 over the icefields, though temporal variations of LWC due to changing meteorological conditions cannot be excluded during the nine days of acquisition. On the other hand variations due to the diurnal temperature cycle are unlikely given the time of the Shuttle overpasses (Table S3).

Values of $\bar{\sigma}^0 < -22$ dB denoting the presence of wet snow are found on large sections of the plateaus. In the north-western part of SPI, a west-east gradient is visible (Fig. S6). Values of $\bar{\sigma}^0$ up to -18 dB are found in the 1800–1900 m range (the mean elevation of the plateaus) and up to -16 dB at elevations up to approximately 2300 m. These ~~e~~values ma~~n~~y be a~~n~~ ttri~~n~~bute~~d~~d~~ica~~ to~~r~~ ~~of~~ wet snow with a rough surface (Nagler and Rott, 2000). Above 2300 m $\bar{\sigma}^0$ ~~inc~~rea~~s~~ches up to -12 dB (excluding steep fore-slopes~~ in layover~~). Here nocturnal freezing of the upper snow layer is more likely, implying a displacement of the scattering phase centre in the order of decimetres (Floricioiu and Rott, 2001; Reber et al., 1987). This analysis was previously presented by Abdel Jaber (2016).

~~T~~Considering the analysis of $\bar{\sigma}^0$, it can be concluded that the SRTM elevations are not affected by a bias due to C-band radar signal penetration ~~on mos~~except fo~~f~~r ~~the ice~~fi~~e~~ld.w ~~A~~areas at high~~er~~ elevations with higher likelihood of penetration. These have been outlined (Fig. S6) and are c~~e~~o~~u~~n~~te~~sid~~ fo~~ered in the error budget.

~~O~~The good agreement of our ~~e~~vo~~ne~~lume change rates~~i~~ 2000 to~~n~~ ~~is~~2012 ~~supp~~over NPI with the~~d~~ results of ~~by~~Dussaillant et al. (2018) bas~~y~~ed on optical data ~~mea~~supports the~~d~~ validity ~~an~~of ~~AWS~~our ~~ne~~appr~~ t~~oach~~e~~ ~~fro~~an~~t~~d ~~of~~ the ~~Per~~conclusi~~t~~ons ~~Mo~~regardin~~o~~g ~~G~~signal~~aci~~ penetr~~-~~at~~ 198 m~~ion. ~~D~~Regardi~~ly averan~~ng~~e~~ ~~a~~possi~~r t~~ble~~m~~ penetration issu~~r~~es ~~wer~~of the SRTM DEM, the~~xtr~~ a~~p~~nalysis of Dussaillant et al. (2018) also indicate~~d u~~s~~ing~~ lack ~~la~~of p~~s~~ene~~-~~trat~~e~~ion of ~~−0.65 °C/100 m (Bippus, 2007)~~ t~~o~~he C-ba~~rou~~nd~~ 0 °C~~SRTM ra~~t 1800 m~~ da~~.~~r s~~.~~ignal~~.~~ ~~w~~int~~h~~o snow and ~~slightly~~firn excep~~osi~~ti~~ve t~~for~~end du~~a region~~g th~~above 29~~days~~00 ~~of~~m a~~equi~~.si~~tion~~.l.

3.3 Uncertainty of SECR and mass balance

This section reports on the estimation of the different error sources affecting the SECR maps and the mass balance computed with the geodetic method.

3.3.1 Random error

The random error of each SECR sample σ_{SECR} was computed~~ as~~ ~~th~~pixe~~ ~~lwis~~quar~~e ~~root~~as ~~of ~~the quadrature sum of the random errors σ_h of the ~~subtracted ~~elevation samples~~,~~ of maseeter and slave DEM, divided by the corresponding Δt~~.~~ in years:

$$\sigma_{\mathrm{SECR}}\left(x,y\right) = \sqrt{\sigma_{h_m}\left(x,y\right)^2 + \sigma_{h_s}\left(x,y\right)^2} / \Delta t\left(x,y\right). \tag{3}$$

For TDM elevations the random error is given in the HEM raster, which ~~contain~~expresses the interferometric standard error for each sample~~ (x,y)~~ computed assuming a normally distributed error as (Rossi et al., 2010):

$$\sigma_h\left(x,y\right) = \sigma_\phi\left(x,y\right)\frac{h_a}{2\pi} \tag{4}$$

where h_a is the height of ambiguity and $\sigma_\phi\left(x,y\right)$ is the standard deviation of the interferometric phase which depends on the coherence and on the number of looks (Lee et al., 1994). The HEM does not include any systematic error components (phase unwrapping errors, etc.), these are discussed in Sect. 3.3.3. Concerning SRTM, the NASADEM also comes with a corresponding height error map providing σ_h. ~~T~~Where performed (section of SPI covered by the 2011/2012 summer SECR), the random error contribution of the pixelwise seasonal correction (Sect. 3.1.3) was also ~~inclu~~added ~~where~~in ~~pe~~quadr~~fo~~atur~~m~~ed ~~on SPI~~. The resulting random error maps for the two epochs are shown in Fig. S7.

3.3.2 Spatial correlation and spatial averaging

The standard error (SE) of a spatial average of several SECR samples ~~ca~~is given by $\mathrm{SE} = \sigma/\sqrt{N}$, where ~~computed~~$\sigma$ ~~a~~is ~~$\mathrm{SE} = \sigma_{\mathrm{SECR}}/\sqrt{N}$, w~~the random error and N is the number of uncorrelated samples. To determine N the spatial correlation of the SECR maps was estimated by means of semivariograms. Two different regions of interest (ROIs), both verifying the assumptions of first- and second-order stationarity, were selected on ice-free terrain. ROI 1 features a relatively flat topography similar to the one of the CRs (Sect. 3.1.2), ROI 2 features varied slope and aspect distribution, simulating the icefield topography. The empirical omnidirectional semivariograms obtained on the two ROIs for the TDM–SRTM and TDM–TDM SECR were furthermore fitted with an exponential model and are shown in Fig. S8. Among the model parameters reported in Table S6 the range of the semivariogram is an estimate of the correlation distance d_c of the SECR map, which was conservatively increased by $\sim 40\,\%$, to account for possible higher slopes on the averaged regions, among other factors. For the TDM–SRTM and TDM–TDM SECR maps we used, respectively, $d_c = 120$ m and $d_c = 60$ m to compute the standard error of the mean height offset on each CR (Sect. 3.1.2) and, respectively, $d_c = 200$ m and $d_c = 100$ m to compute the standard error of the mean SECR on the elevation intervals. For the estimation of N the theory of geostatistics was applied as in Rolstad et al. (2009) by integrating the exponential semivariogram model (they used a spherical model) in polar coordinates over a circular integration area A. The assumption of a negligible nugget (representing the uncorrelated component of the variance for the applied sampling interval) leads to the following expression for the number of uncorrelated samples N within A:

$$N = \left[-\frac{2}{9}\frac{A_c}{A}\left(3\sqrt{\frac{A}{A_c}}e^{-3\sqrt{\frac{A}{A_c}}} + e^{-3\sqrt{\frac{A}{A_c}}} - 1\right)\right]^{-1}, \tag{5}$$

where $A_c = \pi d_c^2$ is the correlation area. Equation (5) simplifies to $N = \frac{9}{2}\frac{A}{A_c}$ for the common case where $A \gg A_c$.

3.3.3 Systematic errors

Systematic errors are not reduced when spatial averaging is applied, they can hence have a significant impact on the mass balance of large areas. We defined four systematic error components.

1. An error linked to the coregistration to the reference DEM (Sect. 3.1.2) was defined for each Raw DEM and for the SRTM DEM of NPI and SPI as the interquartile range (IQR) of the μ_r (mean of Δh on CR r) used to estimate the height offset of that DEM. This error ranges between 0.04 m and 0.3 m. The corresponding systematic error component on the SECR ε_{reg} is obtained pixelwise as the ~~s~~quadrature ~~root~~sum of the ~~quad~~coregistrat~~u~~ion error~~e sum~~ of the~~ of~~ master and slave DEMs~~,~~ scaled by Δt in years, similarly to Eq. (3).

2. To account for signal penetration we used the penetration height offsets assigned to critical regions on each DEM mosaic~~e~~ ~~(Sect. 3.2)~~ as local systematic errors, ranging between 1 m and 6 m according to σ^0, look angle and radar frequency (Sect. 3.2). Furthermore a bulk systematic error of 0.1 m was assigned to all remaining pixels above 1000 m a.s.l. to account for undetected regions and for possible small offsets on refrozen upper layer of snow and firn (Sect. 3.2). The systematic error component on the SECR ε_{pen} was obtained analogously ~~ab~~to~~ve~~ ε_{reg}.

3. An additional bulk systematic error was assigned to all glacier samples to account for unmodelled sources (e.g. residual GIA effects, residual tilts, unmasked local errors due to PU or layover, etc.). This source includes effects of the curvature-dependent SEC bias caused by the different resolution of the SRTM and TDM DEMs affecting small regions mostly at high elevation (Abdel Jaber, 2016). This additional error was set to 0.05 m for TDM, while for SRTM it was set to 0.2 m on SPI and 0.3 m on NPI to account for residual low-frequency elevation biases (Sect. 2.2). The systematic error component on the SECR ε_{add} was obtained analogously ~~ab~~to~~ve~~ ε_{reg}.

4. To compute the systematic error linked to the seasonal correction (Sect. 3.1.3), the previous three ~~aforementioned~~ systematic ~~s~~error~~u~~r components (ε_{reg}, ε_{pen} and ε_{add}) were estimated separately for the summer 2011/2012 SECR. Here ε_{add} was increased by a factor of 1.5 to account for the different temporal coverage. All three components were summed in quadrature and conservatively further increased by a factor of 3.0 on extrapolated regions (north of SPI and NPI). A pixelwise scaling by the number of corrected days and by the appropriate Δt in years was applied, leading to a fourth~~er~~ systematic error component on the SECR, $\varepsilon_{\text{seas}}$.

The total systematic error $\varepsilon(x,y)$ of each SECR sample was obtained pixelwise as ~~$\varepsilon = \sqrt{\varepsilon_{\text{reg}}^2 + \varepsilon_{\text{pen}}^2 + \varepsilon_{\text{add}}^2 + \varepsilon_{\text{seas}}^2}$.~~ (omitting (x,y) for compactness):

$$\varepsilon(x,y) = \sqrt{\varepsilon_{\text{reg}}^2 + \varepsilon_{\text{pen}}^2 + \varepsilon_{\text{add}}^2 + \varepsilon_{\text{seas}}^2}. \tag{6}$$

The mean values of $\cancel{\varepsilon}\varepsilon\,(x, y)$ and of its components for the four SECR maps are reported in Table S7.

3.3.4 Geodetic mass balance error

The geodetic method was applied to estimate the average SECR on separate elevation bins and the corresponding volume and mass change rates. The total error of the mean SECR on elevation bin b was computed by summing in quadrature the mean systematic error $\overline{\varepsilon}_b$ on bin b and the standard error SE_b of the spatial average on bin b (which is generally negligible compared to $\overline{\varepsilon}_b$ ~~on large integration areas~~), obtained as:

$$\mathrm{SE}_b = \sqrt{\frac{\overline{\sigma^2_{\mathrm{SECR}}}}{N_b}}. \tag{7}$$

where N_b is computed according to Eq. (5).

In the geodetic method the mean of the valid SECR samples of bin b is extrapolated to the unsurveyed area of the bin. On such gaps the total error was increased by a factor of 1.5 when computing the mass balance of a single glacier basin and a by factor of 3.0 when computing ~~a~~it on the entire icefield, to account for the across-basin variability of the SEC, particularly at lower elevations.

To calculate the volume change rate a 2 % error was assigned to the glacier area obtained from the updated outlines (Sect. 2.3). This value is higher than the RGI error suggested by Pfeffer et al. (2014) and in line with the empirical findings of Paul et al. (2013). ~~We limited t~~The uncertainty of the density used for the volume to mass change rate conversion~~ to a rel~~wa~~tivelys~~ s~~mall valu~~et to~~f~~ ~~±17~~±36 $\mathrm{kg\,m^{-3}}$ (~~1.9~~4 %)~~,~~. This num~~po~~ber is based ~~by~~on an est~~h~~imated ~~m~~uncerta~~x~~i~~mum~~nty of ±17 $\mathrm{kg\,m^{-3}}$ for density ~~of~~in the ice areas and ±54 $\mathrm{kg\,m^{-3}}$ in the firn areas. In Sect. 4 the average SECR and VCR errors estimated for each bin are ~~report~~visualized graphically on the hypsometric plots, while the errors estimated for the entire icefields and for the individual glaciers are reported in the results tables.

4 Results

The SECR maps of NPI and SPI after seasonal correction are shown in Fig. 1 for the two main epochs 2000–2012 (epoch 1) and 2012–2016 (epoch 2) along with the TDM DEM mosaic of 2012 used as hypsometric reference to analyze the elevation dependence. Unsurveyed areas in the SECR maps are relatively small and geographically evenly distributed, with the exception of the eastern margin of NPI in 2012–2016 because of layover caused by the steep incidence angle of scenes 6 and 7. In Table 1 the SECR, the volume change rate (VCR), the mass balance and the contribution to sea level rise are specified for the entire icefields. Table 2 provides SECR and VCR for NPI glaciers larger than 2 $\mathrm{km^2}$, Table 3 for SPI glaciers larger than 35 $\mathrm{km^2}$ and Table S8 in the Supplement for SPI glaciers ~~l~~with ar~~ge~~e~~r~~a bet~~h~~ween 35 $\mathrm{km^2}$ and 9 $\mathrm{km^2}$. The tables report also the measured basin areas (based on the updated RGI glacier outlines) and the percentage of SECR coverage for the two epochs. The reference hypsometry and the distribution of unsurveyed areas are shown in Figs. S10 and S11 for NPI and SPI, respectively. The altitude dependence of SECR and VCR is shown in Fig. 9 for NPI and its main glaciers and in Fig~~ure~~. 10 for SPI and its main glaciers, while plots for additional glaciers are reported in Figs. S12 and S13. SECR and VCR are assembled in 50 m elevation bins using the surface of the 2012 TDM DEM as reference. The SECR averaged over each glacier basin is visualized in Fig. S9 together with the 2012 TDM DEM average surface elevatio~~pography~~n.

NPI shows a similar pattern of elevation change during the two epochs, with the highest rates of thinning on the lowest sections of the glacier tongues, gradually decreasing up-glacier. Equilibrium state is reached on average at about 1800 m elevation (Fig. 9). On the south-western sector of the icefield and on San Quintin Glacier the thinning rates at elevations below 1200 m are slightly higher than in the northern and eastern sectors. All glaciers with an area larger than 20 $\mathrm{km^2}$ show volume losses during both epochs except Leones Glacier revealing a modest increase in ice volume (Table 2). The volume loss rate of NPI increased from epoch 1 (VCR = $-4.26\ \mathrm{km^3\,a^{-1}}$) to epoch 2 (VCR = $-5.60\ \mathrm{km^3\,a^{-1}}$). The three ~~m~~la~~in~~rgest glaciers (San Quintin, San Rafael, Steffen) account for 50 % of the NPI volume loss during epoch 1 and for 48 % ~~of the NPI volume loss~~ during epoch 2. During both epochs the highest SECR at basin scale was observed on HPN 1 (VCR = $-2.50\ \mathrm{m\,a^{-1}}$ and $-3.25\ \mathrm{m\,a^{-1}}$, respectively). On all glaciers larger than 20 $\mathrm{km^2}$, except Arco Glacier and Leones Glacier (with positive mass balance), the loss rates were higher during epoch 2. San Quintin Glacier (Fig. 2, Fig. 9) shows the highest increase in volume loss (VCR = $-0.60\ \mathrm{km^3\,a^{-1}}$ and $-0.92\ \mathrm{km^3\,a^{-1}}$). On San Rafael Glacier the loss rate increased slightly from epoch 1 to epoch 2 (VCR = $-0.81\ \mathrm{km^3\,a^{-1}}$ and $-0.87\ \mathrm{km^3\,a^{-1}}$), but the loss pattern changed (Fig. 3, Fig. 9). On the terminus below about 800 m a.s.l. the rate of surface lowering decreased, whereas in the upper reaches loss rates became larger.

On SPI the spatial pattern of surface elevation change is more complex and the temporal trend is less uniform. Contrary to NPI, the volume loss of SPI decreased from epoch 1 (VCR = $-14.87\ \mathrm{km^3\,a^{-1}}$) to epoch 2 (VCR = $-11.86\ \mathrm{km^3\,a^{-1}}$). The three glaciers Upsala, Jorge Montt and Viedma account for 45 % of the SPI volume loss in epoch 1 and for 58 % in epoch 2. On Upsala Glacier the rate of surface lowering decreased on the terminus from epoch 1 to epoch 2 (Fig. 4) associated with a slowdown of calving velocity. The losses increased on Jorge Montt Glacier (Fig. 5) and on Viedma Glacier. Very high loss rates are observed on the lower sections of the Jorge Montt terminus, with SECR ~~up~~(for a 50 m elevation ~~a~~bin) o~~ut~~f ~~−22~~$-16.7\ \mathrm{m\,a^{-1}}$ during epoch 1 and ~~−30~~$-25.6\ \mathrm{m\,a^{-1}}$ during epoch 2. The loss rates decrease gradually up-glacier, but the main sections of the accumulation area of these glaciers, up to elevations of 1800 m to 2000 m, were affected by downwasting during both epochs (Fig. 10).

Other glaciers with volume loss rates > 0.5 $\mathrm{km^3\,a^{-1}}$ are located in the northern sector of SPI (O'Higgins, Bernardo, Greve, Tempano, Occidental), in the centre/west sector of the icefield (HPS 12), and in the south-west (Tyndall Glacier). ~~T~~Average thinning rates up to 40 $\mathrm{m\,a^{-1}}$ are observed on the terminus of HPS 12 Glacier during epoch 1. The HPS 12 terminus, flowing through a deep, narrow fjord, retreated by almost 5 km between 2000 and 2012 and by 4 km between 2012 and 2015. In epoch 2 the ~~m~~avera~~ximum~~ge SECR ~~is eve~~and ~~higher~~VCR ~~b~~cou~~t~~ld not~~h~~ be e~~x~~stima~~e~~t~~ numb~~ed r~~ el~~i~~s~~ably ~~not known ~~because of significant gaps on the terminus in the 2015 DEM due to phase unwrapping errors (Fig. 1b), nevertheless thinning rates higher than 40 $\mathrm{m\,a^{-1}}$ could be observed at the 2012 front. Next to HPS 12 the highest loss rates at basin scale are observed on Jorge Montt Glacier (SECR = $-4.01\ \mathrm{m\,a^{-1}}$ and $-4.95\ \mathrm{m\,a^{-1}}$ during the two epochs) and on Upsala Glacier (SECR = $-3.33\ \mathrm{m\,a^{-1}}$ and $-3.04\ \mathrm{m\,a^{-1}}$).

The only glacier with positive mass balance in both epochs is Pio XI Glacier, showing a significant increase of VCR from ~~0.423~~0.52 $km^3 a^{-1}$ in epoch 1 to 1.26 $km^3 a^{-1}$ in epoch 2 (Fig. 6). SEC rates in the elevation zones up to 1500 m a.s.l. ~~have been~~ were positive during both epochs. During epoch 1 the elevation zone between 100 m and 400 m a.s.l. ~~was~~ accounted for the main ~~source~~ contribution to the ~~f~~total gain in ice mass. During epoch 2 an additional source of significant mass gain was the elevation zone between 1000 m and 1500 m on the ice plateau (Fig. 10).

On the western sector south of HPS 12 (49.6° S) and on the eastern sector south of Upsala Glacier (49.9° S) the average loss rates are smaller than on the northern sector, but all glaciers covering areas > 35 km^2 and the majority of smaller glaciers show negative SECR during epoch 1 (Table~~s~~ 3~~,~~ and S13). On the main ice plateau the surface elevation was either stable or the SECR was slightly negative during epoch 1, becoming slightly positive during epoch 2. During epoch 2 the mass balance of several glaciers of the southern sector switched from negative to slightly positive values. However, the termini of the majority of glaciers were thinning during both epochs. The largest contributors to the SPI mass deficit in the southern sector during epoch 1 were Tyndall Glacier (VCR = −0.79 $km^3 a^{-1}$ ~~during epoch 1~~) and Grey Glacier (VCR = −0.44 $km^3 a^{-1}$ ~~during epoch 1~~). On both glaciers the volume loss rate decreased significantly during epoch 2, on Tyndall Glacier (VCR = −0.48 $km^3 a^{-1}$) mainly due to decrease of losses above 700 m a.s.l. (Fig. 10) and on Grey Glacier (VCR = −0.07 $km^3 a^{-1}$) at all elevations (Fig. 7, Fig. 10). Other glaciers with distinctly different hypsometric VCR between the two epochs are Penguin, Europa, Amalia, HPS 41 (Fig. S13).

Figure 8 shows a map of daily SECR on SPI during summer 2011/2012 based on DEM differencing spanning the periods 18/12/2011 to 26/3/2012 (99 days), 7/12/2011 to 15/3/2012 (99 days) and 29/12/2011 to 31/1/2012 (33 days). During summer the signal of surface lowering in the accumulation areas is mainly related to firn ~~compaction~~ densification and melting of the top snow layers ~~(va~~ (Rivera, 2004). On the firn plateau, at elevations ~~−0.03~~ ≥ 1200 ~~m d−1~~ m, the averaged SECR in summer 2011/2012 was about ~~)~~ −0.03 $m\,d^{-1}$ (blue curve in Fig. S3). In the ablation areas ice melt and dynamic downwasting (varying from glacier to glacier) are the main factors. High loss rates (SECR ~~> −0.08~~ < ∼ −0.08 $m\,d^{-1}$) refer to areas that are subject to significant dynamic thinning, such as the lower terminus of Upsala and Viedma glaciers. Average summer melt rates for ice on the lower terminus of Perito Moreno Glacier (at 300 m altitude) are about 0.05 $m\,d^{-1}$ (Stuefer et al., 2007). On a glacier in balanced state surface lowering due to melt is in summer partly compensated by uplift due to emergence.

The reported volume change and mass balance do not include subaqueous ice volume changes. Subaqueous losses are negligible in respect to the mass change of NPI since there are no large frontal retreats on water bodies. On SPI the main glaciers, and also many smaller ones, terminate in proglacial lakes or in oceanic fjords. For the main retreating glaciers of SPI Abdel Jaber (2016) estimated the subaqueous ice VCR at -0.73 ± 0.22 $km^3 a^{-1}$ for the period 2000 to 2011/2012. This number is obtained by measuring or estimating various parameters at the glacier front, including the glacier width, the water depth, the freeboard height on the two dates and the retreat distance. A bulk error of 30 % is assigned to the total subaqueous volume change rate, accounting also for unsurveyed glaciers. For the basal cross-section at the calving front the shape of a semi-ellipse is assumed except for four glaciers for which bathymetric data is available enabling more precise estimates. For these glaciers a bulk error of 20% is assumed for the subaqueous volume changes, amounting for the whole period to -2.80 ± 0.56 km^3 on the main front of Upsala Glacier, -0.68 ± 0.14 km^3 on Jorge Montt Glacier, -0.59 ± 0.12 km^3 on Tyndall Glacier and -0.05 ± 0.01

km^3 on Ameghino Glacier. The estimated subaqueous volume changes for the period 2000–2011/2012 are reported in Table S9, together with the frontal retreat distance.

5 Discussion

5.1 Spatial and temporal pattern of surface elevation and glacier volume change

Patagonian glaciers and icefields experienced area retreat and shrinkage since the Little Ice Age which accelerated during recent decades associated with tropospheric warming (Davies and Glasser, 2012). Our estimate of mass loss for both icefields during the period 2000 to 2016 is equivalent to ~~0.047 ± 0.005~~0.047 ± 0.003 mm a^{-1} eustatic sea level rise. This corresponds to 6 % of the ensemble mean contribution to sea level rise of glaciers and ice caps for the period 2005–2016 of 0.74 ± 0.18 mm a^{-1}, based on global mass balance estimates from various sources (Cazenave et al., 2018). Between epoch 1 (2000–2012) and epoch 2 (2012–2016) the rate of mass loss of SPI and NPI combined decreased by 9 % with a contrasting temporal trend between the two icefields. The~~ topographic data~~ s~~how significant losses in ice mass for both icefields, as reported in previous studies, revealing major differences in mass balance and temporal trends between individual glaciers. The s~~patially detailed maps of SECR during the two subsequent epochs, derived from bistatic InSAR DEMs, provide a sound basis for studying the heterogeneous pattern of glacier response on NPI and SPI.

Regarding the ice bodies at large, on NPI the average loss rate increased by 31 % from epoch 1 to epoch 2 (VCR = -4.26 ± 0.20 $km^3 a^{-1}$ and ~~-5.60 ± 0.71~~-5.60 ± 0.74 $km^3 a^{-1}$, respectively). This was reverse on SPI where the loss rate decreased by 20 % (VCR = ~~-14.87 ± 0.51~~-14.87 ± 0.52 $km^3 a^{-1}$ and ~~-11.86 ± 1.90~~-11.86 ± 1.99 $km^3 a^{-1}$, respectively). Reasons for the different behaviour are temporal changes of calving velocities, in particular on SPI, as well as a north-south gradient of air temperature increase in epoch 2 compared to epoch 1. Air temperatures, based on the European Centre for Medium-Range Weather Forecasts Interim Re-Analysis (ERA-Interim) (Dee et al., 2011; Berrisford et al., 2011) show for the ERA grid point 47.25° S, 73.5° W (NPI) in 850 hPa a mean annual temperature of +1.9 °C during the period 2000–2011 and +2.3 °C during 2012–2015. The corresponding values at the grid point 50.25° S, 73.5° W (southern SPI) are: +0.7 °C and +0.8 °C. The temperature difference between the two epochs was slightly larger during the main ablation period (1 November to 31 March): ~~air temperature ~~+4.1 °C (summer 2000/2001 to 2011/2012) and +4.8 °C (summer 2011/2012 to 2015/2016) on the NPI grid point, +2.4 °C and +2.7 °C on southern SPI. The NCEP/NCAR Reanalysis 850 hPa mean temperature (Kalnay et al., 1996) is about 1 °C lower, but shows a similar temporal and spatial trend. Over an area extending from 72.75° W to 74.25° W, 48.00° S to 51.75° S, covering SPI, the mean annual precipitation, derived from ERA Interim data, was slightly higher (8.4 %) in epoch 1 than in epoch 2 ~~(Langhamer, 2017)~~(Langhamer, 2017; Langhamer et al., 2018).

A main factor for the increased mass losses during epoch 2 on NPI is the higher air temperature compared to epoch 1, in particular during the main ablation period. Assuming a degree-day factor of 0.7 cm d^{-1} on ice areas (Stuefer et al., 2007), the melt loss for an increase of surface temperature by 0.7 °C during November to March corresponds to an additional loss of 0.74 m water equivalent~~ per year~~. The hypsometric plot for the whole icefield shows changes of SECR by about −0.7 m a^{-1} up to elevations of 1200 m a.s.l., indicating increased melt losses during epoch 2 not only on glacier termini but also on lower sections of the NPI plateau. At higher elevations the rate of surface lowering in both epochs, including the additional contribution during epoch 2, decreases gradually with elevation, reaching balanced state at about 1800 m in epoch 1 and about 2100 m in epoch 2 (Fig. 9). On NPI surface melt is the dominating process for mass depletion. During the period 2000 to 2009 the ice export due to calving amounted to about 20 % of the annual mass depletion by surface melt (Schaefer et al., 2013).

On lower sections of the main calving glaciers temporal variations of flow velocities are a main factor for the differences in SECR during the two epochs. ~~Fl~~In o~~w~~rder ~~v~~to support the~~loc~~ interpretation of differences in SECR be~~ar~~tween the two epochs, we derived maps of surface vel~~v~~ocity gridded at 50 m for main glaciers from TerraSAR-X 11-day repeat pass data on various dates ~~of~~between 2010 ~~S~~and ~~R~~2016, applying the off~~a~~se~~l~~t ~~Gl~~tracking technique~~r~~. Th~~av~~e ~~r~~uncerta~~e~~inty of the~~d~~ velocity magnitude~~s~~ ~~in~~of ~~exe~~thes~~s~~e pro~~f 7 $\mathrm{km\,a^{-1}}$~~ducts i~~n~~s ~~2~~0.0~~7~~5 ~~(Willis et al., 2012a; Abdel Jaber et al., 2014),~~$\mathrm{m\,d^{-1}}$(Wuite et al., 2015). ~~bu~~Plots of ~~ha~~ve~~-~~locities alo~~w~~ng ce~~d~~ntral ~~d~~flowlines, extracted from ~~4.4~~the ~~$\mathrm{km\,a^{-1}}$~~velocity ma~~fterw~~ps, ar~~d~~s~~e shown in~~g~~ ~~l~~Fig. 11 for Jorge Montt, Pio XI, Upsala and Viedma glaciers.

Flow velocities near the calving front of San Rafael ~~b~~Glacier reached magnit~~w~~udes in excess of 18 $\mathrm{m\,d^{-1}}$ in April 2007 (Willis et al., 2012a), dropping to 1~~2~~6 $\mathrm{m\,d^{-1}}$ in Ma~~nd~~y 201~~6~~2 (Abdel Jaber et al., 2014). ~~V~~Mouginot and Rignot (2015) report for the velocit~~ies~~y at 10 km from the ice front ~~show~~ a temporal peak in 2005 and a decrease by about 20 % until 2014 ~~(Mouginot and Rignot, 2015)~~. The drop in veloci~~s~~ty between epoch 1 and 2 is reflected in the hypsometric curve of SECR, showing reduced loss rates below 800 m elevation during epoch 2 (Figs. 3 and 9). San Quintin Glacier, the largest glacier of NPI, reaches its maximum speed of about ~~1~~3 ~~$\mathrm{km\,a^{-1}}$ at a distance of~~$\mathrm{m\,d^{-1}}$ ~~27~~30 km from the front (Abdel Jaber et al., 2014; Mouginot and Rignot, 2015). ~~B~~Our analysis of TerraSAR-X data shows between May 20~~05~~12 and June 201~~4~~6 on the ~~flow v~~te~~loc~~rmi~~ty 1 km~~ nu~~p~~s~~tream~~ ~~of~~a ~~th~~me~~ fro~~an~~t~~ increase~~d~~ ~~by~~in ~~ab~~velo~~u~~city ~~5~~by 10 %. However, this caused only a minor additional increase of surface lowerin~~g on the~~ g~~lacier terminus~~ (Fig. 9) because for this glacier the ice export due to calving accounts only for a very small part of total mass turnover (Schaefer et al., 2013).

On SPI calving fluxes play a larger role for mass turnover than on NPI. This is reflected in the change of the average hypsometric curve of SECR of the icefield between the two epochs (Fig. 10). In spite of s~~lightly h~~mi~~ghe~~lar air temperatures during epoch 2 the average rate of surface lowering decreased at elevations below 400 m. Between 400 m and 1000 m elevation the differences between the two epochs are very small. On the ice plateau, between 1000 m and 2000 m, the loss rate decreased slightly, mainly brought about by minor changes on the southern sector of the icefield. Local increase in snow accumulation may play a role.

For six glacier basins the VCR between the two epochs changed by more than +0.2 $\mathrm{km^3\,a^{-1}}$, summing up to a combined decrease of volume losses by 2.20 $\mathrm{km^3\,a^{-1}}$ (Table 3). The change of VCR from epoch 1 to epoch 2 amounted for Pio XI Glacier to +0.74 $\mathrm{km^3\,a^{-1}}$, for Grey & Dickson to +0.37 $\mathrm{km^3\,a^{-1}}$, for Upsala & Cono to +0.33 $\mathrm{km^3\,a^{-1}}$, for Tyndall to +0.30 $\mathrm{km^3\,a^{-1}}$, for Europa to +0.24 $\mathrm{km^3\,a^{-1}}$, for Penguin to +0.22 $\mathrm{km^3\,a^{-1}}$~~. There are three glaciers with major increase of losses during epoch 2 (VCR becoming more negative by ≥ 0.2 $\mathrm{km^3\,a^{-1}}$): the change of VCR for Jorge Montt is −0.36 $\mathrm{km^3\,a^{-1}}$, for Viedma −0.28 $\mathrm{km^3\,a^{-1}}$, for Bernardo −0.20 $\mathrm{km^3\,a^{-1}}$~~.

The behaviour of Pio XI Glacier, with frontal advance and positive mass balance since many years is opposed to the general trend of SPI glaciers. The recent frontal advance trend started at the northern section of the terminus in 2006 and at the southern section in 2000 (Wilson et al., 2016). Between 2000 and 2014 a ~~general~~ slowdown of velocity was observed on th~~e~~ ~~c~~e~~ntral and~~ southern section~~s~~ of the terminus (Mouginot and Rignot, 2015; Wilson et al., 2016). The slowdown went on until 2016, whereas the velocity of the northern section more tha~~ece~~n double~~ra~~d between 2013 and 2016 (Fig. 11). ~~T~~Bathymetric data show ~~i~~shallow ~~r~~wate~~fl~~r with ridges running across the fjord ~~in~~at the ~~ma~~present position of the~~l~~ ice~~va~~ front Dowdeswell and Vásquez (2013). Thi~~on~~s impedes c~~h~~alving at the so~~f-~~uthern ~~tw~~ice front, causing during epoch 1 a main increas~~,~~e of s~~how~~urface elevation~~g~~ on the souther~~o~~n~~ge~~ sect~~-~~ion~~ere~~, la~~s~~ter o~~f SECR~~n shifting towards the northern section that calves into Lago Greve (Fig. 6).

On Upsala Glacier the front retreated by 4 km between 2000 and 2014. ~~and t~~The calving velocity reached a maximum in 2009/2010 (Abdel Jaber et al., 2012; Mouginot and Rignot, 2015) and decreased significantly afterwards, dr~~each~~opping ~~a maximu~~from 8 m d^{-1} in March 2~~0~~011 to 5.9~~/~~ m d^{-1} in August 2014 and 4.8 m d^{-1} in August 2016 ~~(Abdel Jaber et al., 2012; Mouginot and R~~ 11). This caused a major decrease in the thinning rate of the lower terminus during epoch 2 (Fig. 4).

The hypsometric curves of Grey and Tyndall glaciers show~~s~~ little change in SECR on the lower terminus close to the calving front and decreasing loss rates in the upper reaches of the terminus and in the accumulation area, an indication for surface mass balance as main cause for the change in SECR (Fig. 10). This is in line with ~~ou~~Terr~~-analysis~~SAR-X ~~of~~ surface velocity ~~from TerraSAR-X da~~sult~~a~~s between December 2011 and August 2016 showing only modest changes near the ice front and slowdown upstream. On Tyndall Glacier the velocity on the central flowline 0.5 km from the front was ~~0.35 ± 0.02~~0.96 ~~km a^{-1}~~m d^{-1} in December 2011, ~~0.32 ± 0.02~~0.88 ~~km a^{-1}~~m d^{-1} in October 2013 and ~~0.35 ± 0.02~~0.96 ~~km a^{-1}~~m d^{-1} in August 2016. On Grey Glacier ~~the veloci~~at~~y on~~ the central flowline 3 km from the front, where the glacier splits into three branches, the velocity was ~~0.41 ± 0.02~~1.13 ~~km a^{-1}~~m d^{-1} in December 2011, ~~0.40 ± 0.02~~1.11 ~~km a^{-1}~~m d^{-1} in October 2013 and ~~0.37 ± 0.02~~1.02 ~~km a^{-1}~~m d^{-1} in April 2016. Further upstream the~~r~~ ve~~-~~loci~~s~~ty decrea~~-slowe~~d~~own of~~by a~~ppr~~bo~~xima~~u~~t~~ely~~ 20 % between 2011 and 2016 on both glaciers. Weidemann et al. (2018) computed the surface mass balance of both glaciers and estimated the calving flux as residual of mean surface mass balance and geodetic mass balance over the period 2000 to 2014, pointing out that ice loss by surface ablation exceeds ice loss by calving. On Europa and Penguin, featuring steep narrow tongues, the SECR switched from slightly negative values to slightly positive values on the ice plateau above 1000 m elevation, indicating also a change in surface mass balance.

There are three glaciers with major increase of losses during epoch 2 (VCR becoming more negative by ≥ 0.2 km^3 a^{-1}): the change of VCR for Jorge Montt is -0.36 km^3 a^{-1}, for Viedma -0.28 km^3 a^{-1}, for Bernardo -0.20 km^3 a^{-1}. Jorge Montt Glacier experienced a frontal retreat by 11 km between 1990 and 2011 (Rivera et al., 2012) and a further retreat by 2 km until 2016. The hypsometric profile shows high loss rates on the terminus at elevations up to 1000 m, with losses increasing during the second epoch (Table 3, Fig. 5) associated with major flow acceleration between 2007 and 2014 (Mouginot and Rignot, 2015). Figure 11 shows flow acceleration 2010 to 2015/2016 ~~(Mouginot and Rignot, 2015)~~extending 30 km up-glacier. On Viedma Glacier the increased mass loss during epoch 2 is caused by a major increase of the thinning rate on the glacier terminus below 1000 m elevation, an indication for changes in dynamic downwasting. This in accordance with a increas~~inge~~ of ice ~~flow~~ velocit~~ies.~~y ~~W~~be~~-d~~twe~~rive~~dn ~~surf~~2010 a~~e~~nd ~~velocity~~2016 ~~maps~~ o~~f~~n ~~Vi~~the~~dma~~ ~~G~~glacier ~~f~~ter~~o~~m~~ TerraSAR-X repeat pas~~inus, ~~da~~notably

~~of~~in ~~August~~t/~~S~~he~~ptember~~ ~~2010 and Ju~~ly/~~Augu~~owest ~~2016,~~5 ~~show~~km (Fi~~n~~g. ~~a~~11). ~~two-fo~~The cal~~d~~ving velocity increas~~e at th~~e ~~calving~~d fro~~ntm~~ ~~and~~2 ~~the~~m $\mathrm{d^{-1}}$ ~~si~~g~~n~~n~~al~~ ~~of~~August ~~accelera~~2010 t~~i~~o~~n~~ ~~reach~~3.8 m $\mathrm{d^{-1}}$ in~~g~~ ~~15 km~~ Augu~~p~~st~~ream~~ 2016.

The heterogeneous spatial pattern of elevation change on the two icefields and its temporal evolution are results of complex interdependencies between surface mass balance, responding directly to climate change signals, and effects of flow dynamics. Differences in surface elevation change and mass balance between individual glaciers and their temporal trends are particularly pronounced on SPI, where the calving fluxes represent a main component of mass turnover for most glaciers. The elevation dependence of the SEC reveals that ice dynamics exerts a main control on topograph~~ic~~y ~~cha~~n~~ge~~ ~~n~~ot only on the glacier tongues, but also on ~~seve~~par~~al~~ ~~sec~~t~~ion~~s of the main ice plateau.

5.2 Comparison with previous estimates

A comparison of published results on volume change rates of SPI and NPI is reported in Table S10 for different epochs between 1968 and 2017, based on various methods including differencing of optical and/or interferometric DEMs and gravimetric time series of the GRACE mission. Similar comparisons are found in Malz et al. (2018) and Foresta et al. (2018). Our results are in line with geodetic mass balance results of NPI and SPI published by other authors, which suggest an overestimation of the mass losses retrieved from gravimetric time series ~~(~~such as those found in Chen et al. (2007), Ivins et al. (2011) and Jacob et al. (2012), the latter referring to Patagonia in general~~)~~.

Our result for NPI during epoch 1 (VCR = -4.26 ± 0.20 $\mathrm{km^3\,a^{-1}}$)~~ is in~~ compli~~n~~es with the numbers re~~sul~~port~~s~~ed ~~of~~by Abdel Jaber (2016) for the period 2000 to 2014 (-4.40 ± 0.13 $\mathrm{km^3\,a^{-1}}$) and Willis et al. (2012a) for 2000 to 2011 (-4.06 ± 0.12 $\mathrm{km^3\,a^{-1}}$), the latter based on SRTM and ASTER DEMs. Willis et al. (2012b) recomputed their previous estimate applying a 2 m offset to the SRTM DEM to account for signal penetration which result~~ing~~s in larger losses (VCR = -4.9 ± 0.3 $\mathrm{km^3\,a^{-1}}$). This correction is not comprehensible given the wet status of the snow surface during the summer acquisition of SRTM as evident from the backscatter data (Sect. 3.2.2, and Abdel Jaber (2016)). Braun et al. (2019) report for NPI a VCR -4.65 ± 0.17 $\mathrm{km^3\,a^{-1}}$ over the period 2000 (SRTM data) to 2011/2015 (TDM data).

Our VCR for epoch 1 is slightly lower than the results of Dussaillant et al. (2018) who applied ~~b~~two methods: differencing of SPOT and SRTM DEMs (VCR = -4.55 ± 0.41 $\mathrm{km^3\,a^{-1}}$) and derivation of temporal elevation trends from ASTER DEM time series (VCR = -4.72 ± 0.34 $\mathrm{km^3\,a^{-1}}$). Our hypsometric curve of SEC shows up to 2800 m of elevation a similar behaviour as their ASTER_trend results, although with slightly lower losses at most elevations. Above 1000 m Dussaillant et al. (2018) report 35 % and 22 % of unsurveyed area for the SPOT-SRTM analysis and ASTER_trend respectively, mostly due to the lack of contrast or the presence of clouds in the optical stereo images. For the same elevation band the unsurveyed area in our 2000–2012 SECR map of NPI is 6 %~~ on NPI~~. On glaciers larger than 100 $\mathrm{km^2}$ the SEC rates with both methods applied by Dussaillant et al. (2018) agree with~~in~~ ~~err~~our ~~ba~~results within error ~~bar~~results. On two medium-sized glaciers, Exploradores (86 $\mathrm{km^2}$) and Grosse (67 $\mathrm{km^2}$), the average SECR of their two methods differs by more than 1.0 $\mathrm{m\,a^{-1}}$, their ASTER_trend being ~ 0.8 $\mathrm{m\,a^{-1}}$ higher than our SECR and ~ 0.6 $\mathrm{m\,a^{-1}}$ higher than those of Willis et al. (2012a).

On SPI Willis et al. (2012b) estimate a VCR of -21.2 ± 0.5 $\mathrm{km^3\,a^{-1}}$ for the period 2000–2011, a much larger value compared to the ~~on~~value reported here for epoch 1 (VCR = ~~-14.87 ± 0.51~~ -14.87 ± 0.52 $\mathrm{km^3\,a^{-1}}$) and to that of Abdel Jaber (2016) for

2000–2011/2012 (VCR = -14.59 ± 0.37 km^3 a^{-1}). The discrepancy largely exceeds the 10 % VCR contribution they attribute to the 2 m correction for signal penetration in the SRTM DEM.

Malz et al. (2018) present SECR maps and mass balance of SPI for the period 2000–2015 based on SRTM and several TDM DEMs of December 2015. We used the same raw data at the end of our epoch 2. They do not account for missing summer days and report a VCR of -13.2 ± 3.6 km^3 a^{-1}. Scaling our VCR results over the two epochs and accounting for the missing summer days in order to cover a period of 16 years, from mid-February 2000 to mid-February 2016, we obtain ~~-14.2 ± 0.9~~-14.1 ± 0.9 km^3 a^{-1}. The difference can probably be explained by the missing 48 to 76 summer days required for spanning a full period of 16 years. Applying the method of Sect. 3.1.3 for the missing summer days, we obtain an icefield-wide average SECR value of -0.12 m a^{-1}, corresponding to~~ an~~ a~~dditional~~ VCR of -1.5 km^3 a^{-1}, which is not taken into account by Malz et al. (2018). For the southern sector of SPI~~,~~ Malz et al. (2018) show SECR maps and hypsometric curves for the periods 2000–2012 and 2012–2015, based on the same TDM raw data used in this study (scenes 7/8 and 13/14). The absence of a correction for 53/59 summer days at the end of the 4~~-~~-year period leads to lower loss rates compared to our numbers for epoch 2.

Average SEC rates for single glaciers are reported by Willis et al. (2012b) and Malz et al. (2018). On several main glaciers, including Bernardo, Tempano, Occidental, Greve, Chico, Europa and Guilardi glaciers, a direct comparison is not possible because of different glacier outlines. Among main glaciers with similar area our SECR estimates are in general lower than those of Willis et al. (2012b). Among glaciers > 200 km^2, average SEC rates deviating by more than -1.0 m a^{-1} from our results are reported for Tyndall, Pio XI and Perito Moreno glaciers.

Foresta et al. (2018) compute the geodetic mass balance of NPI and SPI for six glaciological years between 2011 and 2017 from SEC maps using swath processed CryoSat-2 (CS2) interferometric data with sub-kilomet~~e~~re spatial resolution. The acquisitions dates vary spatially for different pixels. The authors explain that seasonality biases are avoided due to the regular flight path of CS2 ensuring data acquisition within each pixel at the same epochs in each glaciological year. The data coverage is relatively poor (46 % for NPI, 50 % for SPI), in particular on lower sections of glacier tongues. Termini of several main glaciers are not covered at all and the SECR data appear to be relatively noisy. To fill data gaps hypsometric average models are applied, using the values of polynomials (degree 1 to 3) fitted to the observed hypsometric SECR. This is performed for ~~nine~~NPI ~~sub-~~at lar~~e~~g~~ionse~~ ~~i~~and for~~d~~ SPI separately ~~t~~for six o~~bf~~ the main ~~mass bag~~lan~~ce est~~i~~mat~~ers~~,~~ ~~i~~an~~clu~~d~~ing~~ two large ~~g~~sub-regio~~up~~ns each of which comprises many glaciers ~~(NPI,~~of ~~SPI-G1,~~different size and ~~SPI-G2)~~physiographic features. Therefore the resulting maps ~~n~~of SECR do~~n-~~ not reflect the~~g~~ complexi~~g~~ty and spati~~b~~al~~e~~ variability of ~~the~~ SECR ~~patt~~der~~n~~ived ~~a~~from~~on~~ high ~~ba~~resolution~~s~~ geodetic data, particularly at lower elevations.~~-~~

A comparison between~~ their~~ VCR estimates of Foresta et al. (2018) and our results for 2012–2016 is provided in Table S11. The two data sets do not cover exactly the same period. The ERA Interim 850 ~~H~~hPa data over NPI and SPI show for the average air temperature of the main ablation period (November to March) 2011 to 2017 an agreement within 0.1 °C ~~wi~~compared t~~h~~o 2012~~ to ~~–2016, suggesting similar rates of surface melt during the two epochs. Foresta et al. (2018) report a mass balance of -6.79 ± 1.16 Gt a^{-1} for NPI and ~~-14.5 ± 1.60~~-14.50 ± 1.60 Gt a^{-1} for SPI using 900 ± 125 kg m^{-3} for volume-to-mass conversion. This corresponds to a VCR of -7.54 ± 0.75 km^3 a^{-1} and -16.11 ± 1.43 km^3 a^{-1}, respectively. These numbers for volume lo~~s~~s~~e~~s are significantly higher than our results for epoch 2 in all sub-regions, being overall 35 % higher for NPI and 36

% for SPI. Foresta et al. (2018) show also time series of cumulative mean observed elevation change for the nine sub-regions. For NPI and five sub-regions of SPI ~~m~~the plots show in~~i~~ some years minima of the annual elevation ~~a~~dur~~e found ~~ing mid-winter ~~for some years~~. This is not compatible with both the annual cycle of surface mass balance and the seasonal variation of flow velocities on glacier tongues~~,~~ showing a trend for higher velocities in summer compa~~n~~red ~~low vel~~to~~cities in~~ winter (Stuefer et al., 2007; Minowa et al., 2017).

6 Conclusions

We report~~ed~~ on a detailed study focussing on the climate-sensitive Northern and Southern Patagonian icefields, where high resolution maps of surface elevation change were obtained for the epochs 2000–2012 and 2012–2016 from bistatic InSAR DEMs allowing to derive the total net mass balance of most of the glacier basins. We rely on a re-processed version of the SRTM C-band DEM featuring improved absolute height calibration and on a series of TanDEM-X Raw DEMs, processed with a robust phase unwrapping method, leading to almost complete coverage including narrow glaciers and high altitudes. Significant effort was dedicated to reduce systematic errors, especially critical for the mass balance of vast regions: a precise coregistration of the DEMs was performed, seasonal biases due to gaps in th~~e ord~~e~~r~~ ~~o~~full ~~metr~~annual cycle~~s~~ were corrected based on a complementary TDM summer SEC map, the backscatter coefficient of all acquisitions (including SRTM) was analy~~z~~sed to assess signal penetration. A comprehensive uncertainty estimation including all main error sources of the SEC maps and of the mass balance was also performed.

A similar pattern of elevation change is found on NPI for the two epochs, with lowering on most of the termini and well into the main ice plateau with~~ an~~ increased loss rates during ~~tem~~po~~ral~~ch ~~trend~~2. Being mass depletion mainly driven by surface melt on NPI, this trend is likely due to higher average air temperatures during epoch 2. The estimated volume change rate increased by 31 % from -4.26 ± 0.20 km^3 a^{-1} in epoch 1 to ~~-5.60 ± 0.71~~-5.60 ± 0.74 km^3 a^{-1} in epoch 2.

On SPI the spatial pattern and the temporal trend of SECR are more complex. The volume change rates decreased by 20 % from ~~-14.87 ± 0.51~~-14.87 ± 0.52 km^3 a^{-1} during epoch 1 to ~~-11.86 ± 1.90~~-11.86 ± 1.99 km^3 a^{-1} during epoch 2. Increased t~~rend of t~~hinning during epoch 2 is measured on ~~Upsal~~Bernardo, Jorge Montt and Viedma. Pio XI displays increased thickening up to 1500 m. On the accumulation areas south of $\sim 49.5°$ S the SECR was either stable or slightly negative during epoch 1, turning to slightly positive in epoch 2. Air temperature remained relatively stable at the south of SPI, meaning a north-south gradient was present. This, coupled with a possible local increase in snow accumulation may be the cause of the decreased loss rates at elevations above 1000 m. The more complex behaviour of SPI glaciers is caused by the relevance of calving fluxes as a source of mass turnover on this icefield, where the effect of ice dynamics on surface elevation changes extends to the main ice plateau. Significant frontal retreat was observed on SPI during epoch 1, ~~our~~Abdel Jaber (2016) ~~cor~~res~~s~~po~~n~~rted~~ing~~ a coarse estimation of subaqueous volume ~~l~~change o~~ss is~~f -0.73 ± 0.22 km^3 a^{-1} for the period 2000–2011/2012.

The eustatic sea level rise contribution of both icefields, excluding subaqueous changes, was estimated to be 0.048 ± 0.002 mm a^{-1} in epoch 1 and 0.043 ± 0.005 mm a^{-1} in epoch 2. Behind these numbers lies a complex interplay between surface mass balance, responding directly to climate change, and ice flow dynamics, mechanisms which regulate the heterogeneous spatial pattern and temporal evolution of the SEC on NPI and SPI.

This study confirms the potential of bistatic InSAR and particularly of the TanDEM-X mission for accurate, detailed and almost gapless mapping of surface elevation changes of large icefields even for small basins and tongues. We recommend the use of TanDEM-X data—with an appropriate coregistration and care for radar signal penetration—to map SEC of all types of glaciers, as recently shown also in the northern Antarctic Peninsula (Rott et al., 2018). We hope that our results will encourage the development of remote sensing missions capable of repeated bistatic InSAR observations allowing regular worldwide SEC mapping and mass balance estimations with improved temporal sampling.

Data availability. The SECR maps will be made available upon publication of the final version on http://cryoportal.enveo.at

Author contributions. WAJ, HR and DF conceived and designed the study. WAJ selected and processed the TanDEM-X DEMs and produced the results and their visualization. JW processed updated TerraSAR-X ice flow velocities. HR devised the seasonal correction and performed the glaciological analysis of the results. WAJ prepared the manuscript with contributions from all co-authors.

Competing interests. The authors declare that they have no conflict of interest.

Acknowledgements. The work was supported by the European Space Agency, ESA Contract No. 4000115896/15/I-LG, High Resolution SAR Algorithms for Mass Balance and Dynamics of Calving Glaciers (SAMBA). The TanDEM-X data were made available by DLR through the projects DEM_GLAC0787, XTI_GLAC0495, XTI_GLAC6663. We would like to thank Lukas Langhamer (Humboldt-Universitaet zu Berlin) for providing processed climate re-analysis data over the icefields.

<The following bibliography contains references included in both the old and the new version on the manuscript.>

References

Abdel Jaber, W.: Derivation of mass balance and surface velocity of glaciers by means of high resolution synthetic aperture radar: application to the Patagonian Icefields and Antarctica, Dissertation, Technische Universität München, http://elib.dlr.de/109075/, 2016.

Abdel Jaber, W., Floricioiu, D., Rott, H., and Eineder, M.: Dynamics of fast glaciers in the Patagonia Icefields derived from TerraSAR-X and TanDEM-X data, in: 2012 IEEE International Geoscience and Remote Sensing Symposium (IGARSS), pp. 3226–3229, 2012.

Abdel Jaber, W., Floricioiu, D., and Rott, H.: Glacier dynamics of the Northern Patagonia Icefield derived from SRTM, TanDEM-X and TerraSAR-X data, in: 2014 IEEE International Geoscience and Remote Sensing Symposium (IGARSS), pp. 4018–4021, 2014.

Åström, J. A., Vallot, D., Schäfer, M., Welty, E. Z., O'Neel, S., Bartholomaus, T., Liu, Y., Riikilä, T. I., Zwinger, T., Timonen, J., and Moore, J. C.: Termini of calving glaciers as self-organized critical systems, Nature Geoscience, 7, 874–878, 2014.

Benn, D. I., Warren, C. R., and Mottram, R. H.: Calving processes and the dynamics of calving glaciers, Earth-Science Reviews, 82, 143–179, 2007.

Berrisford, P., Dee, D., Poli, P., Brugge, R., Fielding, K., Fuentes, M., Kållberg, P., Kobayashi, S., Uppala, S., and Simmons, A.: The ERA-Interim archive, version 2.0, ERA Report Series, p. 23, https://www.ecmwf.int/en/elibrary/8174-era-interim-archive-version-20, 2011.

Bippus, G.: Modelling mass balance and climate sensitivity of glaciers of the Southern Patagonia Icefield, Master's thesis, Institute of Meteorology and Geophysics, University of Innsbruck, 2007.

Braun, M. H., Malz, P., Sommer, C., Farías-Barahona, D., Sauter, T., Casassa, G., Soruco, A., Skvarca, P., and Seehaus, T. C.: Constraining glacier elevation and mass changes in South America, Nature Climate Change, 9, 130, 2019.

Bravo, C., Quincey, D., Ross, A., Rivera, A., Brock, B., Miles, E., and Silva, A.: Air Temperature Characteristics, Distribution, and Impact on Modeled Ablation for the South Patagonia Icefield, Journal of Geophysical Research: Atmospheres, 124, 907–925, 2019.

Breit, H., Lachaise, M., Balss, U., Rossi, C., Fritz, T., and Niedermeier, A.: Bistatic and interferometric processing of TanDEM-X data, in: EUSAR 2012; 9th European Conference on Synthetic Aperture Radar, pp. 93–96, 2012.

Brown, C. G., Sarabandi, K., and Pierce, L. E.: Validation of the shuttle radar topography mission height data, IEEE Transactions on Geoscience and Remote Sensing, 43, 1707–1715, 2005.

Carabajal, C. C. and Harding, D. J.: SRTM C-band and ICESat laser altimetry elevation comparisons as a function of tree cover and relief, Photogrammetric Engineering and Remote Sensing, 72, 287–298, 2006.

Cazenave, A., Meyssignac, B., Ablain, M., Balmaseda, M., Bamber, J., Barletta, V., Beckley, B., Benveniste, J., Berthier, E., Blazquez, A., et al.: Global sea-level budget 1993-present, Earth System Science Data, 10, 1551–1590, 2018.

Chen, J. L., Wilson, C. R., Tapley, B. D., Blankenship, D. D., and Ivins, E. R.: Patagonia icefield melting observed by gravity recovery and climate experiment (GRACE), Geophysical Research Letters, 34, 2007.

Cogley, J. G.: Geodetic and direct mass-balance measurements: comparison and joint analysis, Annals of Glaciology, 50, 96–100, 2009.

Crippen, R., Buckley, S., Agram, P., Belz, E., Gurrola, E., Hensley, S., Kobrick, M., Lavalle, M., Martin, J., Neumann, M., et al.: NASADEM Global Elevation Model: Methods And Progress, ISPRS - International Archives of the Photogrammetry, Remote Sensing and Spatial Information Sciences, XLI-B4, 125–128, https://doi.org/10.5194/isprs-archives-XLI-B4-125-2016, 2016.

Dall, J.: InSAR elevation bias caused by penetration into uniform volumes, IEEE Transactions on Geoscience and Remote Sensing, 45, 2319–2324, 2007.

Davies, B. J. and Glasser, N. F.: Accelerating shrinkage of Patagonian glaciers from the Little Ice Age (˜AD 1870) to 2011, Journal of Glaciology, 58, 1063–1084, 2012.

Dee, D. P., Uppala, S. M., Simmons, A. J., Berrisford, P., Poli, P., Kobayashi, S., Andrae, U., Balmaseda, M. A., Balsamo, G., Bauer, P., et al.: The ERA-Interim reanalysis: configuration and performance of the data assimilation system, Quarterly Journal of the Royal Meteorological Society, 137, 553–597, https://doi.org/10.1002/qj.828, 2011.

Dietrich, R., Ivins, E., Casassa, G., Lange, H., Wendt, J., and Fritsche, M.: Rapid crustal uplift in Patagonia due to enhanced ice loss, Earth and Planetary Science Letters, 289, 22–29, 2010.

DLR-CAF: TanDEM-X Ground Segment - Raw DEM Specification (Project Internal), German Aerospace Center (DLR) - Cluster Applied Remote Sensing (CAF), CAF, DLR, Oberpfaffenhofen, Germany, 1.1 edn., doc. TD-PGS-TN-3081, 2010.

DLR-CAF: TerraSAR-X Ground Segment - Basic Product Specification Document, German Aerospace Center (DLR) - Cluster Applied Remote Sensing (CAF), CAF, DLR, Oberpfaffenhofen, Germany, 1.9 edn., doc. TX-GS-DD-3302, 2013.

DLR-EOC: TanDEM-X Ground Segment - DEM Products Specification Document, German Aerospace Center (DLR) - Earth Observation Center (EOC), EOC, DLR, Oberpfaffenhofen, Germany, 3.2 edn., https://tandemx-science.dlr.de/, doc. TD-GS-PS-0021, 2018.

Dowdeswell, J. and Vásquez, M.: Submarine landforms in the fjords of southern Chile: implications for glacimarine processes and sedimentation in a mild glacier-influenced environment, Quaternary Science Reviews, 64, 1–19, 2013.

Dussaillant, I., Berthier, E., and Brun, F.: Geodetic Mass Balance of the Northern Patagonian Icefield from 2000 to 2012 using two independent methods, Frontiers in Earth Science, 6, 8, 2018.

Farr, T. G., Rosen, P. A., Caro, E., Crippen, R., Duren, R., Hensley, S., Kobrick, M., Paller, M., Rodriguez, E., Roth, L., et al.: The Shuttle Radar Topography Mission, Reviews of Geophysics, 45, 2007.

Fernández, A. and Mark, B. G.: Modeling modern glacier response to climate changes along the Andes Cordillera: A multiscale review, Journal of Advances in Modeling Earth Systems, 8, 467–495, 2016.

Floricioiu, D. and Rott, H.: Seasonal and short-term variability of multifrequency, polarimetric radar backscatter of alpine terrain from SIR-C/X-SAR and AIRSAR data, IEEE Transactions on Geoscience and Remote Sensing, 39, 2634–2648, 2001.

Foresta, L., Gourmelen, N., Weissgerber, F., Nienow, P., Williams, J., Shepherd, A., Drinkwater, M., and Plummer, S.: Heterogeneous and rapid ice loss over the Patagonian Ice Fields revealed by CryoSat-2 swath radar altimetry, Remote Sensing of Environment, 211, 441–455, 2018.

Fritz, T., Rossi, C., Yague-Martinez, N., Rodriguez-Gonzalez, F., Lachaise, M., and Breit, H.: Interferometric processing of TanDEM-X data, in: 2011 IEEE International Geoscience and Remote Sensing Symposium (IGARSS), pp. 2428–2431, 2011.

Garreaud, R., Lopez, P., Minvielle, M., and Rojas, M.: Large-scale control on the Patagonian climate, Journal of Climate, 26, 215–230, 2013.

Glasser, N. F., Harrison, S., Jansson, K. N., Anderson, K., and Cowley, A.: Global sea-level contribution from the Patagonian Icefields since the Little Ice Age maximum, Nature Geoscience, 4, 303–307, 2011.

Hueso González, J., Bachmann, M., Krieger, G., and Fiedler, H.: Development of the TanDEM-X calibration concept: analysis of systematic errors, IEEE Transactions on Geoscience and Remote Sensing, 48, 716–726, 2010.

Ivins, E. R., Watkins, M. M., Yuan, D.-N., Dietrich, R., Casassa, G., and Rülke, A.: On-land ice loss and glacial isostatic adjustment at the Drake Passage: 2003-2009, Journal of Geophysical Research: Solid Earth, 116, https://doi.org/10.1029/2010JB007607, 2011.

Jacob, T., Wahr, J., Pfeffer, W. T., and Swenson, S.: Recent contributions of glaciers and ice caps to sea level rise, Nature, 482, 514–518, 2012.

Kalnay, E., Kanamitsu, M., Kistler, R., Collins, W., Deaven, D., Gandin, L., Iredell, M., Saha, S., White, G., Woollen, J., et al.: The NCEP/NCAR 40-year reanalysis project, Bulletin of the American Meteorological Society, 77, 437–471, 1996.

Krieger, G., Moreira, A., Fiedler, H., Hajnsek, I., Werner, M., Younis, M., and Zink, M.: TanDEM-X: A satellite formation for high-resolution SAR interferometry, IEEE Transactions on Geoscience and Remote Sensing, 45, 3317–3341, 2007.

Lachaise, M.: Phase Unwrapping of Multi-Channel Synthetic Aperture Radar Data: Application to the TanDEM-X Mission, Ph.D. thesis, Technische Universität München, http://elib.dlr.de/100297/, 2015.

Lachaise, M. and Fritz, T.: Phase unwrapping strategy and assessment for the high resolution DEMs of the TanDEM-X mission, in: 2016 IEEE International Geoscience and Remote Sensing Symposium (IGARSS), pp. 3223–3226, 2016.

Langhamer, L.: Lagrangian Detection of Moisture Sources for the Southern Patagonia Icefield, Master's thesis, Faculty for Geo- and Atmospheric Sciences, University of Innsbruck, Austria, 2017.

Langhamer, L., Sauter, T., and Mayr, G. J.: Lagrangian Detection of Moisture Sources for the Southern Patagonia Icefield (1979-2017), Frontiers in Earth Science, 6, 219, 2018.

Lee, J.-S., Hoppel, K. W., Mango, S. A., and Miller, A. R.: Intensity and phase statistics of multilook polarimetric and interferometric SAR imagery, IEEE Transactions on Geoscience and Remote Sensing, 32, 1017–1028, 1994.

Lopez, P., Chevallier, P., Favier, V., Pouyaud, B., Ordenes, F., and Oerlemans, J.: A regional view of fluctuations in glacier length in southern South America, Global and Planetary Change, 71, 85–108, 2010.

Malz, P., Meier, W., Casassa, G., Jaña, R., Skvarca, P., and Braun, M. H.: Elevation and mass changes of the Southern Patagonia Icefield derived from TanDEM-X and SRTM Data, Remote Sensing, 10, 188, 2018.

Marzeion, B., Champollion, N., Haeberli, W., Langley, K., Leclercq, P., and Paul, F.: Observation-Based Estimates of Global Glacier Mass Change and its Contribution to Sea-Level Change, Surveys in Geophysics, 38, 105–130, https://doi.org/10.1007/s10712-016-9394-y, 2017.

Mätzler, C.: Applications of the interaction of microwaves with the natural snow cover, Remote Sensing Reviews, 2, 259–387, 1987.

Minowa, M., Sugiyama, S., Sakakibara, D., and Skvarca, P.: Seasonal variations in ice-front position controlled by frontal ablation at Glaciar Perito Moreno, the Southern Patagonia Icefield, Frontiers in earth science, 5, 1, 2017.

Mouginot, J. and Rignot, E.: Ice motion of the Patagonian Icefields of South America: 1984–2014, Geophysical Research Letters, 42, 1441–1449, 2015.

Nagler, T. and Rott, H.: Retrieval of wet snow by means of multitemporal SAR data, IEEE Transactions on Geoscience and Remote Sensing, 38, 754–765, 2000.

NASA JPL: NASA Shuttle Radar Topography Mission Global 1 arc second [Data set]. NASA EOSDIS Land Processes DAAC., https://doi.org/10.5067/MEaSUREs/SRTM/SRTMGL1.003, 2013.

NASA JPL: NASA Shuttle Radar Topography Mission Swath Image Data [Data set]. NASA EOSDIS Land Processes DAAC., https://doi.org/10.5067/MEaSUREs/SRTM/SRTMIMGR.003, 2014.

NASA JPL: NASADEM Global Elevation Model (provisional), https://e4ftl01.cr.usgs.gov/provisional/MEaSUREs/NASADEM, accessed 31/1/2018, 2018.

Nuth, C. and Kääb, A.: Co-registration and bias corrections of satellite elevation data sets for quantifying glacier thickness change, The Cryosphere, 5, 271–290, 2011.

Paul, F., Barrand, N. E., Baumann, S., Berthier, E., Bolch, T., Casey, K., Frey, H., Joshi, S. P., Konovalov, V., Bris, R. L., et al.: On the accuracy of glacier outlines derived from remote-sensing data, Annals of Glaciology, 54, 171–182, 2013.

Pfeffer, W. T., Arendt, A. A., Bliss, A., Bolch, T., Cogley, J. G., Gardner, A. S., Hagen, J.-O., Hock, R., Kaser, G., Kienholz, C., et al.: The Randolph Glacier Inventory: a globally complete inventory of glaciers, Journal of Glaciology, 60, 537–552, 2014.

Rabus, B., Eineder, M., Roth, A., and Bamler, R.: The shuttle radar topography mission - a new class of digital elevation models acquired by spaceborne radar, ISPRS Journal of Photogrammetry and Remote Sensing, 57, 241–262, 2003.

Rasmussen, L. A., Conway, H., and Raymond, C. F.: Influence of upper air conditions on the Patagonia icefields, Global and Planetary Change, 59, 203–216, 2007.

Reber, B., Mätzler, C., and Schanda, E.: Microwave signatures of snow crusts modelling and measurements, International Journal of Remote Sensing, 8, 1649–1665, 1987.

RGI Consortium: Randolph Glacier Inventory–A Dataset of Global Glacier Outlines: Version 6.0: Technical Report, Global Land Ice Measurements from Space, Colorado, USA, Digital Media. https://doi.org/10.7265, 2017.

Rignot, E., Rivera, A., and Casassa, G.: Contribution of the Patagonia Icefields of South America to sea level rise, Science, 302, 434–437, 2003.

Rivera, A.: Mass balance investigations at Glaciar Chico, Southern Patagonia Icefield, Chile, Ph.D. thesis, University of Bristol, 2004.

Rivera, A., Benham, T., Casassa, G., Bamber, J., and Dowdeswell, J. A.: Ice elevation and areal changes of glaciers from the Northern Patagonia Icefield, Chile, Global and Planetary Change, 59, 126–137, 2007.

Rivera, A., Koppes, M., Bravo, C., and Aravena, J. C.: Little ice age advance and retreat of Glaciar Jorge Montt, Chilean Patagonia, Climate of the Past, 8, 403–414, 2012.

Rizzoli, P., Martone, M., Gonzalez, C., Wecklich, C., Tridon, D. B., Bräutigam, B., Bachmann, M., Schulze, D., Fritz, T., Huber, M., et al.: Generation and performance assessment of the global TanDEM-X digital elevation model, ISPRS Journal of Photogrammetry and Remote Sensing, 132, 119–139, 2017.

Rodriguez, E., Morris, C. S., Belz, J. E., Chapin, E. C., Martin, J. M., Daffer, W., and Hensley, S.: An assessment of the SRTM topographic products, Tech. Rep. D-31639, Jet Propulsion Laboratory, 2005.

Rolstad, C., Haug, T., and Denby, B.: Spatially integrated geodetic glacier mass balance and its uncertainty based on geostatistical analysis: application to the western Svartisen ice cap, Norway, Journal of Glaciology, 55, 666–680, 2009.

Rossi, C., Eineder, M., Fritz, T., and Breit, H.: TanDEM-X Mission: Raw DEM Generation, in: EUSAR 2010; 8th European Conference on Synthetic Aperture Radar, pp. 1–4, 2010.

Rossi, C., Rodriguez-Gonzalez, F., Fritz, T., Yague-Martinez, N., and Eineder, M.: TanDEM-X calibrated Raw DEM generation, ISPRS Journal of Photogrammetry and Remote Sensing, 73, 12–20, 2012.

Rott, H., Abdel Jaber, W., Wuite, J., Scheiblauer, S., Floricioiu, D., van Wessem, J. M., Nagler, T., Miranda, N., and van den Broeke, M. R.: Changing pattern of ice flow and mass balance for glaciers discharging into the Larsen A and B embayments, Antarctic Peninsula, 2011 to 2016, The Cryosphere, 12, 1273–1291, https://doi.org/10.5194/tc-12-1273-2018, 2018.

Schaefer, M., Machguth, H., Falvey, M., and Casassa, G.: Modeling past and future surface mass balance of the Northern Patagonia Icefield, Journal of Geophysical Research: Earth Surface, 118, 571–588, 2013.

Seal, D. and Rogez, F.: SRTM As-Flown Mission Timeline, Tech. rep., JPL NASA, http://www2.jpl.nasa.gov/srtm/SRTM_TIM_AF.pdf, 2000.

Stiles, W. H. and Ulaby, F. T.: The active and passive microwave response to snow parameters: 1. Wetness, Journal of Geophysical Research: Oceans, 85, 1037–1044, 1980.

Stuefer, M., Rott, H., and Skvarca, P.: Glaciar Perito Moreno, Patagonia: climate sensitivities and glacier characteristics preceding the 2003/04 and 2005/06 damming events, Journal of Glaciology, 53, 3–16, 2007.

Tiuri, M. E., Sihvola, A. H., Nyfors, E. G., and Hallikaiken, M. T.: The complex dielectric constant of snow at microwave frequencies, IEEE Journal of Oceanic Engineering, 9, 377–382, 1984.

Ulaby, F. T. and Stiles, W. H.: Microwave response of snow, Advances in Space Research, 1, 131–149, 1981.

Ulaby, F. T., Long, D. G., Blackwell, W. J., Elachi, C., Fung, A. K., Ruf, C., Sarabandi, K., Zebker, H. A., and Van Zyl, J.: Microwave radar and radiometric remote sensing, vol. 4, University of Michigan Press Ann Arbor, 2014.

Warren, C. and Aniya, M.: The calving glaciers of southern South America, Global and Planetary Change, 22, 59–77, 1999.

Weidemann, S. S., Sauter, T., Malz, P., Jaña, R. A., Arigony-Neto, J., Casassa, G., and Schneider, C.: Glacier mass changes of lake-terminating Grey and Tyndall glaciers at the Southern Patagonia Icefield derived from geodetic observations and energy and mass balance modeling, Frontiers in Earth Science, 6, 81, 2018.

Wendleder, A., Felbier, A., Wessel, B., Huber, M., and Roth, A.: A Method to Estimate Long-Wave Height Errors of SRTM C-Band DEM, IEEE Geoscience and Remote Sensing Letters, 13, 696–700, https://doi.org/10.1109/LGRS.2016.2538822, 2016.

Wessel, B., Huber, M., Wohlfart, C., Marschalk, U., Kosmann, D., and Roth, A.: Accuracy assessment of the global TanDEM-X Digital Elevation Model with GPS data, ISPRS Journal of Photogrammetry and Remote Sensing, 139, 171–182, 2018.

Willis, M. J., Melkonian, A. K., Pritchard, M. E., and Ramage, J. M.: Ice loss rates at the Northern Patagonian Icefield derived using a decade of satellite remote sensing, Remote Sensing of Environment, 117, 184–198, 2012a.

Willis, M. J., Melkonian, A. K., Pritchard, M. E., and Rivera, A.: Ice loss from the Southern Patagonian Ice Field, South America, between 2000 and 2012, Geophysical Research Letters, 39, 2012b.

Wilson, R., Carrión, D., and Rivera, A.: Detailed dynamic, geometric and supraglacial moraine data for Glaciar Pio XI, the only surge-type glacier of the Southern Patagonia Icefield, Annals of Glaciology, 57, 119–130, 2016.

Wuite, J., Rott, H., Hetzenecker, M., Floricioiu, D., de Rydt, J., Gudmundsson, H., Nagler, T., and Kern, M.: Evolution of surface velocities and ice discharge of Larsen B outlet glaciers from 1995 to 2013, The Cryosphere, 9, 957–969, 2015.

Table 1. Results over NPI and SPI for the two epochs. The reported area refers to the beginning of the epoch, the coverage of the SECR map is also reported. Subaqueous ice changes are not included. <This table reports updated uncertainties.>

Icefield	Period	Area $\left[\mathrm{km}^2\right]$	Cov. [%]	Average SECR $\left[\mathrm{m\,a}^{-1}\right]$	Volume change $\left[\mathrm{km}^3\,\mathrm{a}^{-1}\right]$	Mass change $\left[\mathrm{Gt\,a}^{-1}\right]$	Sea level rise $\left[\mu\mathrm{m\,a}^{-1}\right]$
NPI	2000–2012	3975.3	95.4	-1.072 ± 0.049	-4.261 ± 0.196	-3.835 ± 0.236	10.594 ± 0.653
NPI	2012–2016	3914.2	89.8	-1.431 ± 0.188	-5.602 ± 0.735	-5.042 ± 0.693	13.927 ± 1.915
SPI	2000–2012	12999.0	98.0	-1.143 ± 0.040	-14.874 ± 0.518	-13.386 ± 0.712	36.979 ± 1.966
SPI	2012–2016	12846.8	97.0	-0.923 ± 0.155	-11.860 ± 1.987	-10.674 ± 1.839	29.485 ± 5.079

Table 2. Average surface elevation change rate (SECR) and volume change rate (VCR) for NPI and its glaciers larger than 2 km^2 for the two epochs. The reported area refers to the beginning of the epoch, the coverage of the SECR map is also reported. Subaqueous ice changes are not included. <This table reports updated uncertainties.>

RGI Name	2000–2012				2012–2016			
	Area $[km^2]$	Cov. [%]	Average SECR $[m\,a^{-1}]$	Volume change $[km^3\,a^{-1}]$	Area $[km^2]$	Cov. [%]	Average SECR $[m\,a^{-1}]$	Volume change $[km^3\,a^{-1}]$
NPI	3975.3	95.4	−1.072 ± 0.049	−4.2609 ± 0.1955	3914.2	89.8	−1.431 ± 0.188	−5.6018 ± 0.7346
San Quintin	791.7	99.3	−0.758 ± 0.040	−0.5999 ± 0.0313	773.1	99.0	−1.188 ± 0.153	−0.9182 ± 0.1184
San Rafael	724.6	98.5	−1.117 ± 0.058	−0.8094 ± 0.0420	717.7	98.5	−1.213 ± 0.195	−0.8706 ± 0.1396
Steffen	430.0	98.6	−1.669 ± 0.051	−0.7178 ± 0.0217	421.0	97.8	−2.120 ± 0.146	−0.8926 ± 0.0615
Colonia	291.2	96.5	−0.859 ± 0.042	−0.2502 ± 0.0123	288.0	85.0	−1.010 ± 0.154	−0.2909 ± 0.0445
Acodado	269.8	98.2	−1.710 ± 0.051	−0.4614 ± 0.0138	265.3	96.9	−2.367 ± 0.147	−0.6279 ± 0.0390
Benito	163.4	98.7	−1.500 ± 0.047	−0.2452 ± 0.0077	158.9	97.6	−1.972 ± 0.148	−0.3133 ± 0.0236
HPN 1	154.0	98.4	−2.498 ± 0.062	−0.3847 ± 0.0095	149.2	95.2	−3.249 ± 0.155	−0.4847 ± 0.0230
Nef	128.8	93.5	−0.750 ± 0.040	−0.0966 ± 0.0052	128.4	76.6	−1.045 ± 0.161	−0.1343 ± 0.0207
Gualas	128.3	96.9	−1.148 ± 0.044	−0.1468 ± 0.0056	124.6	95.6	−1.543 ± 0.168	−0.1922 ± 0.0209
Exploradores	86.4	57.9	−0.357 ± 0.049	−0.0308 ± 0.0042	86.4	57.3	−1.187 ± 0.170	−0.1025 ± 0.0146
Pared Norte	84.4	90.7	−1.339 ± 0.047	−0.1130 ± 0.0039	84.2	57.1	−1.369 ± 0.181	−0.1153 ± 0.0153
Reichert	73.2	90.1	−0.869 ± 0.044	−0.0636 ± 0.0032	71.9	87.1	−0.931 ± 0.147	−0.0669 ± 0.0106
Grosse	66.8	78.7	−0.763 ± 0.047	−0.0510 ± 0.0031	66.7	84.6	−1.320 ± 0.151	−0.0880 ± 0.0101
Leones	66.2	94.4	0.231 ± 0.040	0.0153 ± 0.0026	66.2	68.2	0.313 ± 0.163	0.0207 ± 0.0108
HPN 4	65.7	97.9	−1.237 ± 0.045	−0.0813 ± 0.0030	65.7	92.7	−1.444 ± 0.149	−0.0948 ± 0.0098
Soler	50.4	95.3	−0.386 ± 0.039	−0.0194 ± 0.0020	50.5	75.2	−0.493 ± 0.161	−0.0249 ± 0.0082
Fiero	43.2	57.9	−0.482 ± 0.063	−0.0209 ± 0.0027	41.7	43.6	−0.949 ± 0.188	−0.0395 ± 0.0078
Cachet	37.2	95.5	−0.254 ± 0.041	−0.0094 ± 0.0015	36.9	86.7	−0.360 ± 0.150	−0.0133 ± 0.0055
Pared Sur	33.5	92.4	−1.210 ± 0.048	−0.0405 ± 0.0016	33.5	70.3	−1.543 ± 0.179	−0.0517 ± 0.0060
Fraenkel	31.5	99.6	−0.547 ± 0.041	−0.0173 ± 0.0013	30.9	97.5	−0.855 ± 0.141	−0.0264 ± 0.0044
Arco	26.3	97.8	−0.326 ± 0.038	−0.0086 ± 0.0010	26.3	85.5	−0.113 ± 0.167	−0.0030 ± 0.0044
U-3	17.8	99.2	0.046 ± 0.045	0.0008 ± 0.0008	17.8	53.5	−0.092 ± 0.196	−0.0016 ± 0.0035
Strindberg	16.9	99.3	−0.510 ± 0.044	−0.0086 ± 0.0007	16.5	98.4	−1.284 ± 0.142	−0.0212 ± 0.0023
U-2	15.9	90.4	−0.031 ± 0.052	−0.0005 ± 0.0008	15.9	53.3	−0.151 ± 0.185	−0.0024 ± 0.0029
Bayo	13.7	41.9	−0.413 ± 0.061	−0.0057 ± 0.0008	13.7	27.6	−0.754 ± 0.191	−0.0104 ± 0.0026
U-4	13.4	87.1	−1.185 ± 0.057	−0.0159 ± 0.0008	13.4	67.4	−1.414 ± 0.171	−0.0190 ± 0.0023
Pissis	13.4	92.9	−0.455 ± 0.049	−0.0061 ± 0.0007	13.1	41.8	−0.382 ± 0.209	−0.0050 ± 0.0027
U-6	10.8	69.6	−0.332 ± 0.068	−0.0036 ± 0.0007	10.8	26.9	0.167 ± 0.208	0.0018 ± 0.0023
Cachet Norte	10.2	86.7	0.135 ± 0.056	0.0014 ± 0.0006	10.2	54.2	−0.280 ± 0.177	−0.0029 ± 0.0018
Hyades	7.7	80.7	0.735 ± 0.081	0.0056 ± 0.0006	7.7	3.8	0.935 ± 0.502	0.0072 ± 0.0039
RGI-17.15835	7.6	80.5	0.097 ± 0.086	0.0007 ± 0.0007	7.6	30.9	−1.210 ± 0.237	−0.0092 ± 0.0018
Verde	7.0	78.4	−0.094 ± 0.080	−0.0007 ± 0.0006	6.9	83.9	−0.631 ± 0.171	−0.0044 ± 0.0012
RGI-17.15869	6.4	99.9	−0.069 ± 0.057	−0.0004 ± 0.0004	6.4	71.6	−0.023 ± 0.156	−0.0001 ± 0.0010
Cristal	5.7	94.0	−0.091 ± 0.059	−0.0005 ± 0.0003	5.6	69.6	0.201 ± 0.171	0.0011 ± 0.0010
U-5	5.6	92.3	−0.614 ± 0.062	−0.0034 ± 0.0003	5.6	45.4	−0.252 ± 0.186	−0.0014 ± 0.0010
Andree	6.0	100.0	−0.688 ± 0.057	−0.0041 ± 0.0003	5.4	99.8	−1.114 ± 0.147	−0.0061 ± 0.0008
Mocho	5.3	91.1	0.329 ± 0.078	0.0018 ± 0.0004	5.3	23.5	0.831 ± 0.244	0.0044 ± 0.0013
RGI-17.15816	5.1	67.5	−0.102 ± 0.110	−0.0005 ± 0.0006	5.1	61.6	−0.444 ± 0.215	−0.0023 ± 0.0011
RGI-17.15827	4.5	87.5	0.087 ± 0.087	0.0004 ± 0.0004	4.5	85.0	−0.681 ± 0.174	−0.0030 ± 0.0008
U-7	3.1	88.7	0.956 ± 0.110	0.0029 ± 0.0003	3.1	3.2	1.292 ± 0.861	0.0039 ± 0.0026
Circo	2.9	62.6	0.044 ± 0.113	0.0001 ± 0.0003	2.9	66.8	−0.592 ± 0.197	−0.0017 ± 0.0006
RGI-17.15812	2.6	100.0	0.469 ± 0.073	0.0012 ± 0.0002	2.6	99.3	−0.519 ± 0.195	−0.0014 ± 0.0005
Mormex	2.5	87.1	−0.552 ± 0.125	−0.0014 ± 0.0003	2.5	80.1	−1.349 ± 0.203	−0.0034 ± 0.0005
RGI-17.15850	2.3	56.4	−0.515 ± 0.176	−0.0012 ± 0.0004	2.3	22.0	0.196 ± 0.348	0.0004 ± 0.0008
RGI-17.15868	2.0	100.0	−0.194 ± 0.077	−0.0004 ± 0.0002	2.0	61.0	0.196 ± 0.181	0.0004 ± 0.0004

Table 3. Average surface elevation change rate (SECR) and volume change rate (VCR) for SPI and its glaciers larger than 35 km^2 for the two epochs. The reported area refers to the beginning of the epoch, the coverage of the SECR map is also reported. Subaqueous ice changes are not included. The list is continued for glaciers up to 9 km^2 in Table S8 in the Supplement. <This table reports updated uncertainties, the same applies for Table S8 in the Supplement.>

RGI Name	2000–2012				2012–2016			
	Area [km^2]	Cov. [%]	Average SECR [m a^{-1}]	Volume change [km^3 a^{-1}]	Area [km^2]	Cov. [%]	Average SECR [m a^{-1}]	Volume change [km^3 a^{-1}]
SPI	12999.0	98.0	−1.143 ± 0.040	−14.8738 ± 0.5175	12846.8	97.0	−0.923 ± 0.155	−11.8595 ± 1.9871
Pio XI	1237.6	99.4	0.420 ± 0.036	0.5232 ± 0.0449	1246.7	98.5	1.010 ± 0.198	1.2593 ± 0.2470
Viedma	978.8	98.4	−1.987 ± 0.051	−1.9446 ± 0.0501	971.3	98.9	−2.291 ± 0.131	−2.2251 ± 0.1276
Upsala + Cono	848.9	99.2	−3.331 ± 0.076	−2.8278 ± 0.0643	823.5	99.3	−3.039 ± 0.131	−2.5021 ± 0.1077
OHiggins	765.0	99.7	−1.164 ± 0.037	−0.8902 ± 0.0283	764.6	98.2	−1.110 ± 0.158	−0.8484 ± 0.1211
Bernardo	540.7	99.9	−1.319 ± 0.037	−0.7129 ± 0.0202	531.6	99.7	−1.717 ± 0.203	−0.9126 ± 0.1080
Jorge Montt	491.9	99.8	−4.008 ± 0.084	−1.9714 ± 0.0415	471.2	98.6	−4.947 ± 0.216	−2.3309 ± 0.1017
Penguin	469.8	99.7	−0.117 ± 0.035	−0.0551 ± 0.0163	469.8	99.2	0.359 ± 0.124	0.1687 ± 0.0583
Greve	428.9	99.8	−1.867 ± 0.046	−0.8007 ± 0.0198	419.2	99.4	−2.006 ± 0.193	−0.8410 ± 0.0808
Europa	405.9	99.7	−0.276 ± 0.032	−0.1122 ± 0.0132	405.8	99.3	0.322 ± 0.109	0.1307 ± 0.0443
Tempano	334.2	100.0	−1.861 ± 0.045	−0.6218 ± 0.0151	327.0	99.8	−2.189 ± 0.192	−0.7157 ± 0.0626
Grey + Dickson	310.0	99.8	−1.429 ± 0.044	−0.4430 ± 0.0135	304.4	96.4	−0.239 ± 0.121	−0.0726 ± 0.0367
Tyndall	311.0	99.3	−2.525 ± 0.059	−0.7851 ± 0.0182	302.2	98.4	−1.591 ± 0.095	−0.4809 ± 0.0287
Perito Moreno	263.5	96.4	−0.246 ± 0.039	−0.0649 ± 0.0104	263.5	92.3	0.379 ± 0.210	0.0998 ± 0.0554
Chico	239.6	99.6	−1.141 ± 0.035	−0.2735 ± 0.0085	238.2	99.4	−1.519 ± 0.105	−0.3619 ± 0.0249
Occidental	233.1	99.6	−2.681 ± 0.059	−0.6251 ± 0.0137	222.6	94.0	−2.883 ± 0.193	−0.6416 ± 0.0430
HPS 13	213.8	99.9	−0.136 ± 0.045	−0.0291 ± 0.0095	213.8	99.7	0.180 ± 0.147	0.0384 ± 0.0314
HPS 31	167.0	95.0	−0.200 ± 0.037	−0.0333 ± 0.0062	167.1	92.6	0.116 ± 0.174	0.0193 ± 0.0291
Guilardi	165.7	99.6	−0.446 ± 0.034	−0.0740 ± 0.0056	165.5	99.2	0.212 ± 0.105	0.0350 ± 0.0174
HPS 19	163.2	99.8	−0.036 ± 0.035	−0.0058 ± 0.0057	163.2	99.4	0.313 ± 0.120	0.0510 ± 0.0197
Lucia	164.6	98.4	−0.806 ± 0.032	−0.1326 ± 0.0053	162.3	97.0	−1.097 ± 0.195	−0.1780 ± 0.0316
Amalia	163.5	100.0	−0.712 ± 0.034	−0.1164 ± 0.0055	161.1	99.7	−0.169 ± 0.124	−0.0273 ± 0.0200
HPS 12	165.5	89.6	−5.055 ± 0.096	−0.8365 ± 0.0159	155.0	85.6		
HPS 34	153.2	99.1	−0.229 ± 0.032	−0.0351 ± 0.0050	153.2	98.2	0.280 ± 0.131	0.0429 ± 0.0200
Spegazzini	120.0	98.1	−0.245 ± 0.028	−0.0295 ± 0.0034	120.0	98.3	0.216 ± 0.107	0.0259 ± 0.0129
Asia	113.7	99.8	−0.331 ± 0.031	−0.0376 ± 0.0035	113.7	99.2	0.142 ± 0.094	0.0162 ± 0.0106
Calvo	104.3	98.2	−0.250 ± 0.041	−0.0260 ± 0.0043	104.3	93.6	0.528 ± 0.196	0.0551 ± 0.0204
Bravo	104.7	99.6	−1.083 ± 0.035	−0.1135 ± 0.0037	102.5	99.3	−1.185 ± 0.182	−0.1215 ± 0.0186
HPS 15	99.3	99.8	−0.081 ± 0.036	−0.0081 ± 0.0035	99.3	99.6	−0.023 ± 0.131	−0.0023 ± 0.0130
Ofhidro	84.1	99.9	−0.531 ± 0.028	−0.0447 ± 0.0024	81.2	99.7	−1.188 ± 0.181	−0.0964 ± 0.0147
Pascua	81.9	98.9	−1.740 ± 0.045	−0.1425 ± 0.0037	79.6	96.3	−2.263 ± 0.189	−0.1802 ± 0.0151
HPS 29	79.4	98.4	−0.170 ± 0.032	−0.0135 ± 0.0026	79.4	97.9	0.347 ± 0.102	0.0276 ± 0.0081
HPS 41	79.9	94.6	−1.327 ± 0.042	−0.1061 ± 0.0033	73.0	85.9	0.195 ± 0.093	0.0143 ± 0.0068
RGI-17.04863	75.3	99.6	−2.597 ± 0.061	−0.1954 ± 0.0046	71.9	96.6	−1.881 ± 0.129	−0.1353 ± 0.0092
Pingo	70.2	99.8	−0.581 ± 0.032	−0.0408 ± 0.0023	69.7	99.1	0.745 ± 0.083	0.0519 ± 0.0058
HPS 28	68.7	96.0	−0.365 ± 0.034	−0.0251 ± 0.0023	68.7	97.4	0.351 ± 0.115	0.0241 ± 0.0079
HPS 10	67.6	96.1	−0.492 ± 0.031	−0.0333 ± 0.0021	66.8	92.7	−0.390 ± 0.194	−0.0260 ± 0.0130
RGI-17.04982	62.0	99.8	−0.143 ± 0.028	−0.0088 ± 0.0017	62.0	98.6	0.209 ± 0.104	0.0130 ± 0.0065
Ameghino	59.8	92.9	−2.002 ± 0.053	−0.1198 ± 0.0031	59.3	93.0	−1.930 ± 0.125	−0.1144 ± 0.0074
Agassiz	54.4	99.7	−0.360 ± 0.028	−0.0196 ± 0.0015	54.3	99.8	0.230 ± 0.087	0.0125 ± 0.0047
Balmaceda	56.7	94.0	−2.736 ± 0.067	−0.1552 ± 0.0038	54.0	96.5	−2.389 ± 0.100	−0.1291 ± 0.0054
RGI-17.04843	54.4	97.9	−1.813 ± 0.050	−0.0986 ± 0.0027	53.5	90.8	−0.971 ± 0.123	−0.0520 ± 0.0066
HPS 9	54.2	99.3	−0.651 ± 0.032	−0.0353 ± 0.0017	52.4	96.0	−0.955 ± 0.198	−0.0501 ± 0.0104
HPS 38	52.3	98.1	−2.456 ± 0.060	−0.1284 ± 0.0031	50.0	95.6	−1.774 ± 0.123	−0.0888 ± 0.0061
Frias	48.6	61.1	−0.667 ± 0.051	−0.0324 ± 0.0025	48.6	96.5	−1.366 ± 0.107	−0.0663 ± 0.0052
Onelli	49.7	88.0	−0.708 ± 0.037	−0.0352 ± 0.0018	48.4	94.3	−1.333 ± 0.179	−0.0645 ± 0.0086
Oriental	47.8	97.9	−0.523 ± 0.028	−0.0250 ± 0.0014	47.4	97.8	−0.881 ± 0.092	−0.0418 ± 0.0044
RGI-17.04904	46.6	99.4	−0.779 ± 0.040	−0.0363 ± 0.0019	45.5	98.1	−0.276 ± 0.121	−0.0126 ± 0.0055
RGI-17.05363	41.4	98.4	−0.197 ± 0.029	−0.0082 ± 0.0012	41.4	98.0	−0.597 ± 0.183	−0.0247 ± 0.0076
Mayo	41.4	90.4	−0.506 ± 0.037	−0.0209 ± 0.0015	41.4	95.2	−0.404 ± 0.124	−0.0167 ± 0.0051
RGI-17.04963	40.4	99.4	−0.088 ± 0.033	−0.0036 ± 0.0013	40.4	98.6	0.336 ± 0.112	0.0136 ± 0.0045
RGI-17.04915	38.9	96.6	−0.236 ± 0.038	−0.0092 ± 0.0015	38.9	95.5	0.310 ± 0.128	0.0121 ± 0.0050
Mellizo Sur	37.5	92.6	−0.221 ± 0.032	−0.0083 ± 0.0012	37.0	91.6	−0.401 ± 0.126	−0.0148 ± 0.0046
HPS 8	35.5	99.8	−0.369 ± 0.032	−0.0131 ± 0.0011	35.4	98.8	−0.625 ± 0.190	−0.0221 ± 0.0067

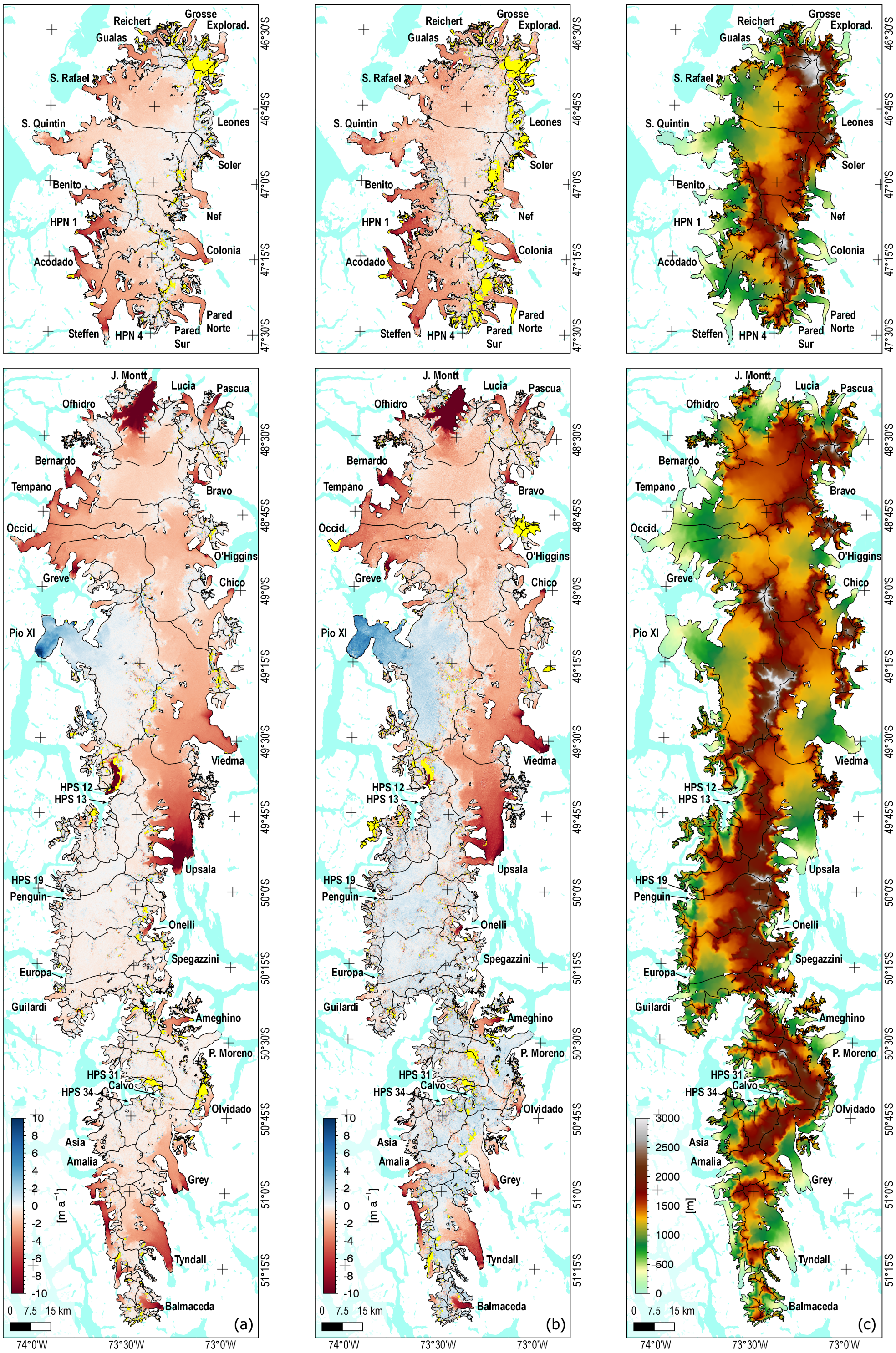

Figure 1. SECR maps of NPI and SPI for the two epochs (a) 2000–2012 and (b) 2012–2016. Unsurveyed areas are marked in yellow. (c) The TDM DEM of 2012 used as reference for the geodetic mass balance.

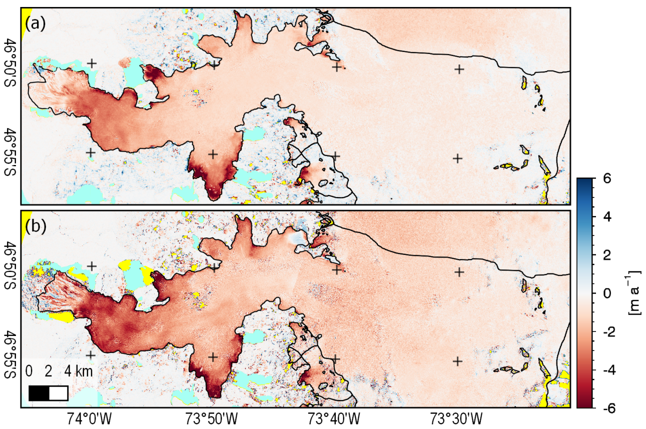

Figure 2. SECR of S. Quintin: (a) 2000–2012 , (b) 2012–2016.

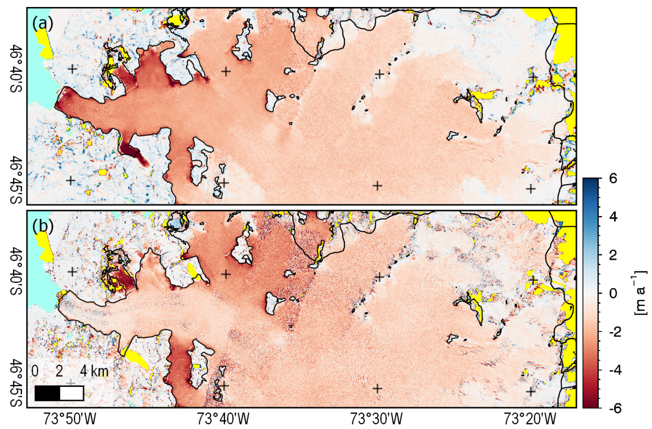

Figure 3. SECR of S. Rafael: (a) 2000–2012, (b) 2012–2016.

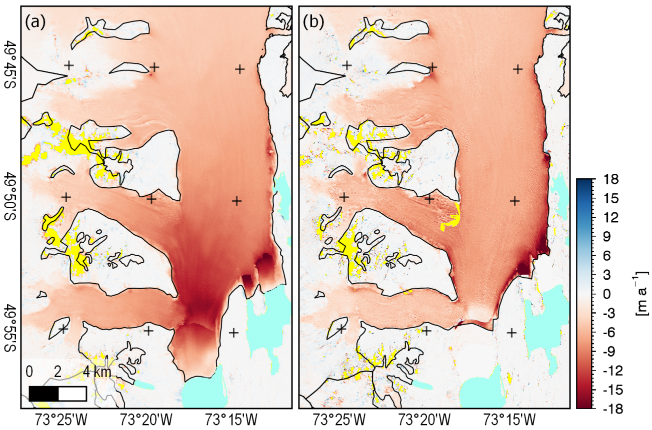

Figure 4. SECR of Upsala: (a) 2000–2012, (b) 2012–2016.

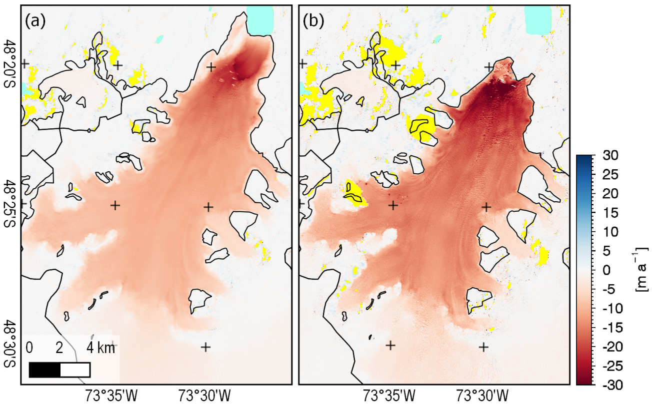

Figure 5. SECR of Jorge Montt: (a) 2000–2012 , (b) 2012–2016.

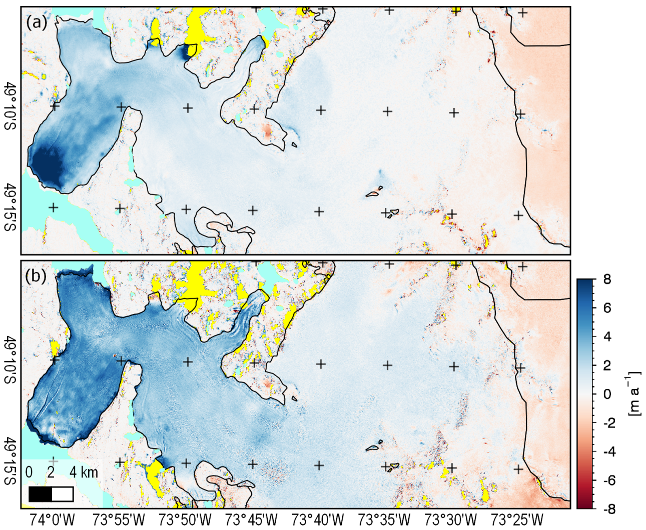

Figure 6. SECR of Pio XI: (a) 2000–2012 , (b) 2012–2016.

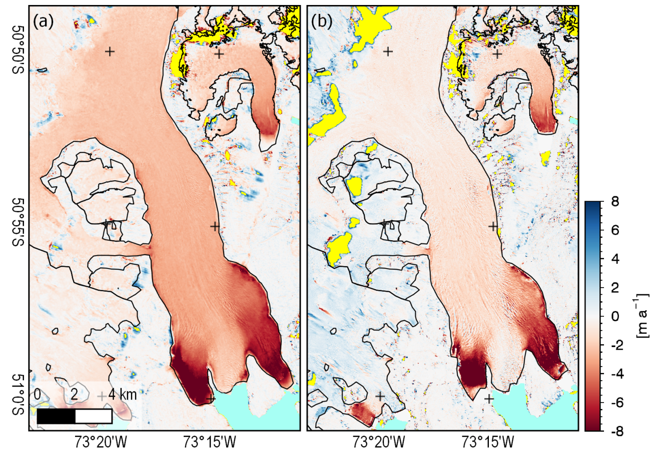

Figure 7. SECR of Grey: (a) 2000–2012 , (b) 2012–2016.

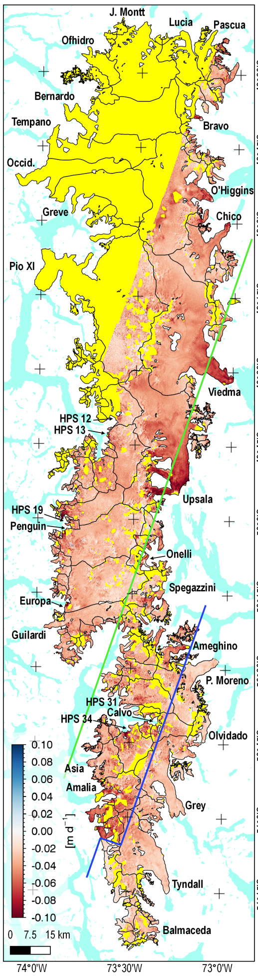

Figure 8. Daily SECR of SPI during summer 2011/2012. Acquisition dates north of green line: 18/12–26/3 (time span: 99 days), between green and blue lines: 7/12–15/3 (99 days), south of blue line: 29/12–31/1 (33 days). Unsurveyed areas are marked in yellow.

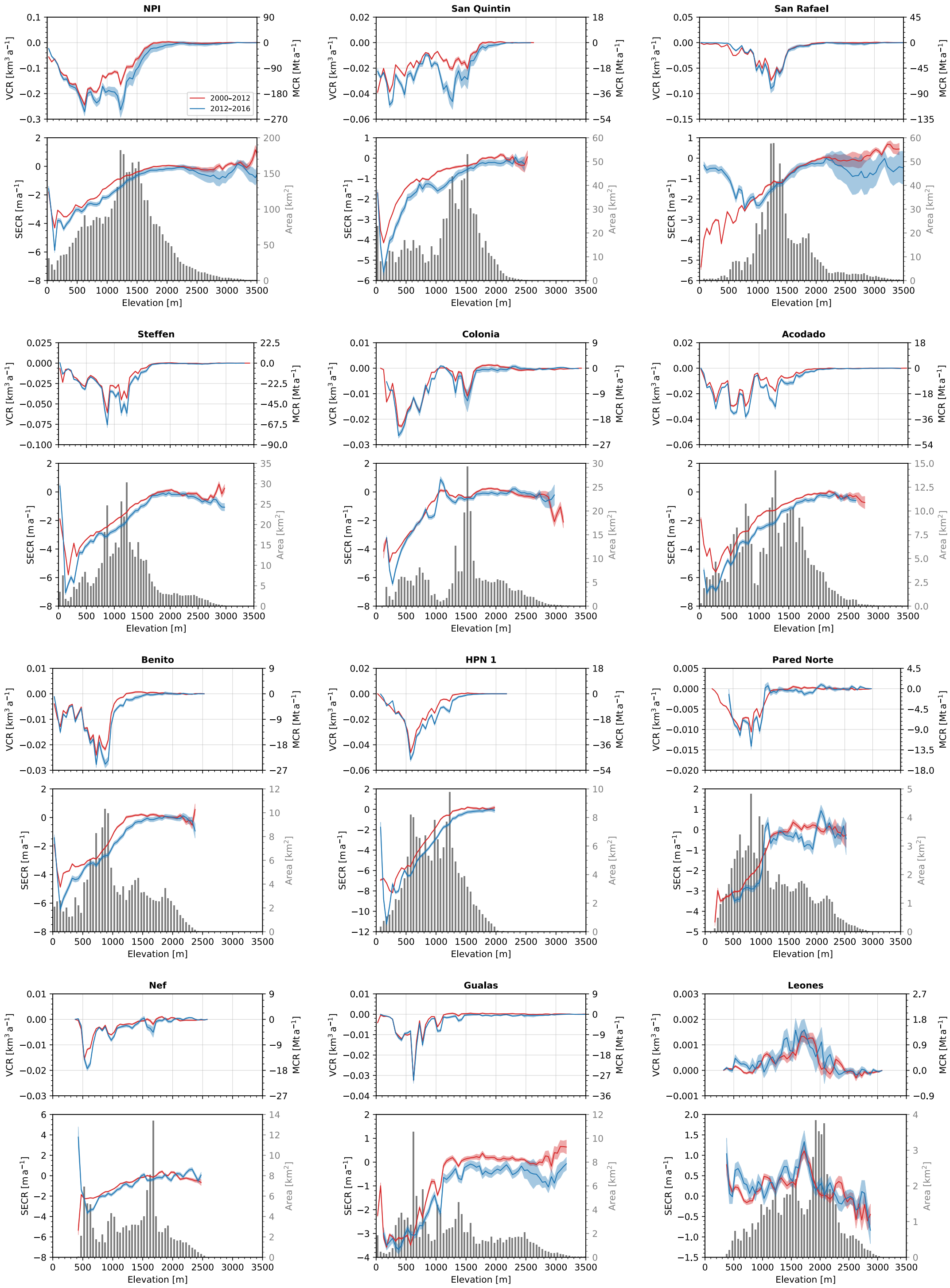

Figure 9. Surface elevation, volume and mass change rates (SECR, VCR, MCR) versus altitude in 50 m intervals for NPI and its main glaciers for epochs 2000–2012 (red) and 2012–2016 (blue). The hypsometric curve of 2011/2012 is shown in grey. <These plot show updated uncertainties, the same applies for Fig. S12 in the Supplement.>

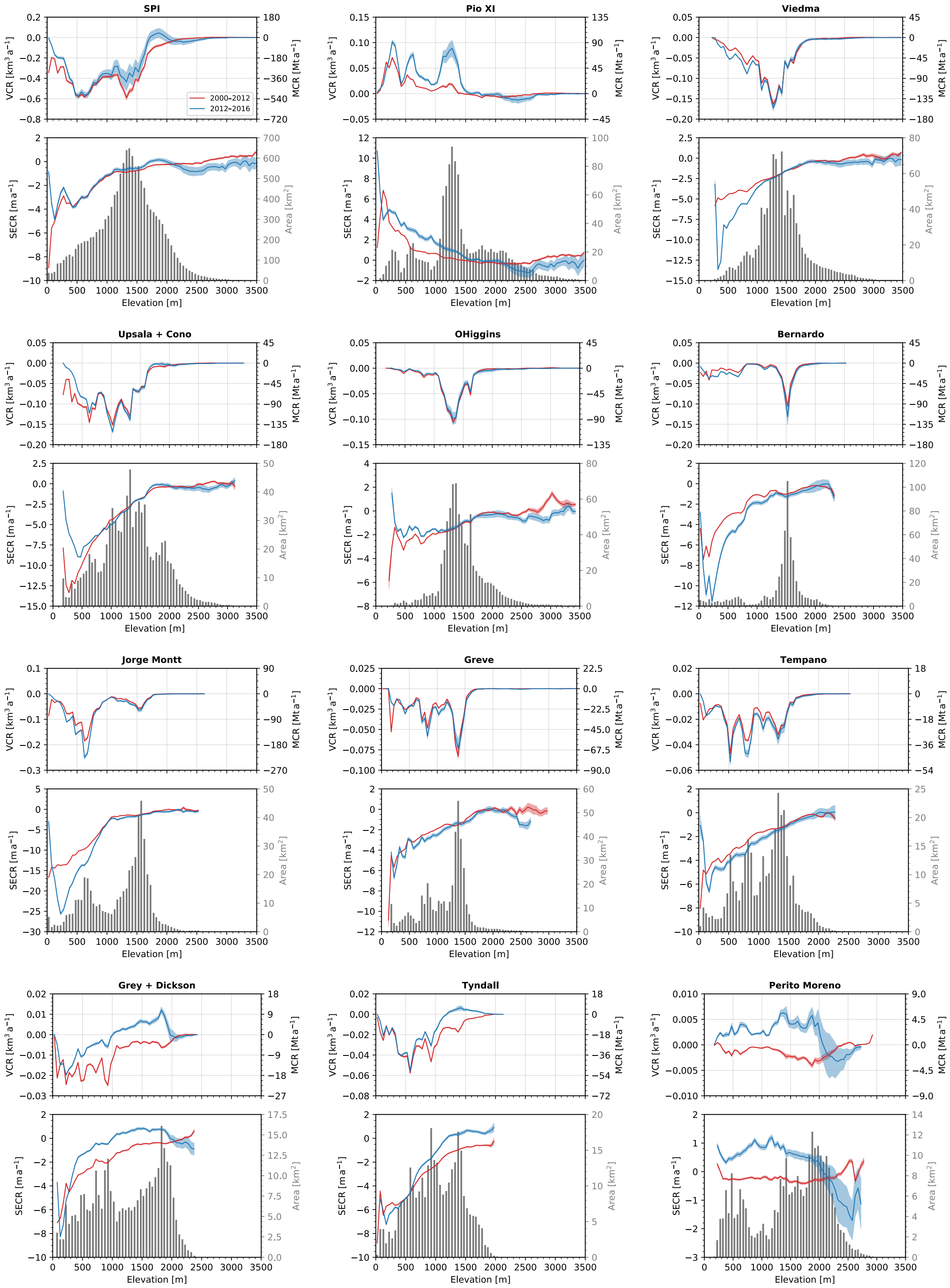

Figure 10. Surface elevation, volume and mass change rates (SECR, VCR, MCR) versus altitude in 50 m intervals for SPI and its main glaciers for epochs 2000–2012 (red) and 2012–2016 (blue). The hypsometric curve of 2012 is shown in grey. <These plot show updated uncertainties, the same applies for Fig. S13 in the Supplement.>

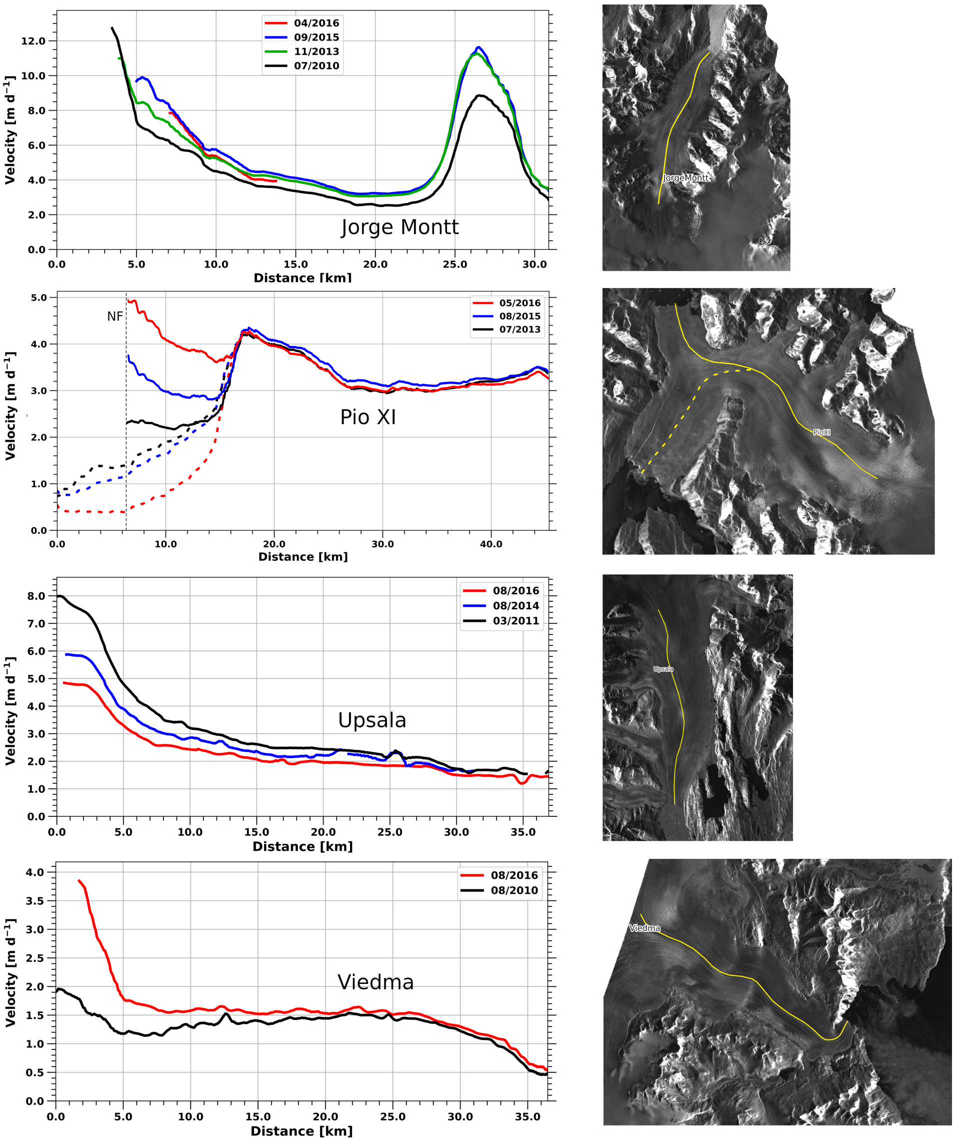

Figure 11. Surface velocities along the central flow lines of Jorge Montt, Pio XI, Upsala, and Viedma glaciers (SPI) on different dates, derived from TerraSAR-X repeat pass data. The distance origin refers to the ice front position on the first date; for Pio XI Glacier to the front of the southern branch, NF to the front of the northern branch. Pio XI Glacier, dashed lines: velocities along the central flowline of the southern branch. Insets: TerraSAR-X images with location of central flowlines. <This figure is new.>

Changes to the Supplement

- Section S4, Fig. S3: the caption was extended and improved. The orange curve was removed since it is not discussed in the manuscript.
- Section S4, Fig. S4: the caption was improved.
- Section S4: an explanation of the procedure for the estimation of mass balance gradients for Jorge Montt, S. Rafael, and S. Quintin glacier was added. It is meant to integrate and complete Sect. 3.1.3. The Contents on page number 1 were updated accordingly.
- Section S7, Fig. S12: the uncertainties were updated.
- Section S7, Fig. S13: the uncertainties were updated.
- Section S7, Table S8: the uncertainties were updated.
- Section S7, Table S9: the description was improved, references to the used bathymetric data were added.
- Section S8, Table S10: the description was improved, the uncertainties of this study were updated.
- Section S8, Table S11: the uncertainties of this study were updated.
- References: the references cited in Fig. S9 were added.